CHAPTER 2

THE STATE OF THE OCEAN

This chapter presents an overview of the current state of knowledge of ocean climate in 2005, placed in historical context. Expert scientists who monitor, observe, and analyze the ocean variables described in this chapter (e.g., sea level, sea surface temperature, ocean carbon, etc.) have produced concise summaries describing what happened during 2005, placing it in the context of what has happened over the course of many years, and discussing why it is important to monitor these ocean variables. The chapter also discusses how the observing system needs to be enhanced to improve ocean analysis and reduce present uncertainties. In presenting these materials, we attempt to address the needs and interests of a broad audience, including decision makers and scientific generalists who are concerned about the role of the ocean in climate.

Contents: The State of the Ocean **Page**

Introduction

Phillip Arkin,
Earth System Science Interdisciplinary Center, University of Maryland, College Park, MD

The material used in this chapter to assess the state of the ocean in the past year comes from three general types of observations and inferences. Many of the original observations used were made by instruments that directly sample the ocean in given locations. For example, sea level is measured by tide gauges at coastal locations, sea surface temperatures (SSTs) are measured by thermometers on ships and buoys, and oceanic carbon is measured by analyzing seawater samples acquired from various locations during research cruises. Inferences from remotely sensed observations, generally from earth-orbiting satellites, are also important, for example as an input to the SST product and for precipitation. Finally, mathematical models of various sorts are used quite substantially to make possible spatially and temporally complete descriptions of many of the parameters discussed.

None of the parameters discussed here are measured in truly continuous fashion for the entire ocean. The diversity of observations and inferred products, and the goal of ensuring a complete description of the full global ocean, implies that we face several crucial challenges. The most immediate of these is the need to convert quantities observed at discrete points in space and time into spatially and temporally complete fields of the value of each parameter on a regular grid. This is often accomplished by a straightforward interpolation of the observations at a given time to each of the points on a regular grid, for example by calculating a weighted average, with weights inversely proportional to distance from the target point, of all the nearby observations. This process of constructing a complete field from irregularly distributed observations is referred to (following the practice in meteorological weather prediction) as *analysis*, and the field that results is called an *analysis*, and you will often see this term used in the chapter.

Since information on the pre-existing state of affairs, or from other observations or physical laws governing the parameter can be useful, much more complex methods are sometimes used. Since we are concerned with the global ocean, which is a fluid for which the governing physical laws can be reproduced reasonably well in a mathematical model, methods are often used that use predictions from such a model jointly with observations to produce complete fields, a process call *data assimilation*. The Global Ocean Data Assimilation System (GODAS) is one such method, and products from GODAS are used on occasion by the authors as a reference for comparison with the analyses derived more directly from observations.

This chapter attempts to describe the state of the ocean climate during 2005 (or, in the case of observations with a lengthy lag in retrieving and analyzing observations, what we **knew** in 2005). While descriptions of the actual observations and the analyses derived from them are very helpful for this, it is also valuable to be able to describe the ocean's state in comparison to that of other years, or to some long-term average state. When possible, we do this by computing and displaying the differences between values from 2005 and from the long-term average for the same location and time of year. Such values are referred to as *anomalies*.

Chapter 2 covers 11 topics, which we have clustered into 5 related groups. We begin with sea level and sea surface temperature (SST), both of which relate to relatively well-observed characteristics of the surface of the ocean. Heat fluxes, precipitation, and a discussion of the exceptional variations in Atlantic Ocean hurricanes during 2005 come next, followed by topics related to motion in the ocean, including surface currents and the thermohaline circulation. We continue with heat content variability and El Niño, which is related to changes in the heat content of the tropical Pacific Ocean, and Arctic variability. We conclude with the important topic of the behavior of the ocean as a source or sink for carbon dioxide.

Sea Level

Mark A. Merrifield[1], Stephen Gill[2], and Gary T. Mitchum[3]
[1] Department of Oceanography, University of Hawaii, Honolulu, HI
[2] NOAA/National Ocean Service, Silver Spring, MD
[3] College of Marine Science, University of South Florida, St. Petersburg, FL

2005 Sea Level Deviation

Tide gauges have long observed sea level, and these instruments still provide the long-term context for understanding climate variations. Since 1992, however, satellite altimetry has provided global views of the sea surface height field. In this report both data sources are exploited to describe spatial patterns of sea level deviations during 2005, which largely are a result of wind forcing, and to consider recent sea level measurements in the context of short-term (e.g., a decade, or the length of the altimeter record) and long-term(length of multi-decade tide gauge records) trend estimates, which are used as a measure of sea level rise. The altimetry data for the TOPEX/Poseidon/Jason missions are obtained from NASA (http://podaac-www.jpl.nasa.gov/) and were processed at the University of South Florida. Tide gauge data for US stations were collected by NOAA's National Ocean Service (http://tidesandcurrents.noaa.gov/nwlon.html), and data for international stations were obtained from the University of Hawaii Sea Level Center (http://uhslc.soest.hawaii.edu/).

Sea level deviations for 2005 are computed as the annual mean sea level at each tide gauge and altimeter grid location relative to a longer-term mean (1993-2001, Figure 1). The spatial patterns of the two datasets are remarkably consistent given differences in ocean dynamics at the coast relative to the open ocean, and the different sample periods of the tide gauge (every hour) and altimeter (every 10 days) time series. Coastal sea level effects are apparent, however, notably along the east coast of North America, where coastal tide gauge sea levels were higher than normal whereas nearby ocean values from altimetry were lower than normal. In many instances, the sea level deviations can be linked directly to anomalous surface winds and their associated upper ocean mass transports (Figure 2). A striking example is a cyclonic (counter-clockwise rotating in the northern hemisphere) wind anomaly centered over the North Atlantic. Cyclonic wind patterns tend to force a divergent upper ocean mass transport and a fall in sea level; the opposite is true for anticyclonic patterns. This anomaly corresponds to a weakening of the Bermuda High and, possibly, an associated weakening of the subtropical wind driven ocean circulation. This would account for the lower than average sea level in the open ocean, and the higher tide gauge sea levels along the North American coast that we noted above to be at odds with the open ocean altimetric heights. Anticyclonic winds associated with an enhanced North Pacific High led to high sea levels over much of the

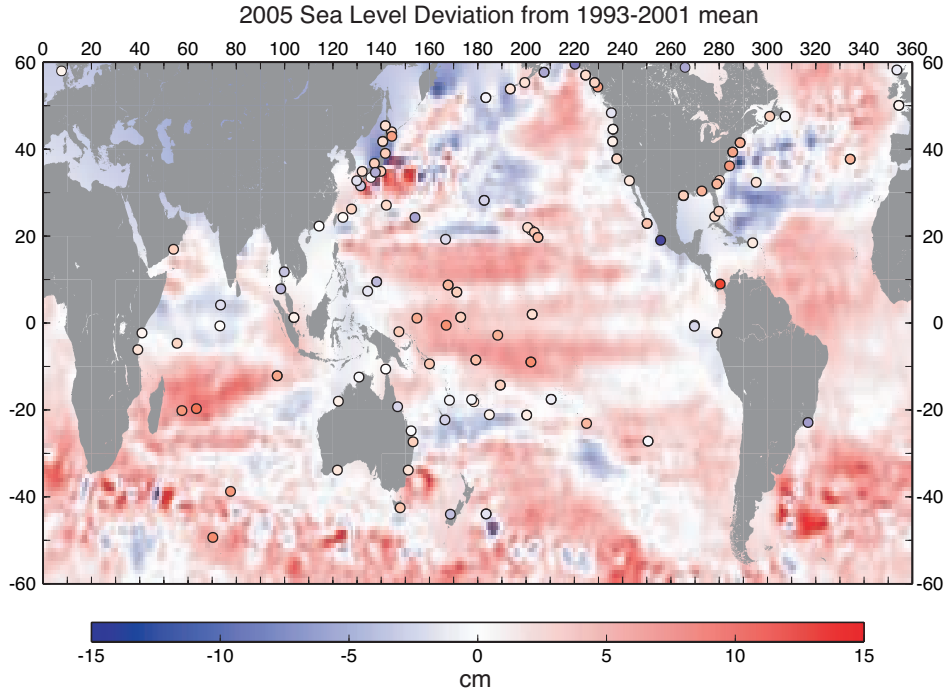

Figure 1. The deviation of 2005 annual average sea level from a 1993-2001 mean, as measured by satellite altimeter (color contour) and tide gauges (circles).

northeast Pacific. Near the equator, increased easterly Trade Winds in the Pacific and Atlantic Oceans led to high sea levels, whereas anomalous westerlies in the Indian Ocean led to low sea levels.

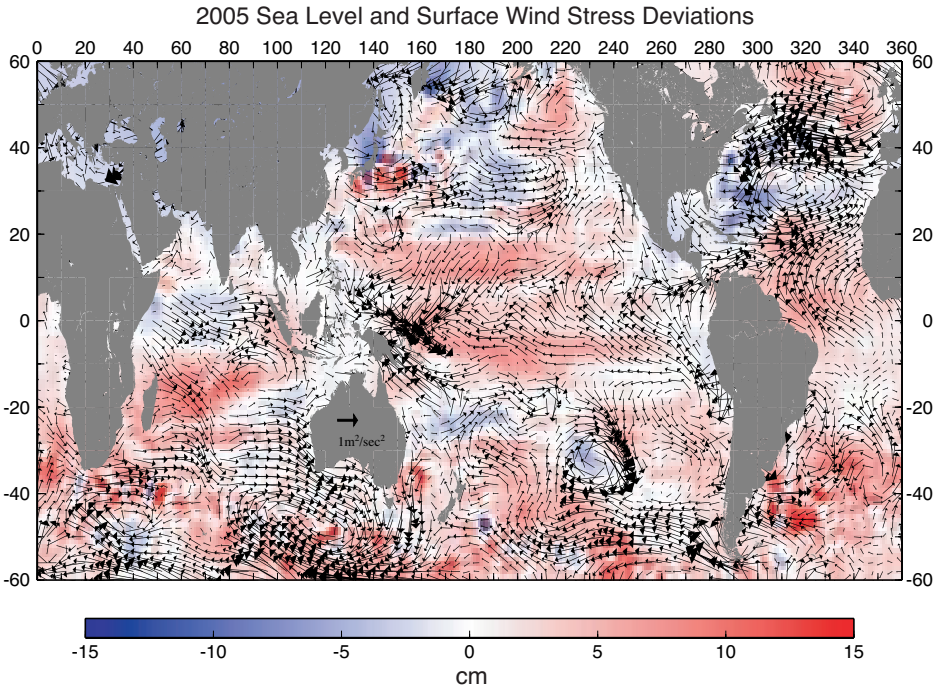

Figure 2. Same as Figure 1, excluding the tide gauge deviations, and including the 2005 deviation of surface winds (data from the National Center for Environmental Prediction).

Relative to the previous year, 2005 saw an increase in sea level in the region of the western tropical Pacific north of the equator and east of the Philippines (Figure 3). The pattern developed in response to increased local anticyclonic wind forcing in 2005 relative to 2004. This region is north of the equatorial zone where precursors to El Niño events are often seen in sea level and heat content (Jin, 1997; Meinen and McPhaden, 2000). In general though, 2005 was a year of relatively weak El Niño/La Niña variability (McPhaden, this report, p. 85). This is consistent with the generally weak sea level changes observed along the equator (Figures 2 and 3 compared to the large changes in equatorial sea level that accompany a typical El Niño or La Niña event (Merrifield et al., 1999)). Other major changes in sea level from 2004 to 2005 occurred in the western boundary currents of the North Pacific and Atlantic, again with corresponding changes in the annual wind forcing.

Global and Regional Sea Level Rise

The deviations shown in Figure 1 were above average over most of the global ocean. Since at least 1993, the time span of Topex/Poseidon/Jason altimeter measurements, global sea levels have been rising at a linear rate of 2.9±0.4 mm/yr (Figure 4, Leuliette et al., 2004; http://sealevel.colorado.edu/; Cazenave and Nerem, 2004). The general increase in globally averaged sea level during 2005 was consistent with this longer trend. At any particular point, however, the rate of sea level change can be very different from the globally averaged rate (Figure 5). A notable example is along the coasts of North America where sea level has fallen in recent years. In the North Pacific, this is presumably associated with a trend in equatorward winds near the coast, which tend to transport surface waters away from the coast (i.e., upwelling favorable). Recent sea level trends appear to be determined by the current polarity of the Pacific Decadal Oscillation (Mantua et al., 1997; Cummins et al., 2005; http://tao.atmos.washington. edu/pdu and it seems likely that the North Pacific sea level trend pattern will reverse sign at some point with a change to rising sea levels near the North American coast.

The primary contribution to the global rise rate (Figure 4) over the past decade is thought to be increased heat content in the upper ocean and the associated increase in volume associated with thermal expansion(Cazenave and Nerem, 2004). Estimates of the heat-related contribution to sea level rise, based on available in situ hydrographic measurements, vary considerably (1.6 +/-0.3 mm/yr, Willis et al. 2004, 1.2 +/- 0.2 mm/yr, Antonov et al., 2005; 2.3 +/-0.8 mm/yr, Carton et al., 2005). Miller and Douglas (2004) conclude that melting ice, resulting in an increase of the mass of the ocean, may account for a larger component of global sea level rise than suggested by the recent estimates of upper ocean heat and volume changes. It is fair to say that there is still considerable uncertainty in specifying the contributions to the global sea level rise budget.

To illustrate how the sea level trends in Figure 5 are highly dependent on record length and residual variability, we examine tide gauge records at locations of recent strong trends in the altimeter data, both for rising (Kwajalein in the western tropical Pacific) and recently falling (San Francisco, CA) sea levels (Figure 6). The recent tide gauge trends (-2.17 mm/yr at San Francisco, 6.64 mm/yr at Kwajalein) are generally consistent with the altimeter derived trends at these locations (Figure 5), even without correcting for land motion at the tide gauges. It is clear that the rates are strongly influenced by recent interannual fluctuations, and that they differ considerably from the longer-term trends estimated over multiple decades (1.95 mm/yr and 1.28 mm/yr, respectively). Zervas (2001) estimates that 50 to 60 year time series are required to obtain a trend with a 1 mm/year confidence interval.

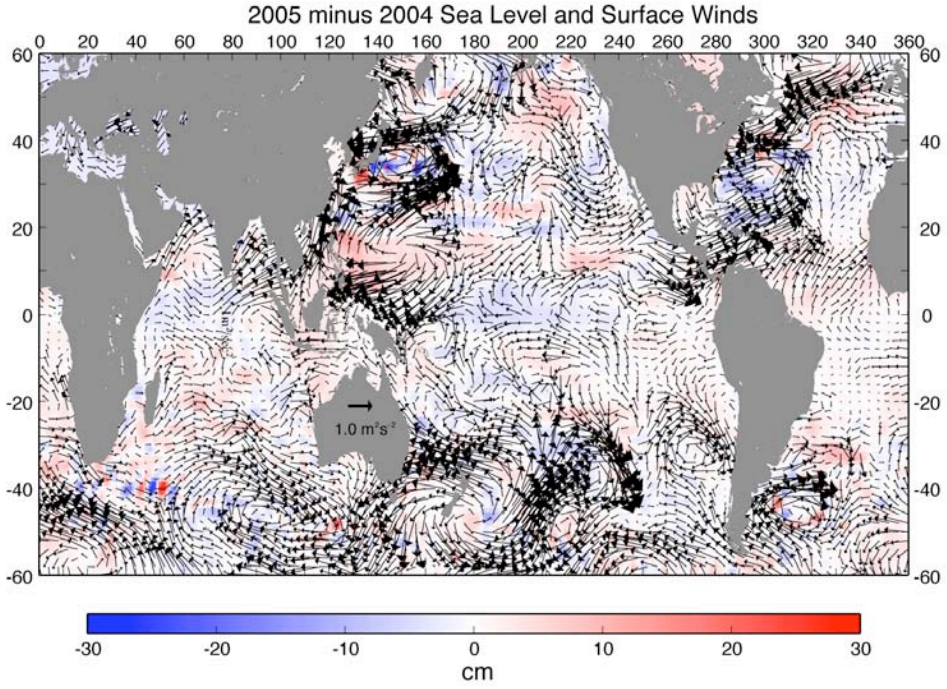

Figure 3. The difference (2005 - 2004) in annual average sea level and surface winds.

New Product Development in 2005

Relative Mean Sea Level Trends

The report of the International Sea Level Workshop (June 10-11, 1997, Honolulu, Hawaii) identified a set of 62 water level stations as a core global network for monitoring long term sea level trends. NOAA National Ocean Service operates and maintains 18 of these proposed climate reference stations and presents routinely-updated analyses of the long-term trends and variability. In support of the program plan objectives of the Office of Climate Observations of NOAA's Climate Program, the sea level trend analysis has been extended to the 44 non-NOS water level stations. The data for these stations were obtained from the Permanent Service for Mean Sea Level (PSMSL, http://www.nbi.ac.uk/psmsl/index.html), the global data bank for long-term sea level information from tide gauges.

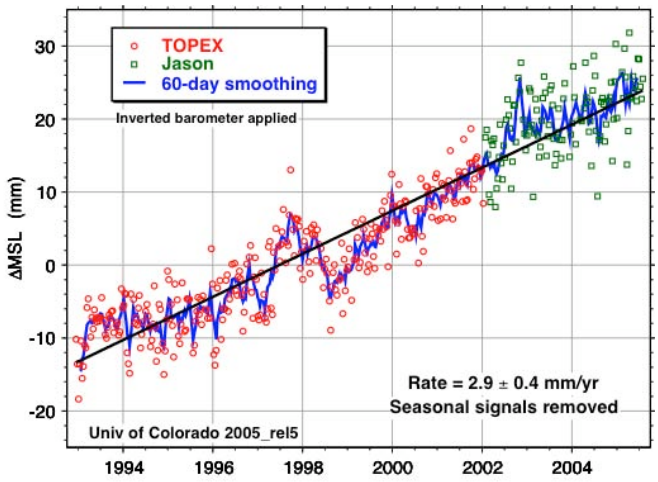

***Figure 4**. Global sea level rise as determined using altimeter measurements from the TOPEX and Jason satellites (source: http://sealevel.colorado.edu).*

Water level records are a combination of the fluctuations of the ocean and the vertical land motion at the location of the station. The sea level variations determined are the linear trend, the average seasonal cycle, and the interannual variability at each station. The trends are available as a table in millimeters/year or feet/century. Sea level trends for these global stations are being incorporated into the NOAA website at

http://tidesandcurrents.noaa.gov in the very near future and follow the product look and feel for the U.S. stations on the web at present.

Exceedance Probability Levels

NOAA has developed a new exceedance probability product from the long-term tide station records. Using an Extreme Value General Extreme Value Analysis (GEV) approach (Zervas, 2005) of the monthly observed highest tides, for example at Honolulu, HI (Figure 7a), exceedance probabilities can be expressed as return periods (Figure 7b) and also can be related to various tidal datums (Figure 7c). This product is being completed for long-term NOAA tide stations and eventually for the set of GLOSS reference stations for sea level as well. It will be provided as a web-based product.

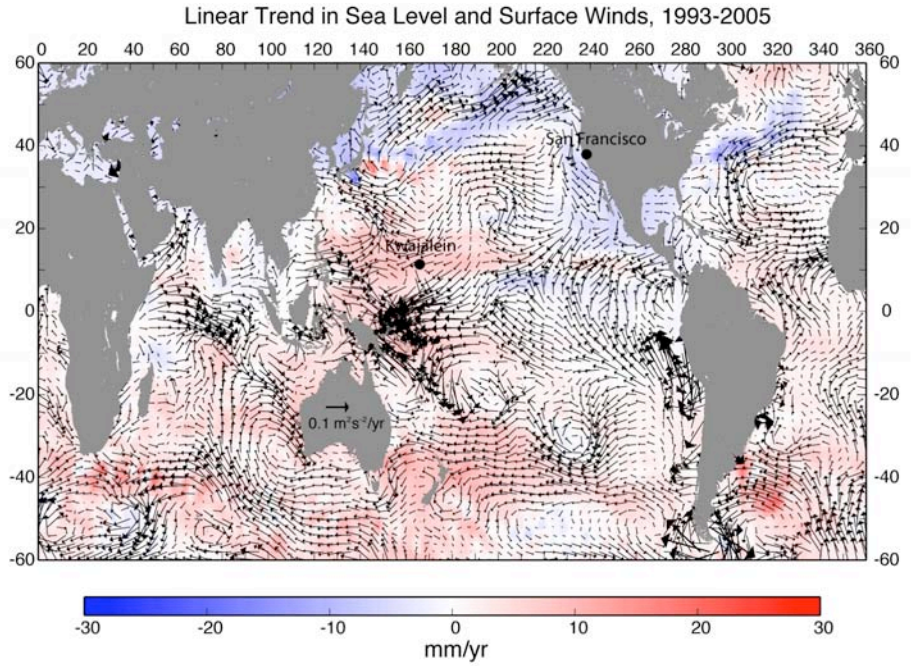

Figure 5. Linear trend in sea level (color contour) and surface winds over the period 1993-2005.

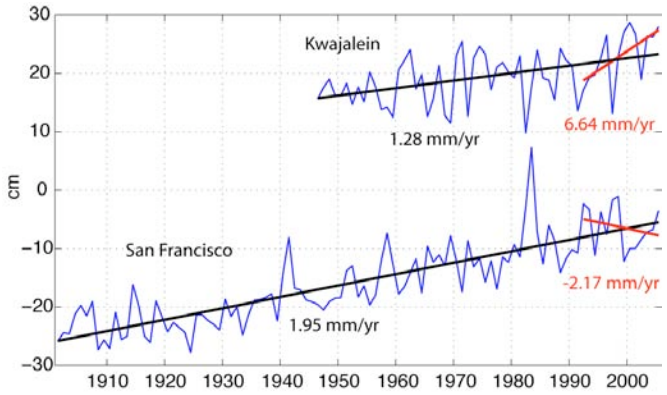

Figure 6. Annual mean sea level from the San Francisco and Kwajalein tide gauges (data courtesy of NOAA-NOS) with estimates of the linear trend for the entire record (in black) and for the time period of the TOPEX and Jason satellite altimeters (in red).

The extreme water level events in 2005 on the east and gulf coasts of the U.S. were dominated by the large number and severity of hurricanes and tropical storms (http://www.nhc.noaa.gov/2005atlan.shtml?). The eastern Pacific also was subject to the effects of several named storms http://www.nhc.noaa.gov/2005epac.shtml?). The severity of the storm surges at many long-term tide station locations redefined the exceedance probability curves when the hurricanes of 2005 were taken into account in the GEV analyses. For instance, the high water levels of Hurricane Katrina

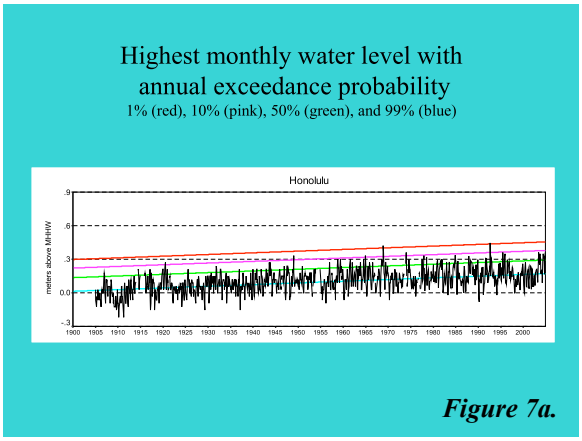

Figure 7a.

raised the 1% exceedance level only slightly at the long-term tide station at Pensacola, FL, but by over one foot at Dauphin Island, AL. Similarly, Hurricane Wilma high water levels at Key West, FL resulted in the

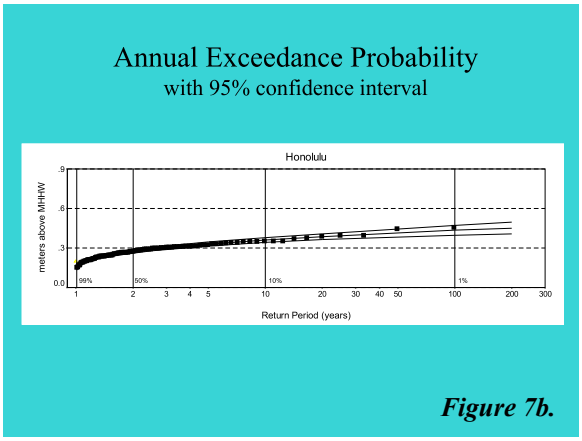

Figure 7b.

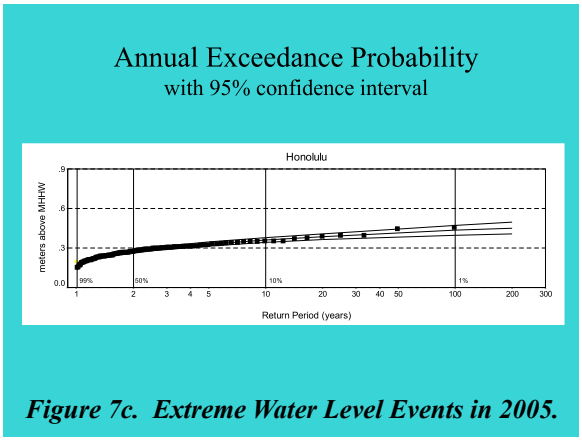

Figure 7c. Extreme Water Level Events in 2005.

1% level being raised slightly. The 1% level can be thought of as representative of the "100-year event" level used in engineering. Figure 8 shows the dominance of the hurricane storm surges in the residual record (observed minus predicted tides) for Pensacola, FL. Figure 9 is the residual for a Pacific island station showing a severe water level event in the winter of 2005.

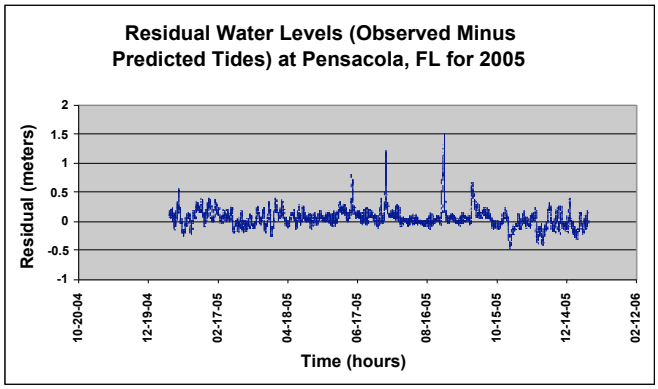

Figure 8. *Atlantic basin example.*

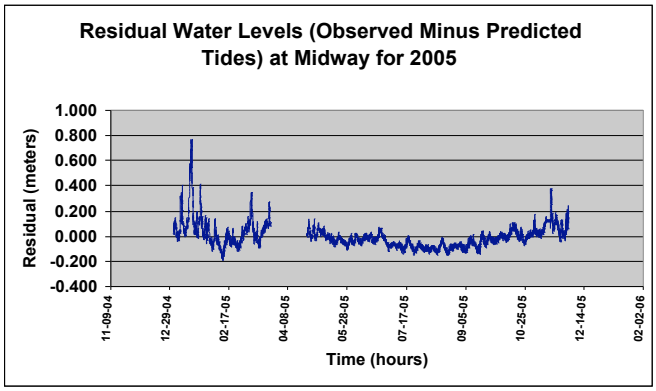

Figure 9. *Pacific basin example.*

References

Antonov, J. I., S. Levitus, and T. P. Boyer, 2005: Thermosteric sea level rise, 1955-203. *Geophys. Res. Lett., 32*, L12602, doi:10.1029/2005GL023112.

Carton, J. A., B. S. Giese, S. A. Grodsky, 2005: Sea level rise and the warming of the oceans in the Simple Ocean Data Assimilation (SODA) ocean reanalysis. *J. Geophys. Res., 110*, C09006, doi:10.1029/2004JC002817.

Cazenave and Nerem, 2004: Present-day sea level change: Observations and causes. *Rev. of Geophys., 42*, RG3001, doi:10.1029/2003RG000139.

Cummins, P. F., G. S. E. Lagerloef, and G. Mitchum, 2005: A regional index of northeast Pacific variability based on satellite altimeter data. *Geophys. Res. Lett., 32,* L17607, doi:10.1029/2005GL023642.

Jin, F.F., 1997: An equatorial recharge paradigm for ENSO. Part I: Conceptual model. *J. Atmos. Sci., 54*, 811-829.

Leuliette, E. W, R. S. Nerem, and G. T. Mitchum, 2004: Calibration of TOPEX/Poseidon and Jason altimeter data to construct a continuous record of mean sea level change. *Mar. Geodesy, 27(1-2)*, 79-94.

Mantua, N. J., S. R. Hare, Y. Zhang, J. M. Wallace, and

R. C. Francis 1997: A Pacific interdecadal climate oscillation with impacts on salmon production. *Bull. Amer. Met. Soc., 78*, 1,069-1,079.

Meinen, C.S. and M.J. McPhaden, 2000: Observations of warm water volume changes in the equatorial Pacific and their relationship to El Niño and La Niña. *J. Clim., 13*, 3551-3559.

Miller, L., and B. C. Douglas, 2004: Mass and volume contributions to twentieth-century global sea level rise, *Nature, 428*, 406-409.

Willis, J. K., D. Roemmich, and B. Cornuelle, 2004: Interannual variability in upper ocean heat content, temperature, and thermosteric expansion on global scales. *J. Geophys. Res., 109*, C12036, doi: 10.1029/2003JC002260.

Zervas, C., 2005: *Relative Sea Level Trends from Tide Stations: How are they determined and what do they tell us?* Poster paper presented at Climate Change Science Program Workshop, Climate Science in Support of Decision Making, 14-16 November 2005, Arlington , VA.

Zervas, C., 2001: Sea Level Variations of the United States 1854-1999, NOAA Technical Report NOS CO-OPS 36, NOAA, Silver Spring, MD, pp186.

Sea Surface Temperatures

Richard W. Reynolds
NOAA/National Climatic Data Center
Asheville, NC

Sea surface temperatures (SST) are an important indicator of the state of the earth climate system as well as a key variable in the coupling between the atmosphere and the ocean. Accurate knowledge of SST is essential for climate monitoring, prediction and research. It is also a key surface boundary condition for numerical weather prediction and for other atmospheric simulations using atmospheric general circulation models. In addition, SST is important in gas exchange between the ocean and atmosphere, including the airsea flux of carbon.

The SSTs are obtained from a variety of data sources. The in situ data are obtained from both ships and buoys. The longest data set of SST observations is based on observations made from ships. From 1870 to present, the number of observations generally increased except for noticeable dips during the First and Second World Wars. In addition to the changes in the number of observations, the method of measuring surface marine observations changed over the period from temperatures measured from uninsulated buckets to temperatures measured from insulated buckets and engine intakes. SST observations from drifting and moored buoys became plentiful in the late 1970s. These observations are typically made by thermistor or hull contact sensor and are usually relayed in real-time by satellites. Although the accuracy of the buoy SST observations varies, the accuracies are usually better than 0.5^{o}C, less accurate than the accuracies from ships.

In late 1981, accurate SST retrievals became available from the Advanced Very High Resolution Radiometer (AVHRR) instrument, which has been carried on many NOAA polar orbiting satellites. These retrievals improved the data coverage over that due to in situ observations alone. The satellite retrievals allowed better resolution of small scale features such as Gulf Stream eddies. In addition, especially in the Southern Hemisphere, where in situ data are sparse, SSTs could now be observed on a regular basis in many locations. Because the AVHRR cannot retrieve SSTs in cloud-covered regions, the most important problem in retrieving SST is to identify areas where clouds are present in the view from space, and to eliminate those areas from the data retrievals. After clouds have been eliminated, the SST algorithm is derived to minimize the effects of atmospheric water vapor. The satellite SST retrieval algorithms are "tuned" by regression against quality-controlled buoy data using the multichannel SST technique of McClain et al. (1985). This procedure converts the satellite measurement of the "skin" SST (roughly a micron in depth) to a buoy "bulk" SST (roughly 0.5m). The tuning is done when a new satellite becomes operational or when verification with the buoy data shows increasing errors. During the last decade additional satellite instruments became available. These include Microwave instruments, which can retrieve SSTs even under persistent cloud cover.

The analysis discussed below is produced using AVHRR and ship and buoy data. Figure 1 shows a sample of the daytime and nighttime AVHRR (upper panels) and ship and buoy (lower left panel) SST anomaly data for one week on a 1° grid. Anomalies are defined as differences from a 1971-2002 climatological base period as described by Xue et al. (2003). The white areas in these panels show the regions with missing data. This is especially evident in the panel showing the in situ data. The purpose of an analysis is to produce a complete field on a regular grid. This is done by weighting the different data sources by their relative accuracy and distance from the grid point to be analyzed. The lower right panel, showing the resulting analysis, demonstrates how the satellite and in situ data combine to create a high resolution data set that is more accurate than that derived from satellite retrievals alone. The formal method is formally defined as optimum interpolation (OI) and is as an objective analysis method described in Reynolds et al. (2002). As discussed there, the OI method assumes that the data do not contain long-term biases. Because satellite biases do occur in our period of interest, a preliminary step using Poisson's Equation is carried out to remove satellite biases relative to in situ data before the OI analysis is begun. This method adjusts any large-scale satellite biases and gradients relative to the boundary conditions defined by the in situ field. The satellite data are adjusted by these

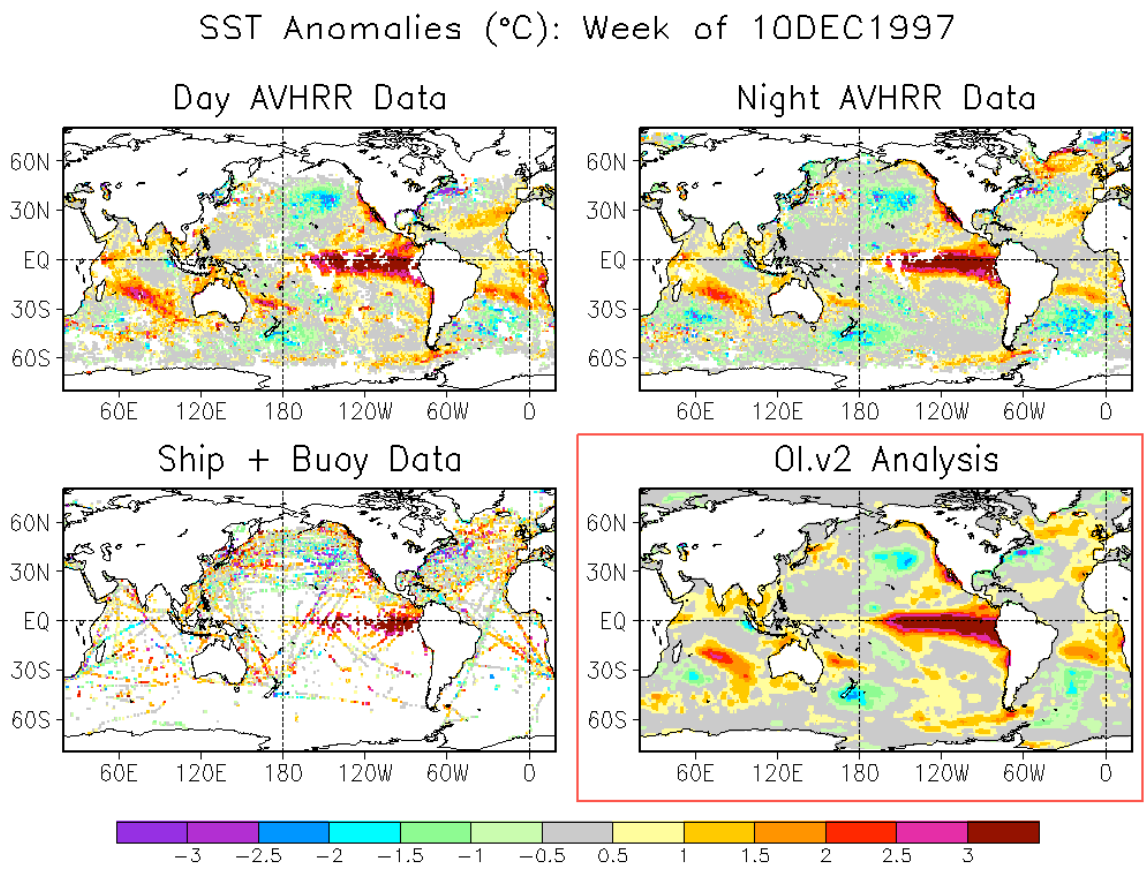

Figure 1. Weekly anomalies on a 1° grid for 10 December 1997. The top two panels the anomalies based on daytime and nighttime AVHRR satellite data, respectively. The left lower panel shows the anomaly based on ship and buoy data. The right lower panel shows the OI analysis using the other panels as input.

smoothed bias corrections before they are used in the OI.

To illustrate the overall changes in 2005, the yearly averages of the monthly anomalies are shown for 2004 and 2005 in Figure 2. The overall impression is that the anomalies are primarily positive. This is due to the overall warming trend of the global SSTs from 1971 to present relative to the mean of the climatological base period. Comparisons of the two years show two important changes: the first in middle latitudes (40°N - 66°N) and the second in the tropical North Atlantic (0° - 30° N). In the middle latitude regions, there is a tendency for the positive anomalies to increase from 2004 to 2005 in the eastern Pacific and western Atlantic. To illustrate the changes with time, monthly anomaly time series are shown for the middle latitude eastern Pacific and western Atlantic in Figure 3. Both regions show an overall warm anomaly over the 1995-2005 period, although the monthly to seasonal variability in the Pacific is less than the Atlantic. There is also evidence of regular summer warming in the Pacific region from 2000 - 2005. This signal is only clearly evident in the Atlantic region in 2003 which is the oceanic response to that summer's European heat wave.

During 2005, there was a record number of strong Atlantic hurricanes. In the recent literature, there has been some discussion to determine if changes in SSTs can imply statistically significant changes in hurricanes (Webster, et al. 2005) or not (Trenberth, 2005). All the reports state that SSTs are not the only variable affecting hurricanes. Because of the changes in the northern tropical Atlantic SSTs from 2004 to 2005, Figure 2, time series are shown for the North Atlantic (10°N - 30°N) and for the Gulf of Mexico in Figure 4. The tropical Atlantic region shows overall warm anomalies with irregular variability on 2 to 5 year periods which is not strongly correlated with the seasonal cycle or ENSO. However, a relatively strong maximum anomaly

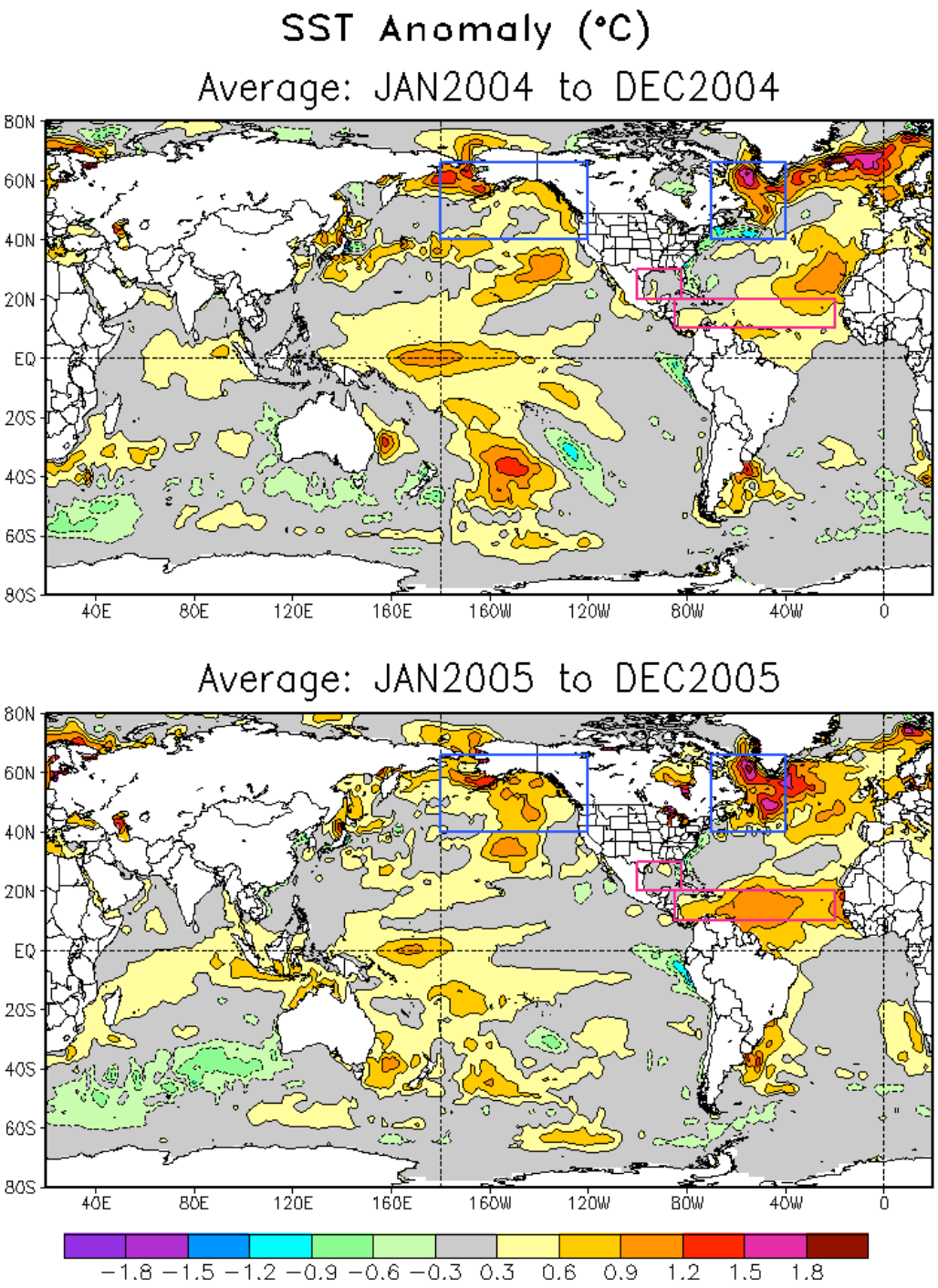

Figure 2. Yearly SST anomalies for 2004 (top) and 2005 (bottom). The anomalies are computed relative to a 1971-2000 base period.

occurs in the summer of 2005. The time series from the Gulf of Mexico appears to be noisier without any no-

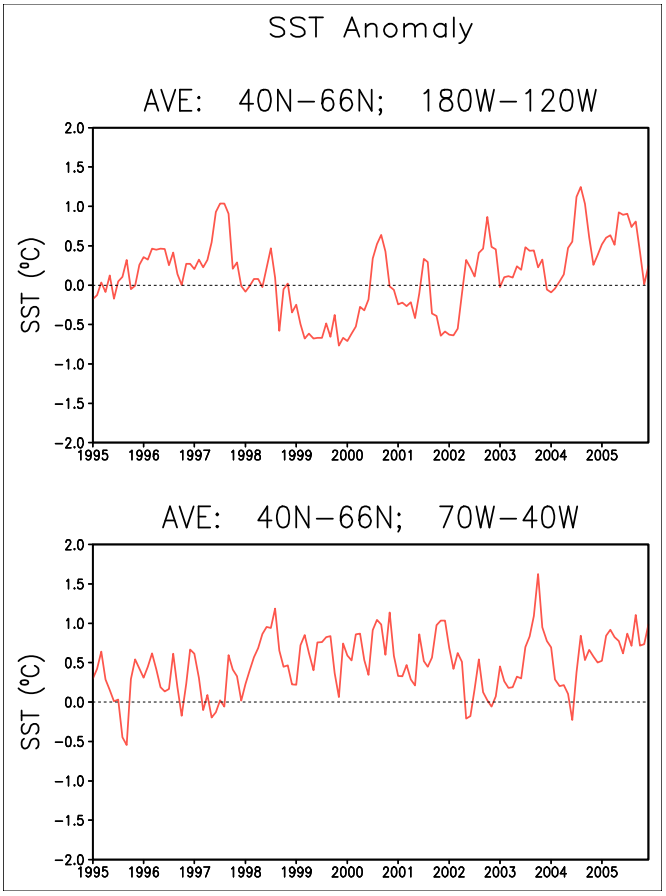

Figure 3. Time series of monthly SST anomalies for the eastern middle latitude North Pacific (top) and the western North Atlantic (bottom). The time series period is January 1995 through December 2005. Regions are indicated in Figure 2.

ticeable signal. To examine the recent summer anomalies in more detail, Figure 5 shows the 2004 and 2005 tropical Atlantic anomalies for July, August and September. In the figure, the 26, 27 and 28°C isotherms of the total SST (anomaly + climatology) are shown for the respective month. Goldberg, et al., (2002) state that local SSTs greater than 26.5°C are needed to generate hurricanes. The figure shows that areas greater than 26.5°C are similar in the corresponding months for 2004 and 2005. However, areas greater than 28°C are larger in July and August 2005 than July and August 2004. As expected, these maps are only of modest help in determining actual hurricane development. However, they are useful background for recent media reports. For example, Time Magazine's October 3, 2005, issue had the bold question on its front cover, "Are we making hurricanes worse?"

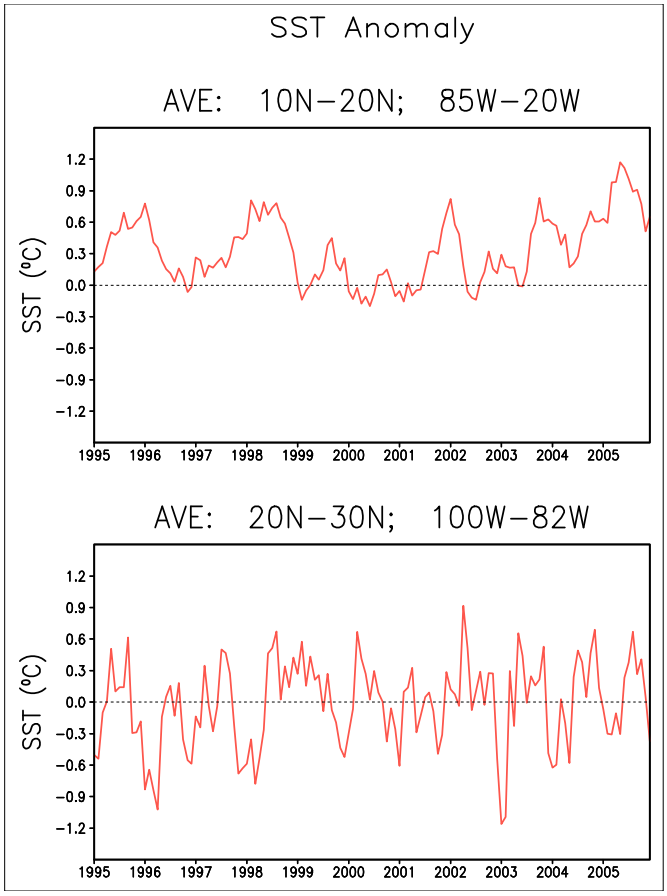

Figure 4. Time series of monthly SST anomalies for the tropical North Atlantic (top panel) and the Gulf of Mexico (bottom panel), otherwise as in Figure 3.

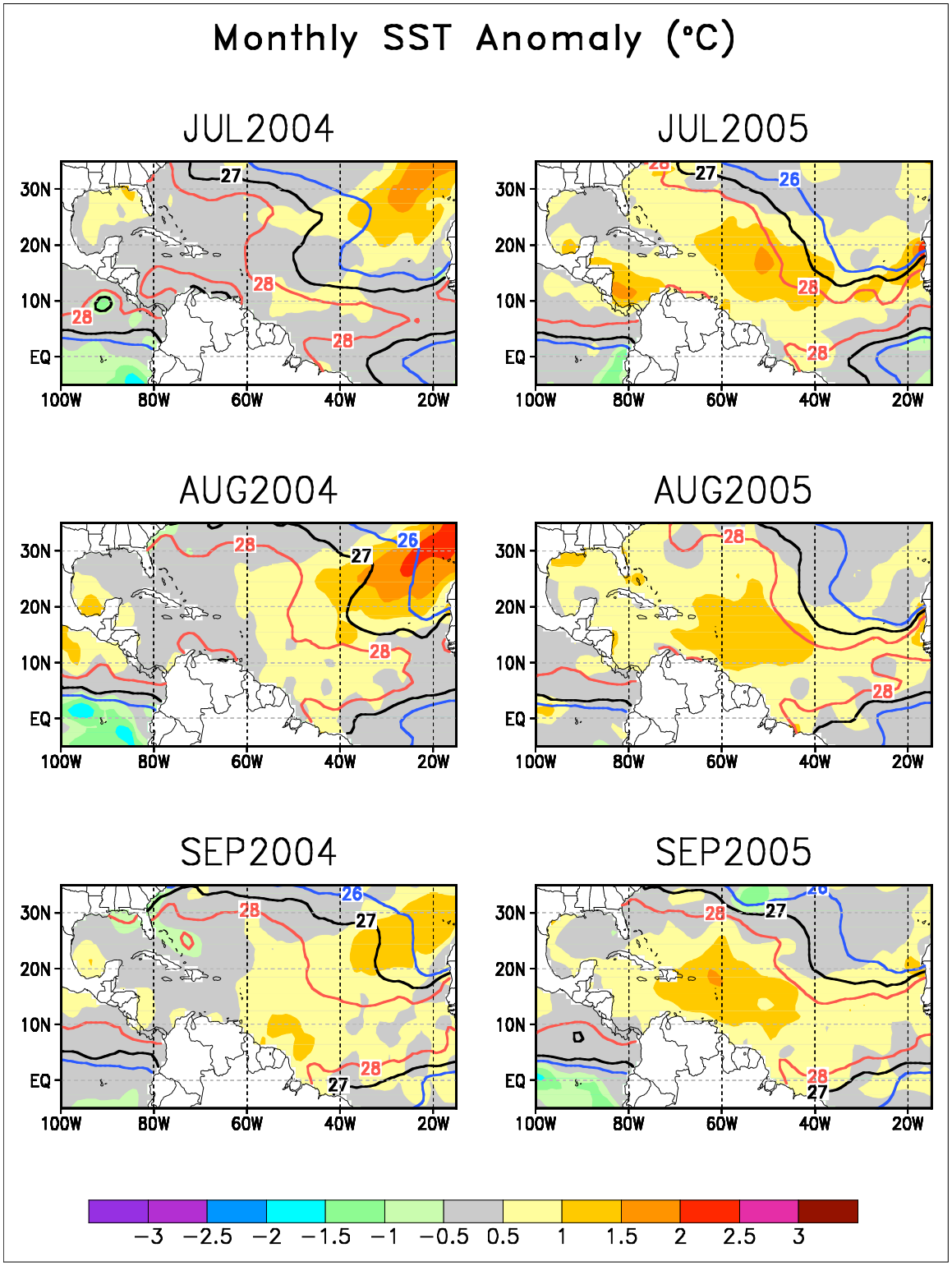

Figure 5. Tropical monthly SST anomalies for July, August and September 2004 (left panels) and for July, August and September 2005 (right panels). Contours show the corresponding monthly total (anomaly + climatology) SST for 26, 27 and 28°C.

References

Goldenberg, S. B., C. W. Landsea, A. M. Mestas-Nuñez, and W. M. Gray, 2001: The recent increase in Atlantic hurricane activity: Causes and implications. *Science*, **293**, 474–479.

McClain, E. P., W. G. Pichel, and C. C. Walton, 1985: Comparative performance of AVHRRbased multichannel sea surface temperatures. *J. Geophys. Res.*, **90**, 1158711601.

Reynolds, R. W., N. A. Rayner, T. M. Smith, D. C. Stokes and W. Wang, 2002: An improved in situ and satellite SST analysis for climate. *J. Climate*, **15**, 1609-1625.

Trenberth, K., 2005: Uncertainty in hurricanes and global warming. *Science*, **308**, 1753–1754.

Webster, P. J., G. J. Holland, J. A. Curry, and H.-R. Chang, 2005. Changes in Tropical Cyclone Number, Duration, and Intensity in a Warming Environment, *Science*, **309**, 1844–1846.

Xue, Y., T. M. Smith, and R.W. Reynolds, 2003: A new SST Climatology for the 1971-2000 Base Period and Interdecadal Changes of 30-Year SST Normal. *J. Climate*, **16**, 1601-1612.

Ocean Heat Fluxes

Lisan Yu and Robert A. Weller
Woods Hole Oceanographic Institution, Woods Hole, MA

Introduction

The oceanic latent heat flux (LHF) is heat energy released by evaporation of sea surface water, and sensible heat flux (SHF) is heat energy transferred by conduction and convection at the air-sea interface. These two fluxes vary with near sea-surface circulation, humidity, and temperature and influence weather and climate processes (Cayan, 1992). Accurate air-sea heat fluxes over the global oceans are required virtually for every aspect of climate studies. For example, air-sea heat fluxes are forcing functions for ocean models that study the generation and distribution of upper ocean temperature anomalies in response to atmospheric forcing. Because ocean influences the atmosphere through sea surface temperature (SST), the relationship between heat fluxes and SST is key to understanding the interaction between the atmosphere and the ocean, and whether such interaction manifests itself in one direction only or in both directions. In the latter case, SST both affects and is affected by heat fluxes; such feedback interaction is called air-sea coupling. The regions where coupled atmosphere-ocean interaction takes place are regions of great climate interest, because any perturbation in SST will lead to changes in the atmospheric circulation and changes in the weather and the climate system. Maps of patterns of air-sea coupling can be derived from coupled atmosphere-ocean models, but, because the models are not error-free, confidence in those patterns rests upon validation with good flux datasets.

However, the structure and variability of the global heat flux fields cannot be obtained from direct observations of fluxes because such direct flux measurements are sparse; instead our knowledge of the global air-sea heat fluxes and their spatial and temporal variability is gained through flux estimates based on bulk parameterizations using basic surface meteorological variables, such as wind speed, temperature, humidity, etc. These variables can be obtained from one of the following three sources: marine surface weather reports from Voluntary Observing Ships (VOS) collected by Comprehensive Ocean-Atmosphere Data Set (COADS), satellite remote sensing, and outputs of numerical weather prediction (NWP) models such as those at the National Centers for Environmental Prediction (NCEP) and the European Centre for Medium-Range Weather Forecasts (ECMWF). None of the three data sources are perfect, as each of them suffers from at least one of the following four deficiencies: (1) incomplete global coverage, (2) relatively short time series, (3) systematic biases, and (4) random errors. While improving the quality of each data source is essential, our project, the Objectively Analyzed air-sea Fluxes (OAFlux) (Yu and Weller, 2006; the project website http://oaflux.whoi.edu/), shows that we can produce a synthesized flux product with good temporal coverage, improved space and time resolution, and improved quality by combining the advantages in the three surface meteorological data sources using an objective analysis (Yu et al. 2004).

"Objective analysis" is a method for synthesizing measurements/estimates from various sources. The methodology is based on the Gauss – Markov theorem, a standard statistical estimation theory that states, when combining data in a linear fashion, that utilization of a linear least squares estimator is the most efficient process for reducing error in each input data source while producing an estimate that has the minimum variance (Daley, 1991). In the case of our flux analysis, objective analysis allows us to formulate a least-squares problem using available satellite/in situ surface meteorological observations and NWP model outputs to search for a solution that best fits the input datasets. The procedure is applied to each flux-related variable (i.e., wind speed, air and sea surface temperatures, and specific air humidity), from which the fluxes are computed using a bulk flux parameterization (Fairall et al. 2003). In this study, the input datasets are derived from multiple sources, including satellite microwave SST retrievals from TRMM Microwave Imager (TMI) and Advanced Microwave Scanning Radiometer for EOS (AMSR-E) (Chelton and Wentz, 2005), wind speed retrievals from Special Sensor Microwave/Imager (SSM/I) (Wentz, 1992), the weekly optimum interpolation (OI) analyses of Reynolds et al. (2002) (which is described elsewhere in this report), and surface meteorology from the NCEP and ECMWF reanalysis/forecast models. The resulting flux fields have been validated against more than 100 flux buoy measurements acquired by the WHOI Upper Ocean

Processes group (e.g. Moyer and Weller, 1997) and by the PIRATA in the Tropical Atlantic and TAO/TRITON in the equatorial Pacific. These flux fields, produced from the objective analysis, are used below to examine the variability of the global LHF and SHF fields in 2005.

Change of latent and sensible heat fluxes from 2004 to 2005

The 2005 annual mean fields of LHF, SHF, LHF plus SHF over the global oceans (Figure 1) show that large oceanic latent and sensible heat losses occur over the regions associated with three major western boundary currents (WBCs), i.e., the Kuroshio off Japan, the Gulf Stream off the United State, and the Agulhas current off the South Africa. In these regions, near-surface vertical gradients of humidity and temperature are largest and the wind speeds are greatest in the respective hemisphere's fall and winter seasons, and the cold season variability of LHF and SHF dominates the annual mean pattern.

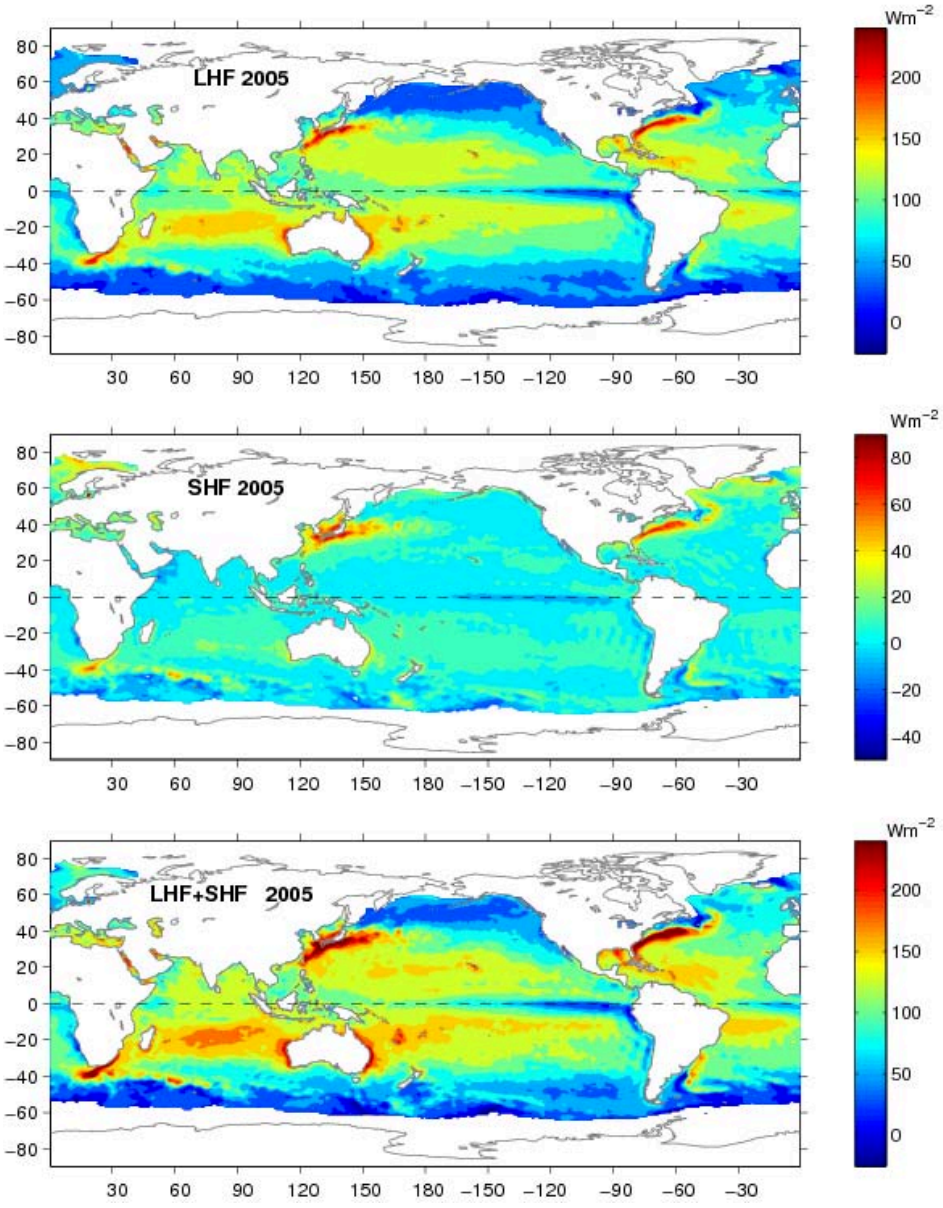

Figure 1 The 2005 annual mean latent heat flux (upper panel), sensible heat flux (mid panel), and latent plus sensible heat flux (bottom panel) in 2005. The sign is defined as upward (downward) positive (negative).

In general, the annual mean SHF has a pattern similar to that of LHF but the magnitude is much smaller. The annual mean LHF plus SHF field reflects primarily the enhanced LHF field. On a year-to-year basis, the three WBC regions are the ocean regions that exhibit greatest variability in LHF and SHF. This is clearly shown from the differences of the 2004 and 2005 annual mean LHF, SHF, and LHF plus SHF (Figure 2). Three additional features are worth noting. First, the anomalies in the difference map of SHF have the same sign as those of LHF in most global basins. Second, the magnitudes of the SHF anomalies are smaller than those of LHF, except for the region of the Kuroshio where the anomalies are both about 40 Wm^{-2}. Finally and most interestingly, the signs of the anomalies associated with different WBC systems are different. For example, the oceanic latent and sensible losses were enhanced (large positive anomalies) from 2004 to 2005 over the Kuroshio region, but reduced (large negative anomalies) over the Gulf Stream region.

Influence of eddy-scale structures is evident in the two-year difference maps. Nevertheless, the change in both LHF and SHF fields from 2004 to 2005 is large-scale: the anomalies are primarily negative over the global basins – sug-

gesting that the oceanic heat loss was overall reduced in 2005.

Linking the State of Latent and sensible heat fluxes in 2005 with past record

The reduction in the global oceanic heat loss in 2005 is more evident in the plot of year-to-year variations of the annual mean LHF, SHF, LHF plus SHF averaged over the global basins from 1981 to 2005 (Figure 3). The time series is constructed from daily analysis fields produced by the OAFlux project. Over the entire analysis record there is a persistent, long-term increase in the global averaged annual mean LHF, although that trend appears to decrease in recent years. It is not clear yet whether or not the reduction in oceanic heat loss for 2005 is merely a perturbation of the longer term upward trend or an indication of a change in the trend. The latent heat loss, averaged over the global basins, has increased by about 10 Wm^{-2} in the past 20 years. Overall, the change in the total oceanic heat loss, i.e., LHF plus SHF, is dominated by the change in LHF. There is a slight increase in SHF in the 1990s, but the net increase averaged over the global basins is small, less than 2 Wm^{-2}.

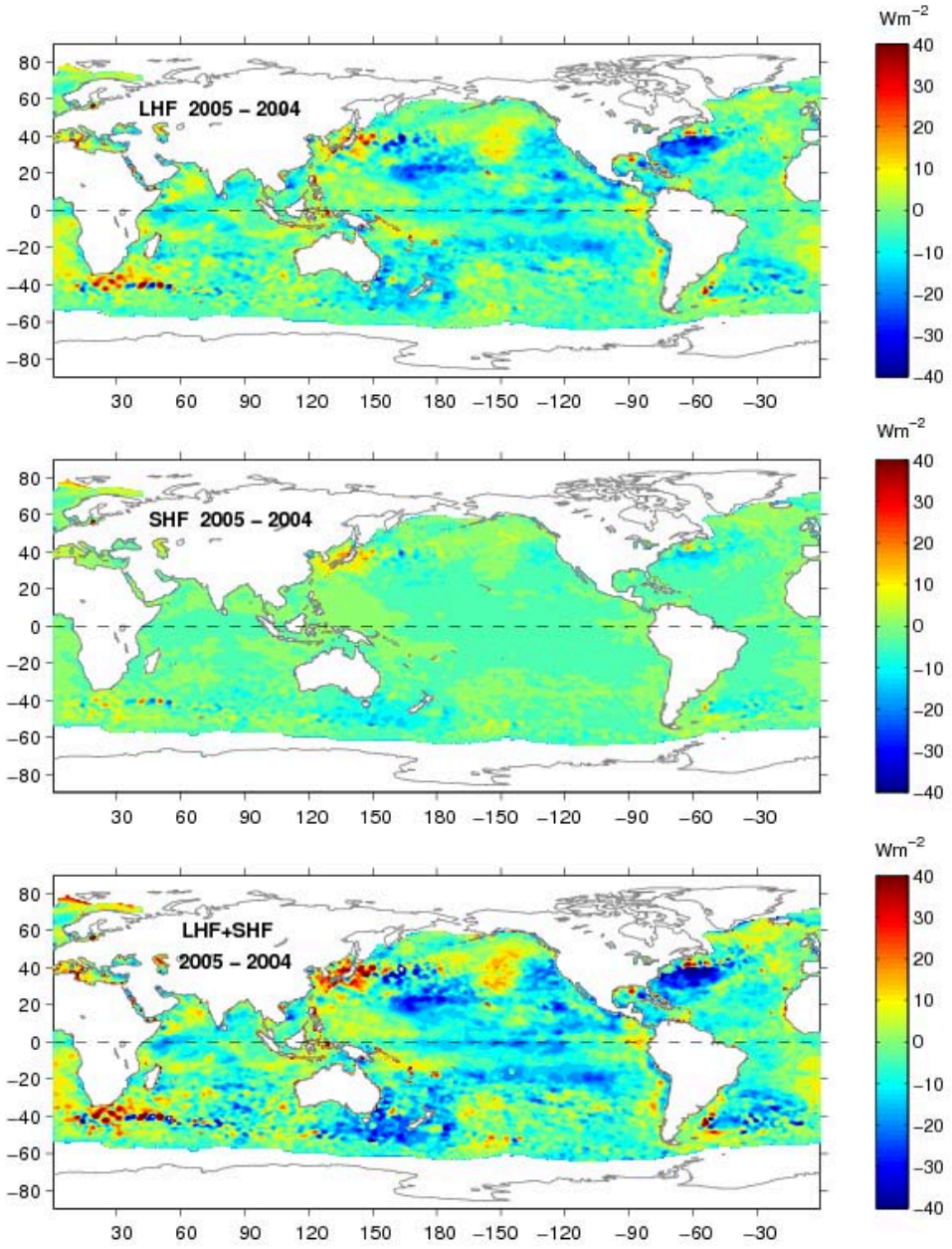

Figure 2 Differences between the 2005 and 2004 annual mean latent heat flux (top panel), sensible heat flux (mid panel), and latent plus sensible heat flux (bottom panel).

Area averages are made for the Kuroshio and Gulf Stream regions (Figure 4) to examine the regional change of LHF and SHF in the past two decades. Clearly, the time series of annual mean LHF plus SHF have a large upward trend in both regions. However, unlike the global averages (Figure 3), the regional averages show strong interannual fluctuations. Unlike the global averages that have a trend starting from the beginning of the analysis record in 1981, the regional averages show a trend toward larger values starting late, in early 1990s. Unlike the trend of the global averages that tends to be flat in recent years, the trend in the two regions is still positive. Furthermore, the slope of the trend in these two regions is twice as great as that of the global averages. Overall, the regional oceanic heat loss has been enhanced by about 20 Wm^{-2} over the past two decades.

Latent evaporation at the air-sea interface results in the transport of energy and water vapor into the atmosphere. The increase of latent heat evaporation in the past 20 years should increase the transport of water vapor into the atmosphere, leading to three questions. First, water vapor is a key element of the hydrological

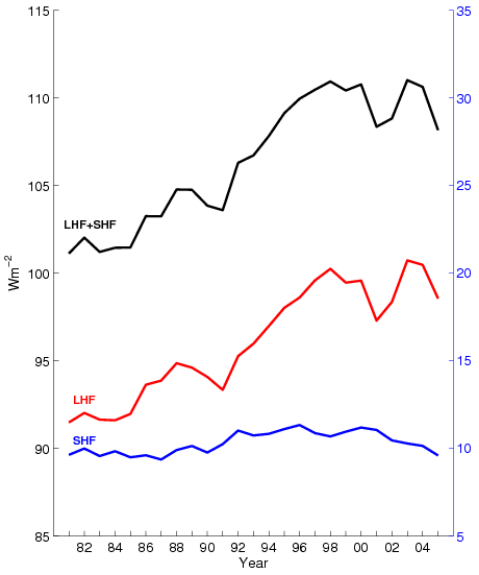

Figure 3 Year-to-year variations of global averaged annual mean latent heat flux (red), sensible heat flux (blue), and latent plus sensible heat flux (black).

cycle, i.e., the cycling of water, in all three phases, within and between the Earth's atmosphere, oceans, and continents. The movement of water vapor in the hydrological cycle is coupled to precipitation and soil moisture. Globally, 86% of evaporation and 78% of precipitation occur over the oceans. How much has the global precipitation, both over the oceans and over the continents, been impacted by the increased evaporation over

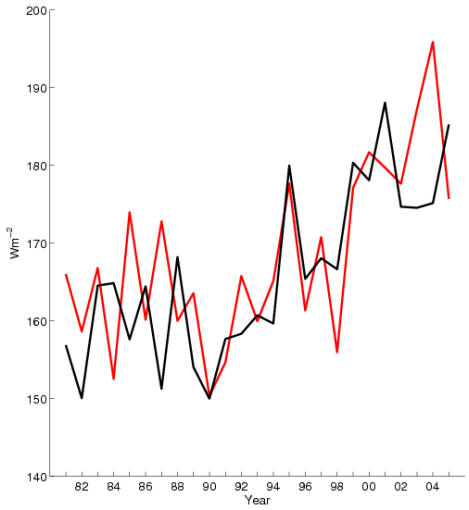

Figure 4 Year-to-year variations of the annual mean latent heat plus sensible heat fluxes averaged over the regions of the Gulf Stream ([85-50W, 25-45N], red) and Kuroshio ([120-150E, 20-40N], black).

the ocean? Second, water vapor is an important greenhouse gas. As the temperature of the Earth's surface and atmosphere increases, the atmosphere is able to hold more water vapor. The additional water vapor, acting as a greenhouse gas, absorbs energy that would otherwise escape to space thereby causing further warming. How much of the global warming can be attributed to the increased water vapor? Finally, the salinity in the ocean mixed layer would increase due to the loss of water vapor to the atmosphere, with consequent impact on the thermohaline circulation that is strongly influenced by the surface salinity differences between the subpolar and the subtropical oceans. The increase in surface salinity also affects the mixed layer structure over the global oceans, which further influences the way that the ocean and the atmosphere interact. To gain a better understanding of the role of evaporation in the ocean climate, salinity observations are needed.

References

Baumgartner, A., and E. Reichel, 1975: The World Water Balance. Elsevier, New York, 179 pp.

Cayan, D. R., 1992: Latent and sensible heat flux anomalies over the Northern Oceans: The connection to monthly atmospheric circulation. J. Clim., 5, 354-369.

Chelton, D. B., and F. J. Wentz, 2005: Global microwave satellite observations of sea surface temperature for numerical weather prediction and climate research. Bull. Amer. Meteor. Soc., 86, 1097-1115.

Moyer, K.A., and R.A. Weller, 1997: Observations of surface forcing from the Subduction Experiment: a comparison with global model products and climatological datasets. J. Clim., 10, 2725-2742.

Reynolds, R. W., N. A. Rayner, T. M. Smith, D. C. Stokes and W. Wang, 2002: An improved in situ and satellite SST analysis for climate. J. Clim, 15, 1609-1625.

Wentz, F. J., 1997: A well-calibrated ocean algorithm for SSM/I. J. Geophys. Res., 102, 8703-8718.

Yu, L., R. A. Weller, and B. Sun, 2004: Improving latent and sensible heat flux estimates for the Atlantic Ocean (1988-1999) by a synthesis approach. J. Clim., 17, 373-393.

Yu, L., and R. A. Weller, 2006: Objectively Analyzed air-sea heat Fluxes (OAFlux) for the global ocean. To be submitted.

Global Oceanic Precipitation Variations

Pingping Xie and John E. Janowiak
NOAA/Climate Prediction Center
Camp Springs, MD

The CAMS-OPI Global Monthly Precipitation Analysis

Prior to 1979, virtually the only information available on oceanic precipitation came from rain gauges at coastal and island stations, along with ship observations of sensible weather. While these data were sufficient to permit the estimation of long-term mean oceanic precipitation (Jaeger 1976; Dorman and Bourke 1979, 1981; Legates and Wilmott 1990), they were not adequate to enable the creation of time series of oceanic precipitation. Significant progress has been made in the last two decades in quantitatively documenting oceanic precipitation, thanks to the advent and continuous operation of earth-observing satellites. Many algorithms have been developed and applied to generate precipitation estimates from satellite-observed radiance emitted or reflected from clouds, precipitation and the earth's surface. Precipitation analyses based on these estimates have been developed to make possible scientific studies of rainfall variation over the globe. Two of the most used of such products are the CMAP (CPC Merged Analysis of Precipitation, Xie and Arkin, 1997) and the GPCP (Global Precipitation Climatology Project, Adler et al., 2004). CMAP and GPCP are both based on the combined use of several estimates of precipitation derived from satellite observations together with observations from rain gauges, and have been shown to be superior to other available data sets for monitoring and studying global precipitation (Adler et al., 2001).

Unfortunately, due to the requirement to collect gauge observations from around the world and to occasional delays in obtaining some of the necessary satellite products, neither CMAP nor GPCP are available until several months following the end of any given time period. Thus near real-time monitoring of global precipitation, such as is discussed here, relies on more promptly available products using similar methods to those used for CMAP and GPCP. One such satellite data set is the outgoing longwave radiation (OLR) observed by the National Oceanic and Atmospheric Administration (NOAA) polar orbiting satellites beginning from June 1974 (Gruber and Krueger 1984). The OLR data measures the intensity of infrared radiation emitted from clouds and the earth's surface toward space. Precipitating clouds, which often exhibit high and therefore cold cloud tops, can be identified in the OLR data as regions of low OLR values because colder clouds emit less infrared radiation. In particular, the convective clouds that produce most of the oceanic precipitation over the global tropics and subtropics tend to produce more precipitation when they have higher tops and therefore less OLR (Janowiak and Arkin 1991). Quantifying this relationship, Xie and Arkin (1998) developed an algorithm to derive estimates of monthly precipitation from the NOAA OLR data based on a set of seasonally and regionally varying empirical relations between precipitation and OLR. The precipitation estimates, which are called the OLR-based Precipitation Index (OPI), have been produced for the 32-year period from 1974 to the present. Verification tests against independent gauge observations have shown that the OPI is able to depict spatial and temporal variations of precipitation over both land and ocean for most of the globe with quantitative accuracy comparable to most other satellite-based products (Adler et al. 2001).

To further improve the quality of precipitation analysis over land, Janowiak and Xie (1999) developed a method to combine the OPI estimates described above with a gauge-based analysis based on the station observations collected in the Climate Prediction Center (CPC) Anomaly Monitoring System (CAMS, Ropelewski et al. 1985). The CAMS is a climate data archive maintained by the NOAA Climate Prediction Center (CPC) that includes monthly surface air temperature and precipitation observation data from ~7000 meteorological stations over the global land areas and islands. The gauge-based analysis of monthly precipitation is constructed by interpolating the observations at the CAMS meteorological stations (Xie et al. 1996) through the algorithm of Shepard (1968) in which the weighting coefficients are inversely proportional to the distance between the station location and the interpolation grid point. This gauge-based analysis and the OPI

satellite estimates are then combined over land, where the gauge data are used to determine the magnitude while the satellite data are used to define the distribution patterns of the precipitation fields. The final product of the CAMS-OPI monthly precipitation analysis is composed of this combined analysis over land and the OPI satellite-based precipitation estimates over ocean (Janowiak and Xie 1999). The CAMS-OPI is generated at NOAA/CPC on a real-time basis and is available for a 32-year period from 1974 to the present. Figure 1 presents an example of the spatial distribution of the OPI satellite estimates (top), the CAMS gauge-based analysis (2nd from top), number of the CAMS gauges in each 2.5°lat/lon grid box (2nd from bottom), and the CAMS-OPI product (bottom) for July 2005. Gauge stations collected in the

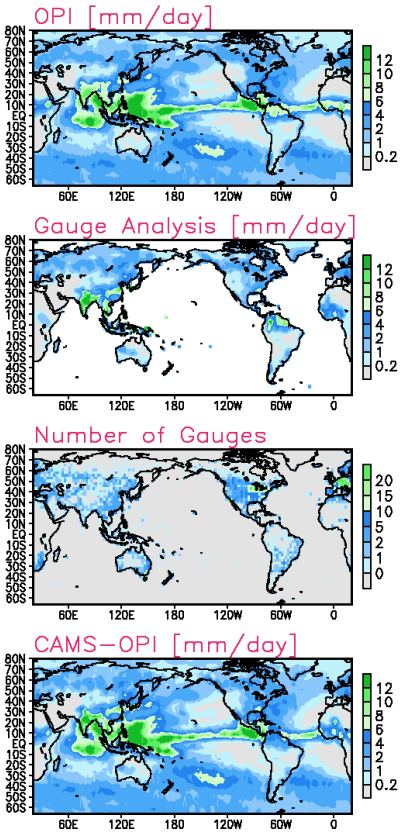

Fig.1: Spatial distribution of the OPI satellite precipitation estimates (top), the CAMS gauge-based analysis (2nd from top), number of the CAMS gauges in a 2.5°lat/lon grid box (2nd from bottom), and the gauge-satellite merged CAMS-OPI precipitation analysis (bottom), for July 2005.

CAMS data set are primarily located over populated land areas over North America, Europe, east coasts of Australia and China, while no gauges are available over desert areas over land and the vast of the oceanic areas. The OPI satellite estimates are capable of capturing large-scale precipitation patterns over both land and ocean, while merging with the gauge data over land providing more details and improved accuracy of precipitation analysis over land.

Oceanic Precipitation Variations in 2005

Real-time monitoring of global oceanic precipitation is routinely conducted at NOAA's Climate Prediction Center (CPC) with the use of the gauge – satellite merged "CAMS-OPI" data set. As shown in Figure 2 (upper panel), global oceanic precipitation during 2005 is characterized by rain bands associated with the Inter-Tropical Convergence Zone (ITCZ), South Pacific Convergence Zone (SPCZ), and the mid-latitude oceanic storm tracks.

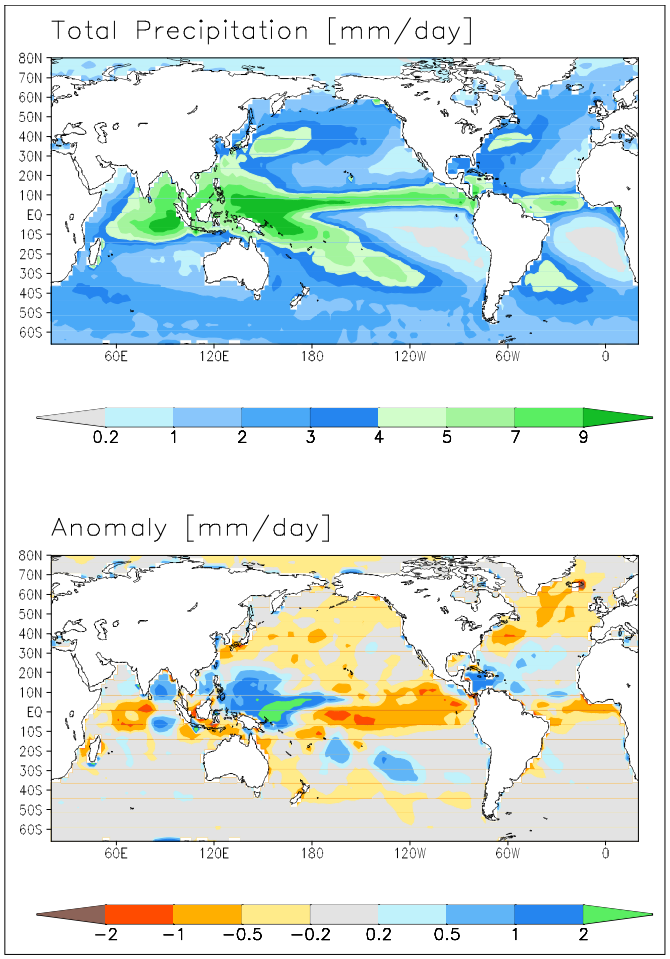

Fig.2: Annual mean total precipitation [mm/day, upper] and annual mean precipitation anomaly [mm/day, bottom] for 2005 as observed by the gauge-satellite merged data set of CAMS-OPI (Janowiak and Xie 1999). Precipitation anomaly is calculated using 1979 – 1995 as the base period.

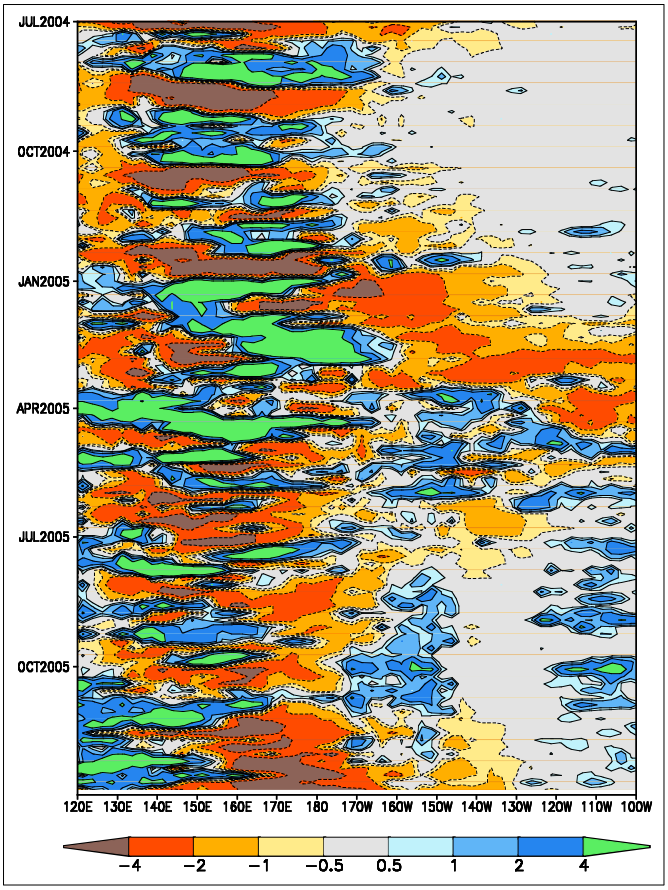

Fig. 3: Time-longitude section of precipitation anomaly averaged over the tropical Pacific [5°S-5°N] as observed by the Global Precipitation Climatology Project (GPCP) pentad precipitation data set (Xie et al. 2003). Precipitation anomaly is calculated using 1979 – 1995 as the base period.

Mean precipitation over the entire global oceans during 2005 was 2.840 mm/day, equivalent to a fresh water influx of 1036.6 Kg/m^2. Maximum annual precipitation rates of over 10 mm day^{-1} are observed during the year over the tropical western Pacific where the ITCZ merges with the SPCZ. Meanwhile, relatively light precipitation was recorded over several oceanic dry zones over the southeast Pacific, northeast Pacific off the coast of Southwest United States, southeast Atlantic, tropical North Atlantic near western Africa, and the eastern Indian Ocean.

The distribution of precipitation anomalies during 2005 indicates a dipole pattern of wet and dry anomalies over the western and eastern tropical Pacific, respectively (Figure 2, bottom). Although weak El Niño conditions prevailed over the tropical Pacific in the second half of 2004 and continued into early 2005 (Lyon and Barnston 2005), enhanced precipitation was limited mostly to the tropical Pacific west of the dateline. This pattern is different from that typical of a medium or strong El Niño event when large positive precipitation anomalies occur over the central and eastern Pacific (Ropelewski and Halpert 1989, Xie and Arkin 1997).

Enhanced convection, and attendant above normal precipitation, was first observed in late 2004 over the tropical western Pacific north of Indonesia (Figure 2). As the positive precipitation anomaly moved slightly toward the east, it intensified and reached its maximum intensity during January – March of 2005. Strong variations in precipitation over the region at intraseasonal time scales are clearly indicated in Figure 3. These intraseasonal variations are associated with the strong Madden Julian Oscillation (MJO; Madden and Julian 1971) activity that was observed during that period (Climate Prediction Center 2005). The positive precipitation anomaly over the tropical western Pacific gradually shifted westward during the second half of 2005 as the coupled ocean-atmosphere system evolved toward a weak La Niña.

The second half of 2005 witnessed the most active tropical storm season on record. A total of 27 tropical storms occurred of which 14 developed into hurricanes, and 7 of those were classified as major hurricanes. These totals eclipse the previous records for the number of tropical storms (21 in 1933), number of hurricanes (12 in 1969) and 1 short of the record year for the number of major hurricanes (1950). As a result, a substantial positive precipitation anomaly was observed over the regions of strong hurricane activity, especially over the Caribbean Sea. Note that the Atlantic ITCZ was located slightly north of its climatological latitude, which is reflected by two parallel bands of positive and negative precipitation anomalies over the tropical Atlantic (Figure 2, bottom).

Also noticeable during 2005 is the substantially depressed precipitation over the northwestern Atlantic. A brief examination of monthly precipitation and atmospheric circulation fields suggest that the bulk of the negative precipitation anomaly over the region was the result of below normal winter storm activity in the oceanic storm track, which is a climatological feature over the western North Atlantic during the cool season. This reduced storminess was associated with the strong anticyclonic blocking activity over the high latitudes that was observed during the winter season.

References:

Adler, R., G. Huffman, A. Chang, R. Ferraro, P. Xie, J.E. Janowiak, B. Rudolf, U. Schneider, S. Curtis, D. Bolvin, A. Gruber, J. Susskind and P. Arkin, 2004: The version 2 Global Precipitation Climatology Project (GPCP) monthly precipitation analysis (1979-present). *J. Hydrometeorology,* **4**, 1147–1167.

Adler, R.F., C. Kidd, G. Petty, M. Morrissey, and H.M. Goodman, 2001: Intercomparison of global precipitation products: The third Precipitation Intercomparison Project (PIP-3). *Bull. Amer. Meteor. Soc.*, **82**, 1377 – 1396.

Climate Prediction Center, 2005: Climate Diagnostics Bulletin: January 2005. U.S. Dept. of Commerce, NOAA, NWS, Climate Prediction Center, 5200 Auth Road, Camp Springs, MD 20746-4304.

Dorman, C.E., and R.H. Bouke, 1979: Precipitation over the Pacific Ocean, 30°S to 60°N. *Mon. Wea. Rev.*, **107**, 896 – 910.

Dorman, C.E., and R.H. Bouke, 1981: Precipittaion over the Atlantic Ocean, 30°S to 50°N. *Mon. Wea. Rev.*, **109**, 554 – 563.

Gruber, A., and A.F. Krueger, 1984: The status of the NOAA outgoing longwave radiation data set. *Bull. Amer. Meteor. Soc.*, **65**, 958 – 962.

Jaeger, L., 1976, Monatskarten des Niederschiags fur die Ganze Erde. Berichte des Deutscher Wetterdienstes, Offenbach, 33pp, And plates.

Janowiak, J.E., and P. Xie, 1999: CAMS-OPI: A global satellite-rain gauge merged product for real-time precipitation monitoring applications. *J. Climate*, **12**, 3335 – 3342.

Legates, D.R., and C.J. Willmott, 1990: Mean seasonal and spatial variability in gauge corrected, global precipitation. *Int. J. Climatol.*, **10**, 111-127.

Lyon, B., and A.G. Barnston, 2005: The evolution of the weak 2004-2005 El Nino. U.S. CLIVAR Variations, 3(2), US CLIVAR Office, Washington, DC, pp.1-4.

Madden, R. A., and P. R. Julian, 1971: Detection of a 40-50 day oscillation in the zonal wind in the tropical Pacific. *J. Atmos. Sci*., **28**, 702-708.

Ropelewski, C. F, J. E. Janowiak, and M. S. Halpert, 1985: The analysis and display of real time surface climate data. *Mon. Wea. Rev.* **113**, 1101-1106.

_____ and M.S. Halpert, 1989: Precipitation patterns associated with the high index phase of the Southern Oscillation. *J. Climate*, **2**, 268 – 284.

Shepard, D, 1968: A two dimensional interpolation function for irregularly spaced data. *Proc. 23rd National Conf. of American Computing Machinery*, Princeton, NJ, Association for Computing Machinery, 517 – 524.

Xie, P., R. Rudolf, U. Schneider, and P.A. Arkin, 1996: Gauge-based monthly analysis of global land precipitation from 1971 – 1994. *J. Geophys. Res.*, **101(D14)**, 19023 – 19034.

Xie, P., and P.A. Arkin, 1997: Global precipitation: A 17-year monthly analysis based on gauge observations, satellite estimates, and numerical model outputs. *Bull. Amer. Meteor. Soc.*, **78**, 2539 – 2558.

Xie, P., and P.A. Arkin, 1998: Global monthly precipitation estimates from satellite-observed outgoing longwave radiation. *J. Climate*, **11**, 137 – 164.

Xie, P., J.E. Janowiak, P.A. Arkin, R. Adler, A. Gruber, R. Ferraro, G.J. Huffman, and S. Curtis, 2003: GPCP pentad precipitation analyses: An experimental dataset based on gauge observations and satellite estimates. *J. Climate*, **16**, 2197 – 2214.

Atlantic Monthly Air-Sea Fluxes and the 2005 Hurricane Season

Mark A Bourassa, Shawn R. Smith, Paul Hughes, and Jeremy Rolph
Center for Ocean-Atmospheric Prediction Studies
The Florida State University
Tallahassee, FL

Air-sea fluxes in the 10˚-20˚N belt across the Atlantic exhibited anomalies that are consistent with the increased tropical activity during 2005. An assessment of Atlantic fluxes is conducted with a newly completed version of the Florida State University air-sea flux fields (the FSU3). The FSU3 are produced using an objective analysis technique (Bourassa et al. 2005) that produces fields of surface turbulent fluxes and related variables. Much of the energy that goes into increasing the intensity of a tropical disturbance or tropical cyclone (TC: tropical depressions, tropical storms, and hurricanes) comes from latent heat release related to condensation (i.e., water vapor changing phase to liquid water. This water vapor (and the energy associated with it) originates as liquid water in the ocean. The latent heat flux (LHF) is the rate (per unit area) at which energy associated with the phase change of water is transferred from the ocean to the atmosphere. In the Atlantic hurricane generation region, the area averaged 2005

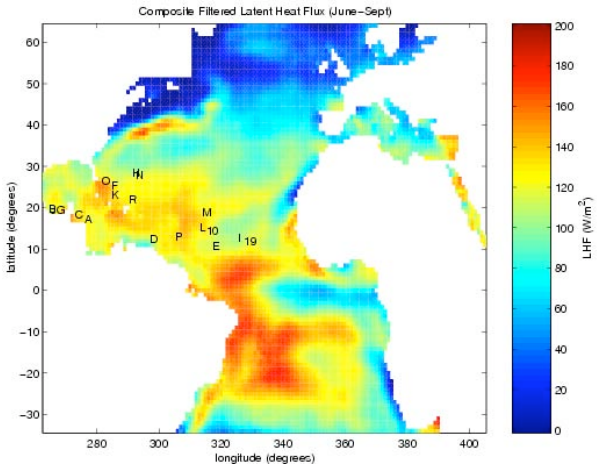

Figure 1. Composite latent heat flux from June to September 2005. The letters are the first letters of the named storms, located where they were first identified as TCs by the National Hurricane Center. The numbers indicate similar positions for tropical depressions that did not become named storms. TC formation favored areas of high LHF, but were found outside areas of maximum LHF.

LHF anomaly is 10 Wm^{-2}, 20% greater than the largest similarly averaged anomalies seen in the 1978 to 2003 time series.

Latent heat fluxes are largely dependent on the wind speed and the difference in humidity between the surface and an arbitrary height above the surface (typically 10 meters). In 2005 the mean wind speeds were near average. However, there was a small drop in the 10m humidity with a large increase in the near surface humidity (due to an increase in the SSTs). The drop in 10m humidity associated with a prolonged increase in moisture flux suggests that the moisture is being spread over a larger boundary layer and/or removed from the boundary layer with unusual efficiency. It is likely that TCs were responsible for removing an unusually large amount of moisture from the boundary layer. In addition, SSTs in 2005 were atypically greater than the air temperature, resulting in relative instability in the boundary layer. This relative instability implies a thicker boundary layer and more easily generated convection, which would lead to more tropical disturbances growing into TCs. A thicker boundary layer could result in more moisture in the boundary layer despite a reduction in 10m humidity.

The LHF varied considerably across the Atlantic Ocean with peak anomalies near 55 Wm^{-2} on the southern side of the ITCZ in July and August. In September, the highest positive LHF anomalies shifted northwestward to the region from east of Florida to Bermuda. September tropical cyclone formation mimicked this NW shift. A June-September composite (Fig. 1), with the location where TCs were first identified, shows that preferred genesis regions were areas of high LHF. The hurricane genesis region had unstable stratification in the boundary layer; meaning that information about the low level winds was relatively well translated to the surface (10m) winds. The 10 m wind anomalies indicated a weakening of the normal low-level easterlies, which would tend to reduce low level vertical wind shear. Low shear is a positive factor for development of tropical

systems. We suspect that the combination of abundant energy (in the form of water vapor) combined with increased boundary layer instability and reduced vertical shear led to exceptionally favorable conditions for the genesis of tropical cyclones in 2005.

References

Bourassa, M. A., R. Romero, S. R. Smith, and J. J. O'Brien, 2005: A new FSU winds Climatology. *Journal of Climate*, **18**, 3692-3704.

Surface Currents

Rick Lumpkin and Gustavo Goni
NOAA/Atlantic Oceanographic and Meteorological Laboratory
Miami, FL

Ocean surface currents (Fig. 1) carry water, heat, salt, nutrients and other properties over vast distances and play a major role in regional and global climate. The Ocean Observing System for Climate measures surface currents in-situ by an array of satellite-tracked drifting buoys and by moored current meters at a number of sites. NOAA/AOML processes and distributes the drifter data as part of the Global Drifter Program, while data from the fixed-location moorings are processed and distributed by NOAA/PMEL as part of the Tropical Atmosphere Ocean Project.

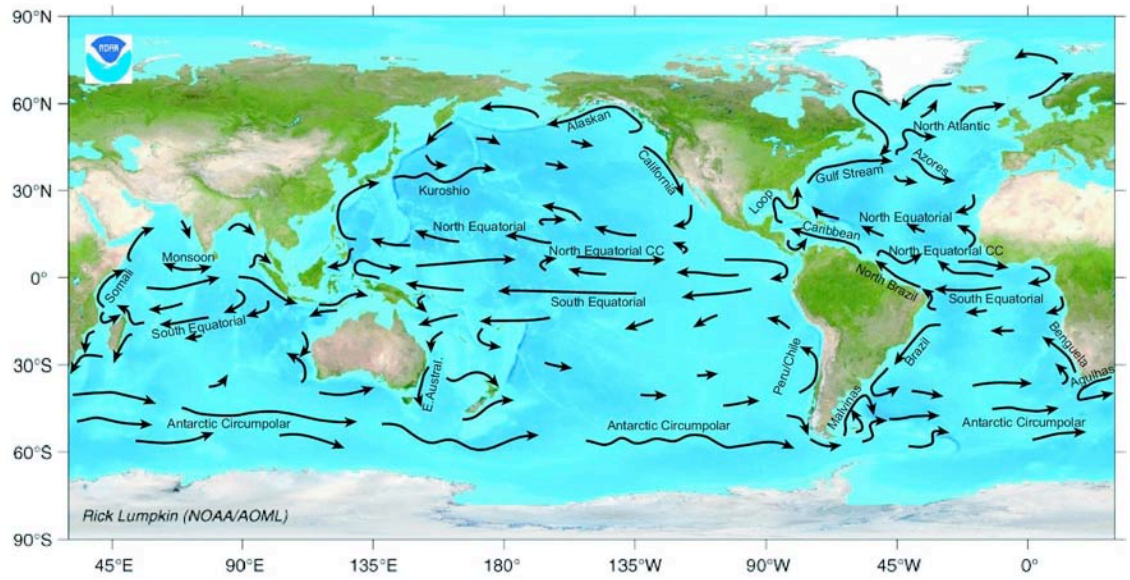

Fig. 1: Major ocean surface currents of the world, derived from drifter data. "CC" stands for counter-current.

Why surface currents are important for climate

Ocean surface currents are a critical part of the earth's heat engine. Incoming solar heat in the tropics must be carried poleward by the ocean and atmosphere to achieve a steady-state balance; ocean transport by currents dominates the net transport for tropical latitudes (Trenberth and Caron, 2001). This tropical heat is lost to the atmosphere at higher latitudes (poleward of about 20º), creating the largest air-sea heat fluxes on earth and associated with the formation of denser water masses and the Meridional Overturning Circulation (MOC).

Time-mean heat advection can be calculated from averaged drifter trajectories and sea surface temperature (SST) measured by the drifters. The convergence or divergence of this transport (Fig. 2) shows where heat must be exchanged between the ocean and atmosphere in the form of air-sea heat fluxes. Heat convergence in Fig. 2 exceeds 200 W/m^2 in the Gulf Stream and Kuroshio Current, indicating enormous heat loss to the atmosphere in these regions. For reference, the largest sea-air heat flux in time-mean NCEP climatology is 255 W/m^2, found in the Gulf Stream extension. Large areas of heat divergence (blue in Fig. 2) are found in the Southern Ocean, particularly in the Indian Ocean sector, indicating where the ocean must absorb large amounts of heat from the atmosphere. (Interestingly, climatologies of air-sea fluxes, based on extremely sparse observations, are ambiguous about this feature; *c.f.,* Grist and Josey, 2003).

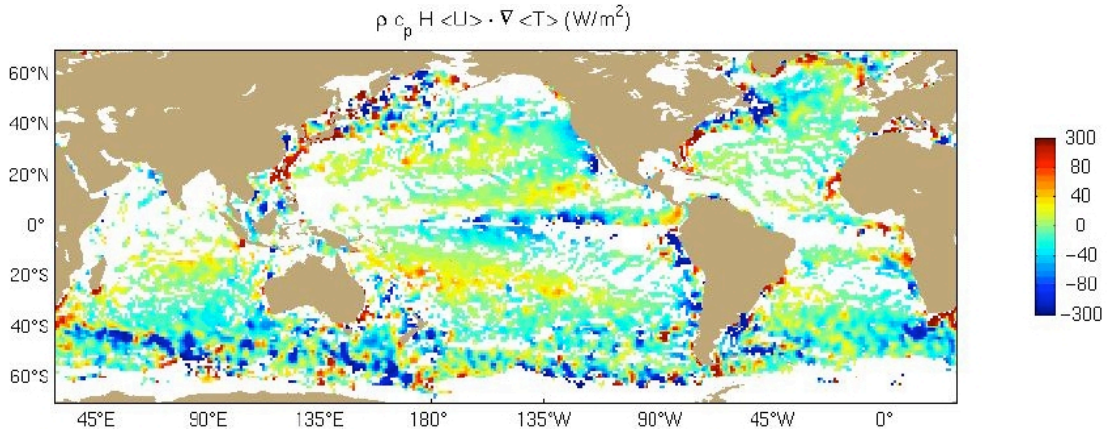

Fig. 2: Heat convergence (negative: divergence) driven by time-mean currents in the upper 30m of the ocean, in Watts per square meter. Red areas show where currents heat the atmosphere; blue areas are where the ocean cools the atmosphere. White areas are not resolved by the data.

Changes in the paths or strengths of surface currents can play a major role in climate fluctuations by altering the air-sea heat fluxes. For example, it is well known that SST differences between the northern and southern tropical Atlantic play a major role in setting rainfall rates in the Americas and Africa (Nobre and Shukla, 1996; Giannini et al., 2000), and that there should be a dynamical link between SST in these two regions via a positive feedback mechanism (Chang *et al.,* 1997). However, this link is not supported by observations (Enfield and Mayer, 1997), suggesting that heat advection by eddying currents acts as a major negative feedback (Seager *et al.,* 2001) that must be accounted for in order to improve seasonal rainfall forecasts.

What we can and cannot resolve with the existing observing array

The present in-situ observing system is capable of resolving time-mean currents and time-averaged eddy variability at 1º resolution throughout most of the world's oceans (Fig. 3). Coverage remains too sparse in a few regions, including the Gulf of Guinea in the eastern tropical Atlantic and in the northwestern Indian Ocean.

While the observing system is capable of a broad range of time-mean calculations, it is a greater challenge to produce continuous time series of current variations about this mean. Drifter observations can be averaged in extended zonal bins to map monthly anomalies (see below), while the moored observations provide continuous time series at points.

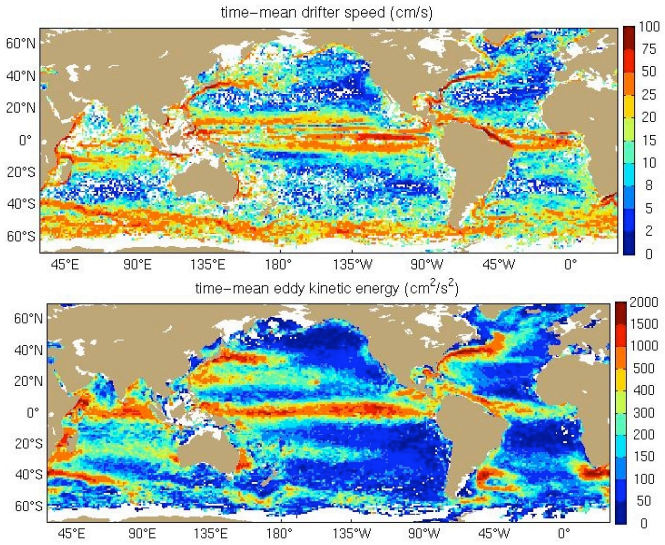

Fig. 3: Time-mean speed of drifters at 1º resolution (top). No interpolation has been used. White areas are not resolved by the data due to insufficient observations and/or extremely weak mean speeds. Bottom: eddy variability about the time-mean state (intensity of current fluctuations).

Current variations are associated with several types of motion. Large and mesoscale variations caused by sea level height can be inferred from satellite altimetry. These observations can be combined with in-situ observations of temperature, salinity and/or drifter trajectories (Fig. 4) for improved mapping of currents to investigate their spatial and temporal variability (Goni *et al*., 1996; Niiler et al., 2003). The availability of near-real time drifter and altimetry data also allow researchers to estimate and validate global current

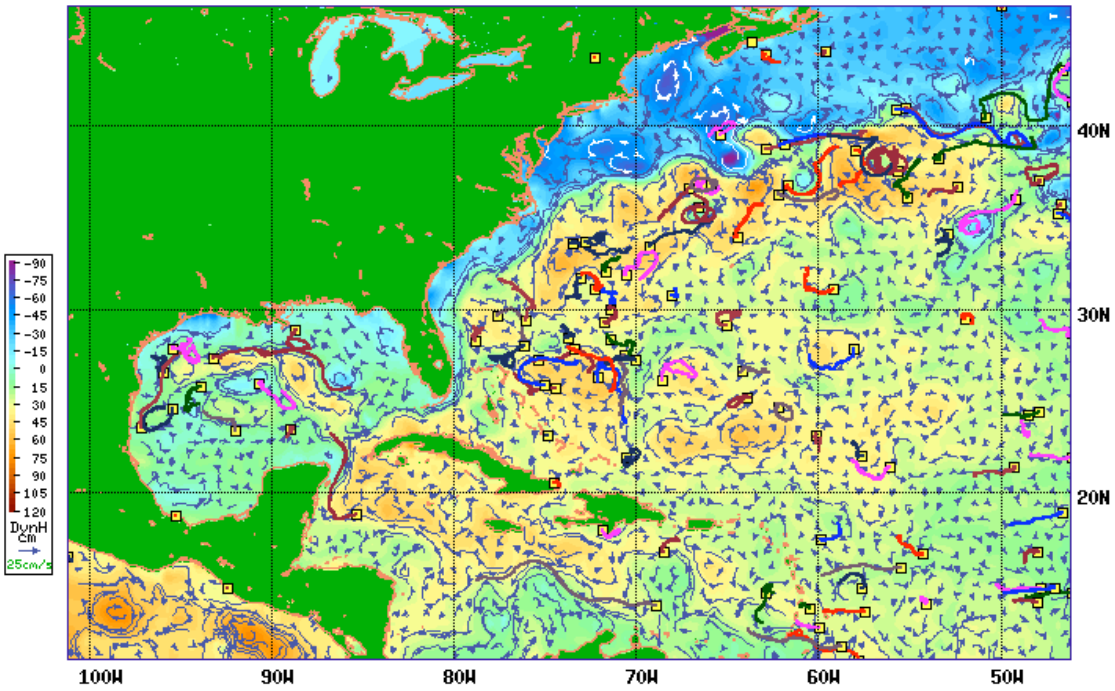

Fig. 4. Surface geostrophic current field in the North Atlantic derived from satellite altimetry during the period February 9-18, 2005, with drifter trajectories (color lines) corresponding during the period February 4-18, 2005. The dynamic height (color scale) derived from satellite altimetry is included in the map.

fields. Smaller scale, shallower changes are forced directly by wind stress anomalies, and can be estimated globally from satellite-based wind products using empirical models calibrated from the in-situ observations (Ralph and Niiler, 1999).

Ocean current measurements in 2005

For many years, the Global Drifter Program aimed at achieving an array of 1250 drifters, the number required to cover the world's oceans at a nominal resolution of 5ºx5º. In September 2005 the drifter array reached this target goal, becoming the first fully realized component of the Global Ocean Observing System. Growth of the array and its spatial coverage is shown in Fig. 5. By early 2006, the size of the drifter array had slightly exceeded 1250 due to near-concurrent dense deployments on some research cruises. With sustained funding, the drifter array will be maintained at 1250 with an instantaneous size fluctuating about this number. Future efforts must focus on improving the coverage of the array: some regions are very densely sampled, while other regions (typically upstream of the major shipping routes of Voluntary Observation Ships) are poorly sampled.

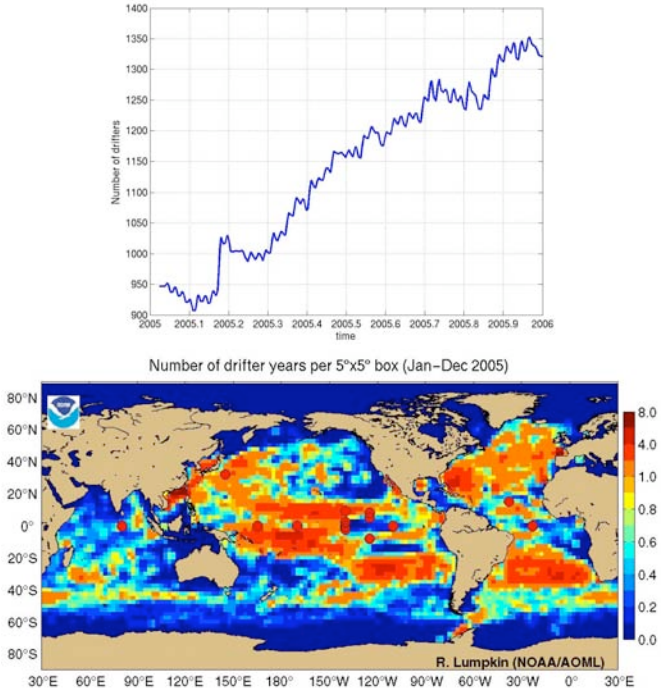

Fig. 5: Top: number of drifters in the Global Drifter Array. Bottom: drifter years of data at 5ºx5º resolution (shading) and location of moored near-surface current observations (red bullets) for January—December 2005.

Moored observations were collected at 14 sites (red bullets in Fig. 5), including equatorial regions of surface divergence where drifting buoys do not reside for long. Studies of the continuous currents at these sites have greatly improved our understanding of how current variations drive off-equatorial heat fluxes (e.g., Grodksy et al., 2005).

During 2005, surface currents were well sampled except in the far northern Pacific, the southwest Pacific between 20—40ºS, 150ºE to the dateline, the Arabian Basin of the Indian Ocean and the extreme Southern Ocean south of 55ºS.

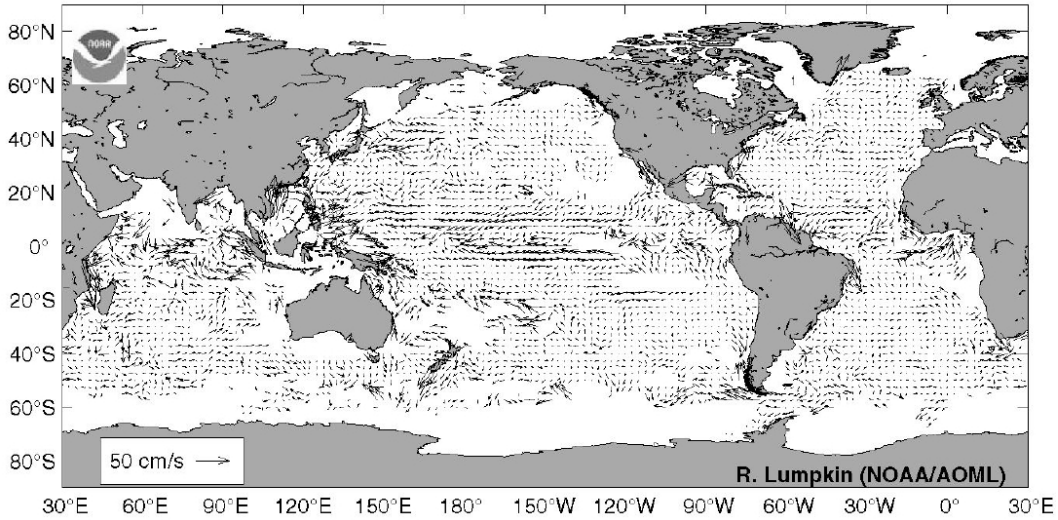

Fig. 6: 2005 mean anomalies from ten year surface current climatology.

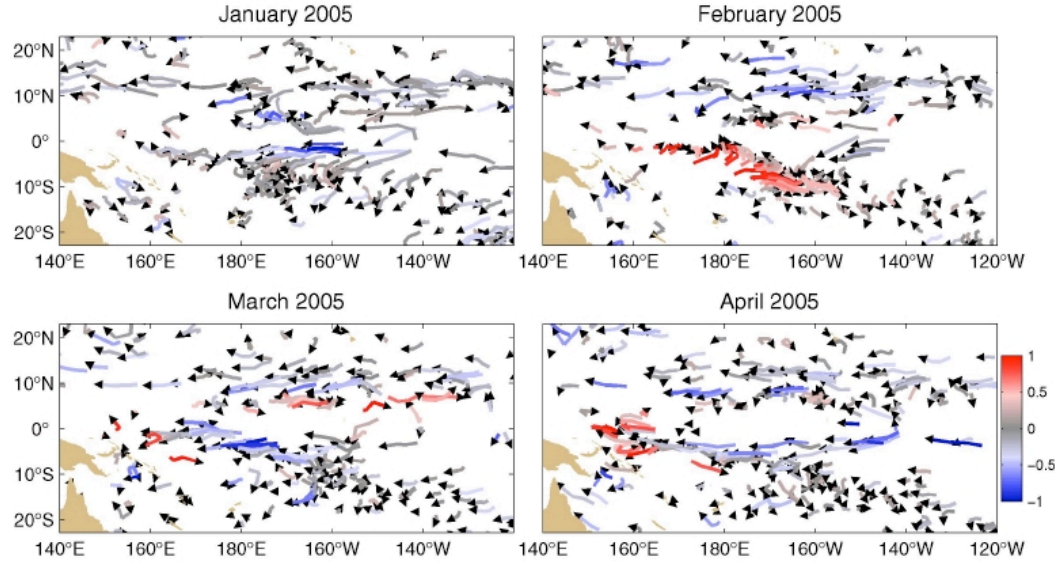

Fig. 7: drifter trajectories during January—April 2005 in the tropical Pacific. Arrowheads indicate direction; color indicates zonal speed anomaly (m/s, positive eastward).

State of Ocean: Currents in 2005

A climatology of monthly mean currents was computed from all drifter observations, 1994—2004, using the methodology of Lumpkin and Garraffo (2005). Anomalous currents (Fig. 6) were calculated with respect to this climatology.

Indo-Pacific Basins: Annual mean anomalies from climatology (Fig. 6) were most prominent in the tropical Pacific Ocean. Westward anomalies of nearly 20 cm/s were observed on the equator between 120ºW and the dateline. Weaker anomalies of 5-10 cm/s were seen in the North Equatorial Current (NEC) region (10-20ºN) (see Fig. 1). The drifter observations did not indicate anomalously strong eastward currents in the Kuroshio Extension, at odds with the simple hypothesis of a more intense than average wind-driven clockwise gyre.

The strongest intraseasonal (timescales between mesoscale eddies and the seasonal cycle) anomalies were observed in early 2005 in the western and central tropical Pacific, associated with equatorial wave activity driven by intraseasonal ("Madden-Julian Oscillation") wind fluctuations (c.f., Eisenman *et al*., 2005). In January (Fig. 7), very strong westward anomalies were measured in the northern branch of the South Equatorial Current (nSEC). The nSEC at 160ºW-170ºE, 0-5ºS was 80-100 cm/s westward, compared to a climatological January speed of 40-60 cm/s. During February, a dramatic reversal was seen from 155ºW—180º, 6—12ºS where several drifters moved eastward at 50-100 cm/s. Drifters suggested the passage of a second equatorial wave in March and April, when strong westward, then eastward, anomalies were seen west of the dateline (Fig. 7). These anomalies were also present in the continuous time series of near surface currents measured at the Tropical Atmosphere Ocean (TAO) mooring at 0, 170ºW (Fig. 8). The previously noted NEC anomalies were first observed in February. Westward anomalies in the South Equatorial Current (SEC) at 0—6ºS appeared in April. Both the NEC and SEC continued to flow anomalously quickly through the remainder of the year.

For the major western boundary current of the Indian Basin, the Agulhas Current, altimetric estimates of geostrophic transports suggest that the 2005 annual mean remained slightly lower than its historical value, and significantly lower (5-10 Sv) than during 2004 (Fig. 9).

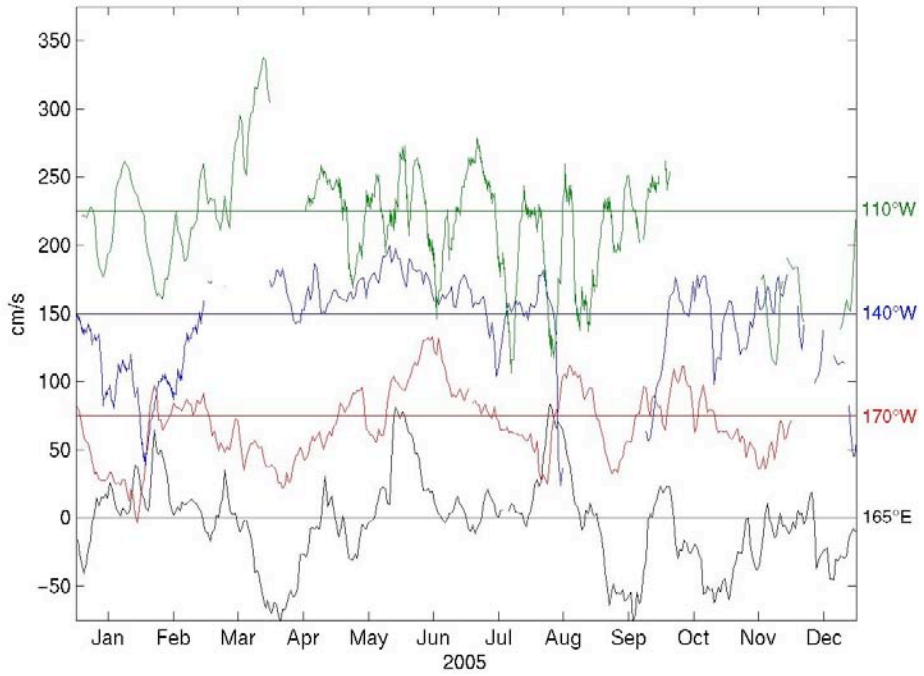

Fig. 8: near-surface zonal current anomalies (daily averages) measured at equatorial TAO moorings. Time series east of the dateline have been displaced vertically; the zero line for each is color-coded.

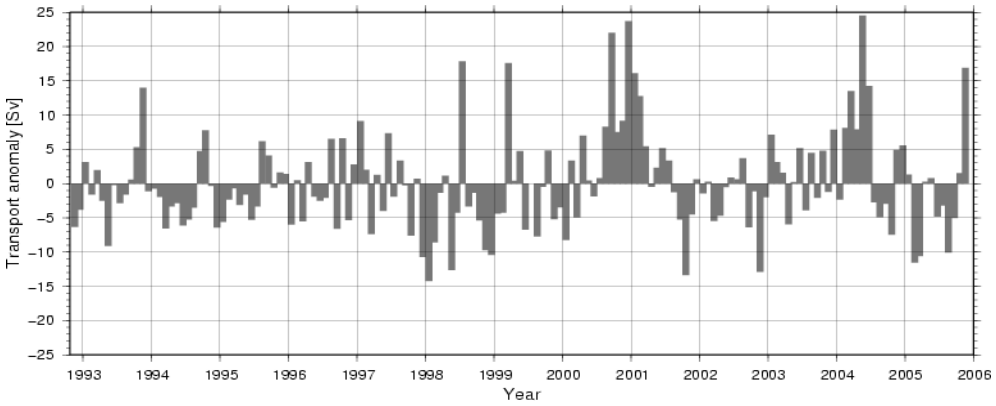

Fig. 9. Monthly geostrophic transport anomalies of the Agulhas Current at 28°W, derived from satellite altimetry observations.

Atlantic Basin: Several key components of the Atlantic Meridional Overturning Circulation can be monitored using altimetry observations. For example, the shedding of Agulhas Current rings is closely related to pulses in the current and represents the main passage of surface waters from the Indian into the Atlantic Ocean. The number of Agulhas Current rings has a very large year-to-year variability and can be monitored from space-time diagrams of sea height anomalies (Fig. 10, left). Similarly space-time diagrams off the coast of NE Brazil can be used to identify and track the rings of the North Brazil Current. These rings contribute with the transfer of South Atlantic surface waters into the North Atlantic (Fig. 10, right). During 2005 the number of rings shed by the Agulhas and North Brazil currents remained close to their mean annual value.

The North Atlantic subtropical gyre –benchmarked by transport through the choke points of the Florida Straits and Yucatan Channel – was close to its decadal climatological strength during 2005. The Western Boundary Current transport through the Florida Straits, measured by cable voltage, averaged 31.4±1.2 Sv during 2005 (C. Meinen, pers. comm.), not significantly different from the 1982—2005 mean of 32.1 Sv. Transport through the Yucatan Channel (from the Caribbean Sea to the Gulf of Mexico), estimated from altimetric sea level anomaly was within 1 Sv of the long-term mean. In the North Equatorial Current region 5—15ºN, 30—50ºW, westward anomalies of 10 cm/s were observed. Drifter deployments during several French cruises seeded the Gulf of Guinea region heavily for the first time; anomalies here were large, but may reflect a poorly-defined climatology for the period 1994—2004. Thus, it is difficult to tell from these data what role anomalous advection may have played in the development of the unusually large cold tongue during 2005.

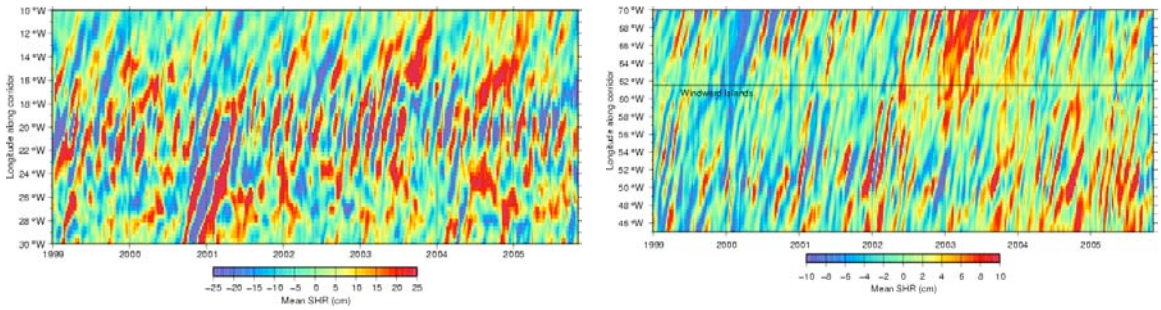

Fig. 10. Space-time diagrams of sea height anomalies depicting the motion of the Agulhas Current (left) and North Brazil Current (right) and the rings shed by these currents during the period 1999-2005. The reds and yellows (blues) indicate large (small) values of sea height anomalies.

Southern Ocean: Drifters did not reveal large-scale anomalies in the strength of the Antarctic Circumpolar Current (Fig. 5). During the period August to December, 18 drifters passed south of Cape Horn. These drifters indicated that the flow entering the Drake Passage was 8±9 cm/s, much weaker than the climatological speed of 23±11 cm/s here. This anomaly was most prominent during August—September. Four drifters passed through this region during February—May, measuring speeds of 27 ±14 cm/s (very close to climatology).

ACKNOWLEDGEMENTS

Drifter data is distributed by NOAA/AOML's Global Drifter Program at the Drifter Data Assembly Center web site (http://www.aoml.noaa.gov/phod/dac/dacdata.html). Moored current meter data is distriubed by NOAA/PMEL's Tropical Atmosphere Ocean project at http://www.pmel.noaa.gov/tao. Altimetric time series of transports may be viewed at http://www.aoml.noaa.gov/phod/altimetry. The authors were supported by NOAA's Climate Program Office and the Atlantic Oceanographic and Meteorological Laboratory.

References

Chang, P., L. Ji and H. Li, 1997: A decadal climate variation in the tropical Atlantic Ocean from thermodynamic air-sea interactions. *Nature*, **385**, 516-518.

Eisenman, I., L. Yu and E. Tziperman, 2005: Westerly Wind Bursts: ENSO's Tail Rather than the Dog? *J. Climate* **18** (24), 5224-5238.

Enfield, D. and D. A. Mayer, 1997: Tropical Atlantic sea surface temperature variability and its relationship to El Niño- Southern Oscillation. *J. Geophys. Res*., **102**, 929-945.

Giannini, A., Y. Kushnir and M. A. Cane, 2000: Interannual variability of Caribbean rainfall, ENSO, and the Atlantic Ocean. *J. Climate*, **13,** 297-311.

Goni, G. J., S. Kamholz, S. L. Garzoli and D. B. Olson, 1996: Dynamics of the Brazil/Malvinas Confluence based on inverted echo sounders and altimetry. *J. Geophys. Res*., **101** (C7), 16273-16289.

Grist, J. and S. Josey, 2003: Inverse Analysis Adjustment of the SOC Air-Sea Flux Climatology Using Ocean Heat Transport Constraints. *J. Climate* **16** (20), 3274-3295.

Grodsky, S.A., J.A. Carton, C. Provost, J. Servain, J.A. Lorenzetti, and M.J. McPhaden, 2005: Tropical Instability Waves at 0°N, 23°W in the Atlantic: a case study using Pilot Research Moored Array in the Tropical Atlantic (PIRATA) mooring data. *J. Geophys. Res*. **110** (C08010), doi:10.1029/2005JC002941.

Lumpkin, R. and Z. Garraffo, 2005: Evaluating the Decomposition of Tropical Atlantic Drifter Observations. *J. Atmos. Oceanic. Techn*. **22** (9), 1403—1415.

Niiler, P. P., N. A. Maximenko, G. G. Panteleev, T. Yamagata, and D. B. Olson: 2003, Near-surface dynamical structure of the Kuroshio Extension. *J. Geophys. Res*., **108**, 3193, doi:10.1029/2002JC001461.

Nobre, P. and J. Shukla, 1996: Variations of Sea Surface Temperature, Wind Stress and Rainfall over the Tropical Atlantic and South America. *J. Climate*, **9**, 2464-2479.

Ralph, E. A. and P. P. Niiler: 1999, Wind-driven currents in the Tropical Pacific. *J. Phys. Oceanogr.*, **29**, 2121–2129.

Seager, R., Y. Kushnir, P. Chang, N. Naik, J. Miller and W. Hazeleger, 2001: Looking for the Role of the Ocean in Tropical Atlantic Decadal Climate Variability. *J. Climate*, **14**, 638-655.

Trenbert, K. and J. Caron, 2001: Estimates of Meridional Atmosphere and Ocean Heat Transports. *J. Climate,* **14** (16), 3433-3443.

The Meridional Overturning Circulation and Oceanic Heat Transport

Molly Baringer[1], Chris Meinen[1] and Silvia Garzoli[1]
[1] NOAA/Atlantic Oceanographic and Meteorological Laboratories, Miami, FL

Introduction

Oceanic and atmospheric circulation drives climate variability through the redistribution of heat about the globe. The contribution of the ocean dominates the system equatorward of 17ºN and 17ºS and plays a sizable role at the higher latitudes according to recent atmospheric reanalyses (Trenberth and Caron, 2001). A prominent example of the physical processes of coupled ocean-atmospheric meridional heat transport is the well-known El Niño-Southern Oscillation phenomenon. On longer time scales, the component of the ocean circulation associated most with variability in heat redistribution is the Meridional Overturning Circulation (MOC), sometimes also called the thermohaline circulation. The MOC is a global circulation cell wherein surface waters in the high latitudes are cooled in winter, thereby becoming denser, and this dense water sinks and flows towards the equatorial regions. In tropical and subtropical regions around the world these waters eventually mix with other waters, becoming less dense, and they return to the sea surface to flow towards the higher latitudes and complete the cell, simultaneously carrying a significant amount of heat to the higher latitudes. The primary locations where deep convection occurs are in the northern North Atlantic and in the subpolar ocean around Antarctica, while the upwelling of new surface waters is spread broadly around the globe.

There are other convective circulation regimes in the global ocean (e.g. Subtropical Overturning Cells), however the term MOC is generally reserved for only the deepest overturning cells. The shallower overturning cells are not insignificant for climate; for instance while the redistribution of anthropogenic carbon in the ocean is dominated by the MOC in the northern North Atlantic, the shallower cells which form the Subantarctic mode waters in the southern hemisphere sequester a substantial amount of carbon (Sabine *et al.,* 2004). These other shallow overturning circulations are intricately tied to gyre scale circulations and as such the variability of these circulations are difficult to quantify using the present ocean observing system and present an active research topic.

This chapter focuses on the current state of knowledge about the MOC and its associated heat transports in part because of the more advanced state of the ocean observing and analysis system in place to describe MOC variability. In the North Atlantic, the MOC can be studied at discrete locations, or choke points, while in the Southern Ocean deep convection is not geographically isolated and is closely tied to the Antarctic Circumpolar Current. Any observing system in the Southern Oceans is a practical challenge for these reasons as well as due to the simple logistical problems of working in the Southern Ocean climate. Present research suggests that the deep convection in the MOC in the North Atlantic (formation of the so called North Atlantic Deep Water, NADW) represents about half of the total deep-water ventilation, the Southern Ocean representing the other half (Orsi *et al* 2001). This chapter will focus on the component of the MOC associated with deep-water formation in the northern North Atlantic where the observing system is more advanced.

Variations in the strength of the overturning circulations are directly related to variations in heat transport (warm water flowing north in the upper layers and returning southward as cold water at depth represents a net poleward heat transport). The current best estimates for the steady state global mass and heat transport can be found in the analyses of Ganachaud and Wunsch (2003) as shown in Figure 1 (see also Talley, 2003). Keep in mind that oceanic heat transport is not just carried by the Atlantic MOC. Many shallow overturning circulations exist that are also important for carrying heat. For example the North Pacific carries about 0.5 PW northward, but most of this heat transport is associated with water mass transformations in the upper layers of the ocean where warm surface water is cooled (transformed) into shallow North Pacific Intermediate Water. On the other hand, the North Atlantic carries a much larger transport of 1.2 PW northward, most of which is carried in the top-to-bottom MOC system where warm surface water is transformed into deep and bottom water. Historical estimates of the net northward Atlantic MOC heat flux in the vicinity of its maximum,

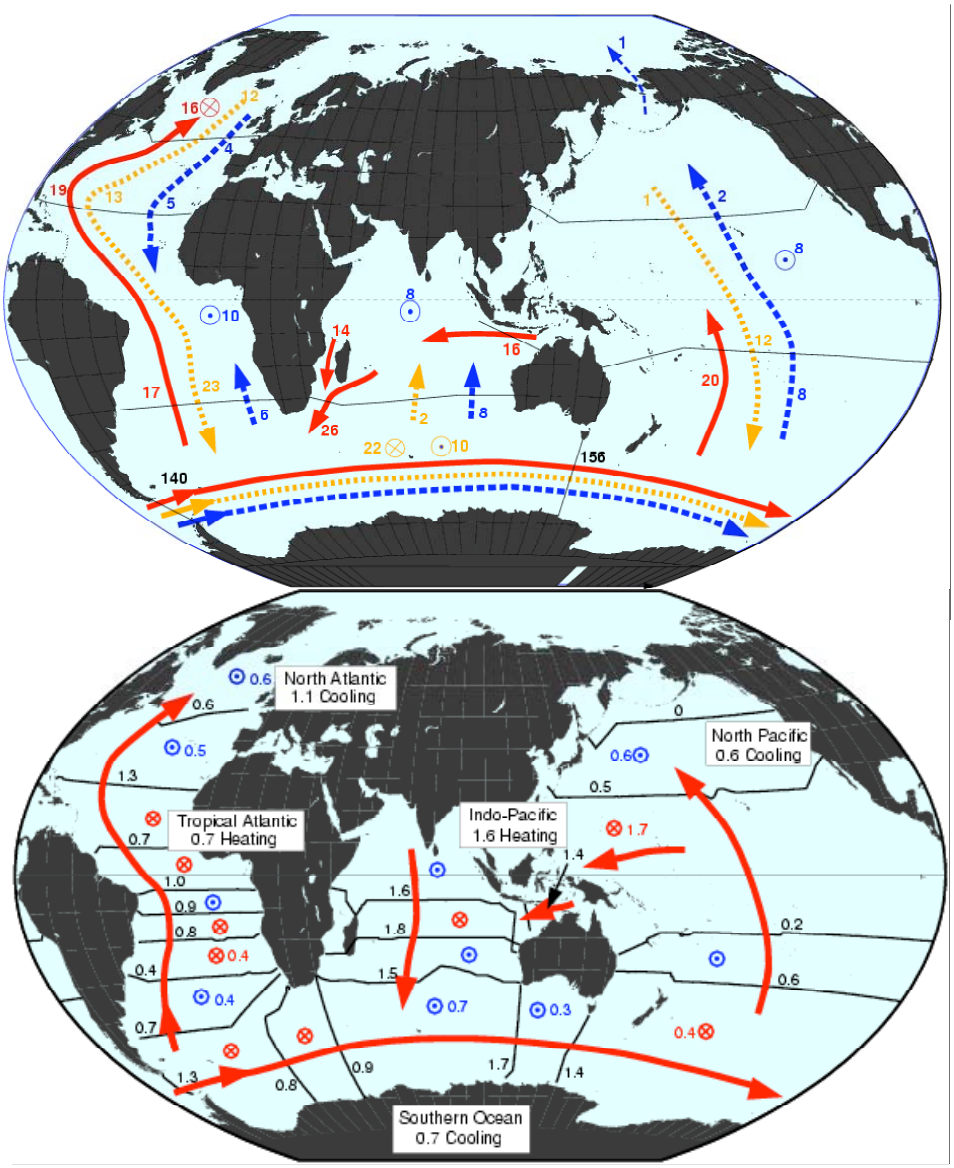

Figure 1: Estimates of the meridional transports of top) mass and bottom) heat from the globally consistent results from Ganachaud and Wunsch (2003 adapted from Macdonald et al 2001), using WOCE era hydrographic sections (black lines). top) Red arrows indicate the direction of mass transport in surface waters, Yellow represents intermediate water masses (e.g. NADW) and Blue represents Bottom waters. Units are in 10^9 kg s^{-1}. Circles with dots are upwelled water, circles with X are downwelled/convected water. bottom) Red arrows represent direction of heat transport (totals given across each section). Blue (red) circles with dots (Xs) are heat loss (gain) to the atmosphere.

which occurs in the North Atlantic roughly at the latitude of the center of the subtropical gyre, range from 0.9 PW[2] to 1.6 PW, while estimates of the oceanic heat transport in the 30°S to 35°S band in the South Atlantic are even more uncertain, ranging from small southward values to more than 1 PW northward.

Direct estimates of the MOC

NOAA maintains some of the longest time series of observations aimed at monitoring the MOC in the North Atlantic. Begun in 1982 as the Subtropical Atlantic Circulation Study (STACS), the NOAA program has been monitoring variations in the upper limb of the MOC by measuring the Florida Current transport almost continuously using a submarine cable across the Florida Straits[3], while the deep limb of the MOC has been monitored through regular hydrographic cruises (more than 20 to date) across the Deep Western Boundary Current east of the Bahamas. Called the Western Boundary Time Series (WBTS) project in its current incarnation, the NOAA program now involves moored inverted echo sounders and bottom pressure gauges east of Abaco Island in the Bahamas as an effort at time series monitoring of the Deep Western Boundary Current in addition to the regular hydrographic cruises. NOAA is also collaborating in an international program to measure the total basin-wide heat transport at 26ºN in the Atlantic

[2] PW is PetaWatt or 10^{15} Watts, a unit of power commonly used for ocean heat transports. One PW is equivalent to the amount of energy produced by about one million nuclear power plants.

[3] Over 24 years of daily mean voltage-derived transports have been obtained for the Florida Current using out-of-service and in-service cables spanning the Straits of Florida. The cable voltages can be converted to physically meaningful transport estimates i.e., intensity of the flow, using electromagnetic induction theory.

using a variety of measuring systems. Called the Meridional Overturning Circulation Heat-Transport Array (MOCHA) by the US contributors (NOAA/AOML and the Univ. of Miami with NSF funding) and the RAPID climate change program by the UK contributors (National Oceanography Centre, Southampton), the program began in 2004 with the stated goal of developing a cost-effective basin-wide MOC monitoring system.

The Florida Current contains most of the upper limb of the MOC as it flows through the Florida Straits, with a smaller contribution being carried by the Antilles Current east of the Bahamas. Fluctuations in the Florida Current show a clear negative correlation with the atmospheric phenomenon known as the North Atlantic Oscillation (NAO); however while the NAO has been trending towards its negative extreme over the past twenty years, the Florida Current transport shows no such long-term trend through 2005 (Figure 2). The

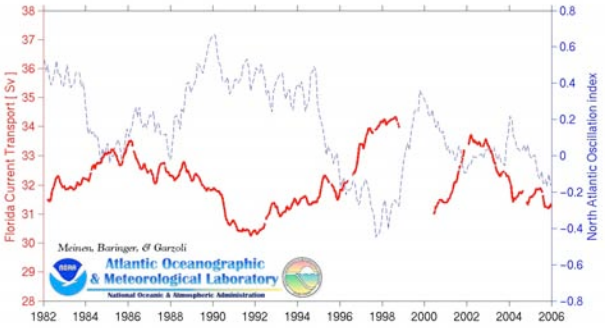

Figure 2: Florida Current transport (red solid) as measured by the NOAA funded submarine cable across the Florida Straits, along with the North Atlantic Oscillation index produced by NCEP (blue dashed).

annual mean transport observed in 2005 (31.4 Sv[4]) falls just within the lowest quartile of historical annual mean transports from the cable, however this transport is still well within one standard deviation from the long-term mean of 32.1 Sv and given the statistical standard error of the mean of 1 Sv, the year 2005 cannot be termed as an unusual year in terms of the Florida Current transport (Figure 3).

Hydrographic observations of the lower limb of the MOC, mostly contained within the Deep Western Boundary Current east of the Bahamas, show the arrival of a pulse of new NADW in 1995, with a gradual

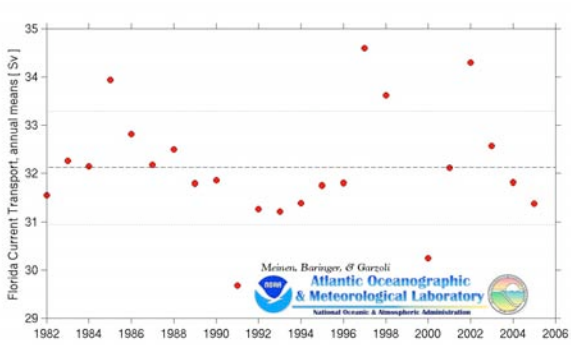

Figure 3: Annual mean transports from the Florida Current measured by submarine cable.

extension of this signal offshore occurring later albeit of smaller magnitude (Figure 4). In 2005 the hydrographic observations showed little change from the previous several years. Coupled with the new NOAA-funded system for monitoring the Deep Western Boundary Current and the new international program for monitoring the basin-wide circulation, in future years it will be possible to state with a much greater degree of certainty what the variations in the integrated,

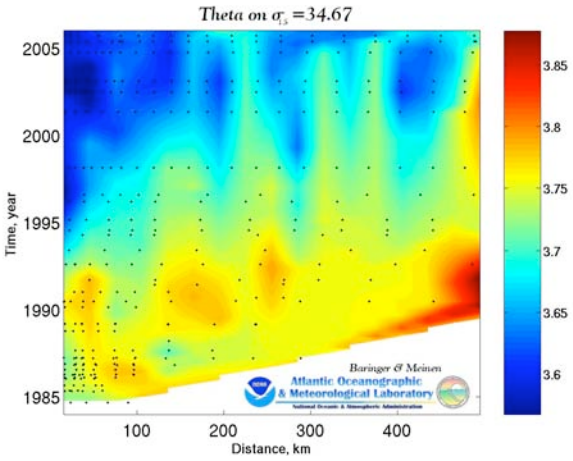

Figure 4: Potential temperature (theta) obtained east of Abaco Island as part of the NOAA Western Boundary Time Series project. Theta is shown on a potential density surface associated with the upper core of the Deep Western Boundary Current. During the 1980's sections only extended 100-300 km offshore that were extended farther offshore in the 1990's to the present.

basin-wide, MOC circulations are and at what time scales they vary. In a recent article, Bryden *et al.*

[4] Sv is a Sverdrup or 10^6 m^3/s, a unit commonly used for ocean volume transports.

(2005), postulated a 30% reduction in the MOC transport between the 1950s and the present day, however that analysis was based on a very limited data set (essentially five points), and other data over the past few decades, such as the moored observations of the Deep Western Boundary Current at the Southeast Newfoundland Rise in the early 1990s and early 2000s showed no indication of such a significant trend in the MOC (Fritz Schott, personal communication).

Heat transport estimates

A basin-wide MOC monitoring system such as the one now in place is truly needed to measure the real ocean variability; however more limited programs currently in place can address individual aspects of the MOC, such as estimating the heat transport using the long time series of expendable bathythermograph (XBT) observations collected on two trans-Atlantic sections by NOAA/AOML. AOML collects XBT data on two lines spanning the subtropical oceans: in the North Atlantic since 1995 (quarterly repeats) along a line running between Spain and Miami, Florida (denoted AX7) and in the South Atlantic since 2002 (twice per year until 2004 and quarterly thereafter) along a line between Cape Town, South Africa and Buenos Aires, Argentina (denoted AX18). These data capture the upper limb of the MOC transport. In the North Atlantic much of the northward transport is confined to a strong boundary current through the Florida Straits, where XBT data can also be usefully augmented with other data from the NOAA funded WBTS program measuring the Florida Current.

Heat transports have already been successfully computed using XBT data (see Roemmich *et al,* 2001, Garzoli and Baringer 2006). Because flux estimates depend upon density, and hence upon salinity, these results have depended on how well salinity profiles could be estimated to complement the XBT data and on how the flux is estimated for depths not sampled by XBT observations. Improving these estimates to achieve more accurate fluxes has been an essential part of this a project at AOML throughout 2005, as has been a careful quantitative assessment of the accuracy of the resulting fluxes.

Estimates of mass and heat transport have been obtained from temperature profiles collected along AX07 and AX18 high-density lines using Sippican T-7 XBT probes, which typically provide data to 800 m or deeper. Salinity was estimated for each profile by linearly interpolating the closest of Levitus' climatological mean salinity and temperature profiles to the XBT temperature and the climatological profiles were used to extend the data to the bottom. In computing velocities the flow is assumed to reverse direction just below the northward flowing Antarctic Intermediate Water (σ_0=27.6 kg m^{-3} in the North Atlantic and σ_0=27.4 kg m^{-3} in the South Atlantic) based on historical studies in the literature and based on what is known about the circulation (hence water deeper than this flows southward). Within strong flows such as the Florida Current or the Malvinas Current the water moves in the same direction down to the bottom and the transport must be specified (e.g. by the utilizing the mean value of the Florida Current from the WBTS submarine cable observations for AX07). The estimated velocities have been adjusted so that the net mass transport across the basin is zero using a single velocity correction for each section. Typically, values of this correction are extremely small, ranging from 10^{-4} to 10^{-6} m s^{-1}.

Using data from 1995 to the present in the North Atlantic, the averaged heat transport was found to vary on inter-annual time scales from 0.8 ± 0.2 PW to 1.2 ± 0.2 PW (Figure 5). The annual average for 2005 was 0.96 PW, indistinguishable from the 1995-2005 average heat transport. Heat transport due to wind-driven Ekman layer flow computed from annual Hellerman winds was relatively small (only 0.1 PW). The observed variability is entirely a function of changes in the

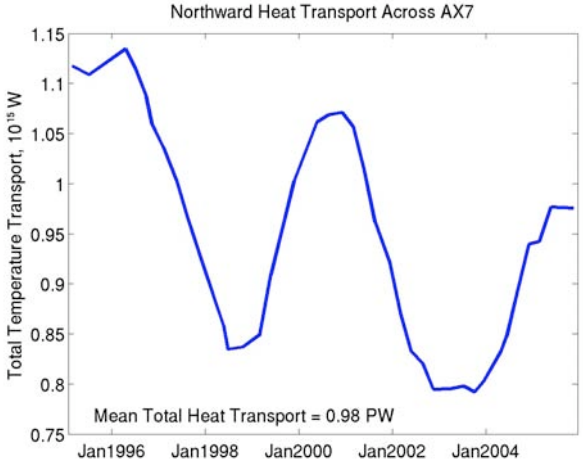

Figure 5: North Atlantic Meridional Heat transport along the AX7 high density XBT line (blue solid line). One PW is equivalent to the amount of energy produced by about one million nuclear power plants. Quarterly values of heat transport vary from 0.5 to 1.6 PW (not shown) for each of the sections (1 PW = 10^{15}W) and here the heat transport and NAO index are subject to a Gaussian filter with e-folding time scale at 1 year.

interior density field; the barotropic Florida Current transport was kept fixed (32 Sv), despite variations in the Florida Current. As shown earlier the 2005 annual mean Florida Current transport of 31.4 Sv was only slightly lower than the 1982-2005 mean value of 32.1 Sv. Planned future improvements to the North Atlantic upper ocean heat transport estimates include (i) taking into account time varying Florida Current transports and wind fields, (ii) improving salinity estimates and extrapolations to the bottom, and (iii) improving error estimates that reflect the effect of the initial reference level, the wind field variability, the importance of barotropic flows, and the uncertainties of the salinity estimates and the extrapolations.

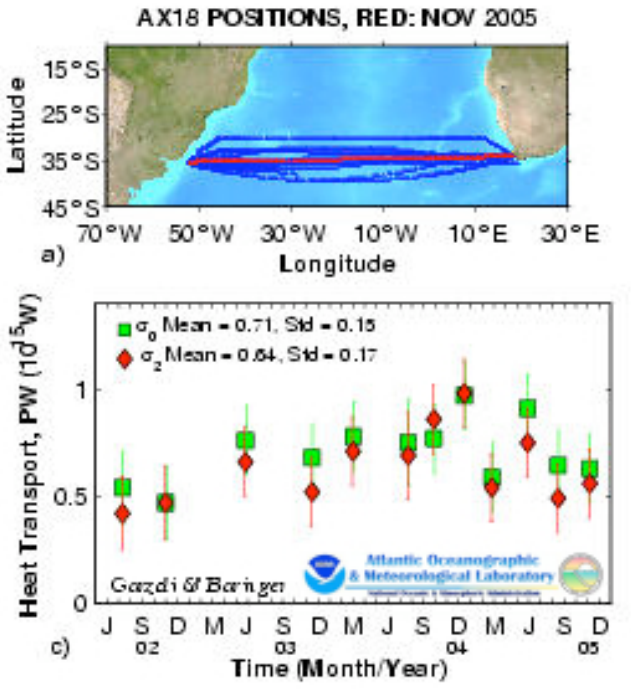

Figure 6: South Atlantic Meridional Heat transport along the AX18 high density XBT line. Heat transports were estimated using two different techniques: one where the flow is assumed to reverse direction just above Antarctic Intermediate Water (green squares) and one where the flow is assumed to reverse direction just above Antarctic Bottom Water (red diamonds).

For the South Atlantic, the transports must be adjusted for the strong flow of the Malvinas Current that is unidirectional (barotropic). Note that in the North Atlantic a good estimate for the barotropic western boundary current is readily available through Florida Current observations and a stable estimate of the mean transport. In the future, current meter moorings deployed by French scientists in the Malvinas Current will provide these values for the South Atlantic, however at this date there is no long-term time series of the Malvinas Current. Based on the limited data available for 2002-2005, the mean heat transport is northward with a mean of about 0.64 +/- 0.3 PW (Figure 6). The 2005 mean heat transport is about 0.59 PW and is indistinguishable from the 2002-2005 mean. Similar improvements to the North Atlantic transports are planned for the South Atlantic. Data collected along the A10 WOCE line located near 30°S have been used to estimate the errors induced by using a climatological deep T, S field from the Levitus product instead of actual data. Results indicated that this procedure can introduce an error of up to 25% and that in order to reduce the errors a better climatology and better T/S relation is needed.

Additional results indicate that the use of different wind products to calculate the wind-driven Ekman component of the flow induced an error of 10%. Particularly in the South Atlantic, the wind-driven Ekman transport estimates vary with latitude and season. One of the main challenges to providing an accurate heat transport is the lack of accurate information on the South Atlantic boundary currents. As a result providing estimates in the South Atlantic is in many ways more challenging than in the North Atlantic.

Summary

Preliminary estimates of the temperature transport in the North Atlantic from the available long-term data sources suggest that the annual mean heat transport estimates range from values near 1.2 PW to values near 0.8 PW with large interannual fluctuations. Changes of the heat transport on the order of 30% such as that postulated by Bryden *et al.* (2005) could have substantial impacts on climate, and time series observations are clearly necessary in order to put one-time hydrographic sections in temporal context. Temporal aliasing is a well-known problem in the use of snapshot sections, and some kind of moored observing system will be needed into the future to monitor fluctuations of the MOC system. Repeated hydrographic sections, however, can play a significant role in measuring and monitoring the MOC system over a broader range of locations than would be feasible with moored instrumentation, particularly when the hydrographic section data is obtained with a fairly high frequency as with the quarterly XBT sections discussed earlier. The programs in place in 2005 are an excellent first step towards the development of such an integrated measurement system, however much work remains before it will be possible to state that the Atlantic MOC system is truly being monitored.

References

Bryden, H. L., H. R. Longworth and S. A. Cunningham, 2005: Slowing of the Atlantic meridional overturning circulation at 25°N. *Nature*, 438, 655-657.

Ganachaud, A., and C. Wunsch, 2003: Large-Scale Ocean Heat and Freshwater Transports during the World Ocean Circulation Experiment. *Journal of Climate*, **16**(4), 696-705.

Garzoli, S. And M. O. Baringer, 2006: Estimates of Meridional Heat Transport in The South Atlantic Ocean. *Journal of Marine Research* (submitted).

Macdonald, A. M., M. O. Baringer and A. Ganachaud, 2001: Heat transport and climate. *Encyclopedia of Ocean Sciences* - Vol. 2 (D-H), 1195-1206.

Orsi, A.H., S.S. Jacobs, A.L. Gordon, and M. Visbeck, 2001: Cooling and ventilating the abyssal ocean. *Geophysical Research Letters*, **28**(15), 2923-2926.

Roemmich, D., J. Gilson, B. Cornuelle, and R. Weller, 2001: The mean and time-varying meridional transport of heat at the tropical/subtropical boundary of the North Pacific Ocean. *Journal of Geophysical Research,* **106**, 8957-8970.

Sabine, C.L., R.A. Feely, N. Gruber, R.M. Key, K. Lee, J.L. Bullister, R. Wanninkhof, C.S. Wong, D.W.R. Wallace, B. Tilbrook, F.J. Millero, T.H. Peng, A. Kozyr, T. Onon, and A.F. Rios, 2004: The oceanic sink for anthropogenic CO2. *Science*, **305**(5682), 367-371.

Talley, L. D. 2003. Shallow, Intermediate, and Deep Overturning Components of the Global Heat Budget, *Journal of Physical Oceanography*, **33**(3), 530-560.

Trenberth, K. E., and J. M. Caron (2001): Estimates of meridional atmosphere and ocean heat transports, *Journal of Climate*, **14**, 3433-3443.

Ocean Heat Content Variability

Gregory C. Johnson[1], Sydney Levitus[2], John M. Lyman[1,3], Claudia Schmid[4], and Joshua K. Willis[5]

[1]NOAA/Pacific Marine Environmental Laboratory, Seattle, WA
[2]NOAA/Nation Oceanographic Data Center, Silver Spring, MD
[3]JIMAR, University of Hawaii, Honolulu, HI
[4]NOAA/Atlantic Oceanographic and Meteorological Laboratory, Miami, FL
[5]NASA/Jet Propulsion Laboratory, Pasadena, CA

Introduction

Assessment of the role of the ocean in global climate variability requires accurate time-dependent estimates of ocean heat and fresh water content as well as transports of both quantities over the globe. Phenomena such as El Niño, the Pacific Decadal Oscillation (Mantua et al. 1997), the North Atlantic Oscillation (Hurrell 1995), and the global water cycle are all aspects of climate in which ocean heat and freshwater content and transport variations play a role. Analyses of how temperature and salinity anomalies enter, circulate within, and leave the ocean lead to increased physical understanding and improved modeling of these and other climate variations.

For example, mixed layer properties (temperature, thickness and heat storage) influence climate over the ocean and adjacent land areas: Sea surface temperature anomalies in the tropical Atlantic Ocean are strongly correlated with rain over northeast Brazil (Nobre and Shukla 1996), the Caribbean and North America (Enfield and Alfaro 1999; Enfield et al. 2001), and the sub-Saharan region (Lamb and Peppler 1992). While sea surface temperature is an important parameter for understanding interactions between ocean and atmosphere, ocean heat storage also plays an important role: A thick layer of warm water supplies more energy than a thin one for hurricane intensification (e.g. Shay et al. 2000).

It was also recognized some time ago that ocean heat content could dominate temporal variability of the earth's heat budget (Rossby 1959). The possibility of a warming ocean due to increasing greenhouse gasses has also been posited for some time (White House 1965), as has the potential for delay of greenhouse-gas induced atmospheric warming due to initial uptake of heat by the world ocean (National Research Council 1979). Ocean heat content estimates and analyses (e.g. Levitus et al. 2000, 2001, 2005a, b) have supported these hypotheses, helped to verify climate models simulating greenhouse-gas induced warming (e.g. Barnett et al. 2001, 2005; Hansen et al. 2005), and have the potential to improve their predictive skill. Ocean heat content is thus a critical variable for monitoring earth's climate system and for detection and attribution of climate change due to the observed increase of greenhouse gases in earth's atmosphere.

Ocean salinity is very important dynamically on a variety of time-scales; for instance, a freshwater cap in the northernmost Atlantic Ocean could reduce the ocean's meridional overturning circulation, greatly affecting the weather of nearby continents (Curry and Mauritzen 2005). In addition, changes in ocean salinity distributions are sensitive indicators of climate variations, allowing tests of climate models (Banks and Woods 2002) In situ salinity measurements are at present insufficient to allow a reasonably certain discussion of interannual upper ocean freshwater content variability globally for 2005. In many locations the historical record may be insufficient to define an ocean salinity climatology, much less analyze interannual variations around that climatology, although linear trends have been computed as a function of latitude alone from 1955 – 1998 in the major ocean basins (Boyer et al. 2005). More detailed regional analyses of interdecadal, and in some cases interannual, ocean salinity variations are possible in better-sampled areas of the ocean like the North Atlantic Ocean (e. g. Curry and Mauritzen 2005) or with oceanographic cruises repeatedly occupied in more remote areas such as the South Indian Ocean (e.g. Bryden et al. 2003). These analyses are usually a few years out of date because there is still a significant time delay in availability of climate-quality ocean salinity data.

However, the Argo Project (Roemmich et al. 2004;

http://www.argo.net/) array of profiling CTD (Conductivity-Temperature-Depth) floats began in 2000 and will allow estimates of global freshwater content variability. It first achieved sparse global coverage in 2004 and is expected to achieve global coverage at its target density within the next few years. When complete, this array will collect temperature and salinity profiles from 2000 m to the surface at 10-day intervals from about 3000 floats spaced roughly every 3 degrees of longitude and latitude throughout the ice-free global ocean. In a few years sufficient salinity data will be collected to allow construction of a robust mean climatology and seasonal cycle (where there is a seasonal cycle in salinity).

Here we focus primarily on upper ocean heat content variability. Ocean transport variations are discussed in another section of this document. Analyses of ocean heat content have traditionally relied solely on in situ data from instruments such as mechanical and expendable bathythermographs (MBTs and XBTs), Conductivity Temperature Depth (CTD) profilers, thermistors on moorings, surface drifters, and more recently, CTD equipped profiling floats and bathythermograph equipped pinnipeds. In situ data, while arguably sparse in space and time with respect to natural variability (Gregory et al. 2004), have been used to generate annual estimates of upper ocean heat content (from 0 – 700 m) throughout the global ocean on annual time scales. Pentadal estimates to greater (0 – 3000 m) depth have also been generated (Levitus et al. 2005a, b), showing an overall warming trend of the ocean from 1955 through 2003. These results are reviewed below. Monthly Atlantic mixed layer properties estimated from in situ data are also analyzed from 1997 through November 2005 in regions where data coverage is sufficient.

In situ estimates of ocean heat content (calculated from the data source mentioned above as anomolies with respect to an ocean temperature climatology) have tended to be sparsely sampled in space and time. Starting in 1993, sea surface height anomalies (SSHA) maps from satellite altimetry (http://www.aviso.oceanobs.com/) provide more complete temporal and spatial coverage of the ocean surface over much of the globe. Because SSHA fields are dynamically related to ocean heat content anomaly (OHCA) fields, satellite-based OHCA fields can be generated by calculating local regressions of in situ upper (0 – 750 m) OHCA data against SSHA data, and then applying these coefficients to the SSHA maps. The OHCA maps derived from SSHA can then be used to fill in areas and times where no in situ OHCA estimates exists. Thus annual OHCA maps can be generated almost globally, even in areas where the density of in situ observations is small (Willis et al. 2003, 2004). Over larger spatial scales and longer time scales, changes in the ocean mass measured by the altimeter likely contaminate SSHA-based OHCA estimates. On regional scales, salinity variability may also contaminate such estimates, because both salinity and temperature affect ocean density, and thus ocean sea surface height. However, maps of OHCA made by combining in situ data with SSHA maps have greater accuracy than OHCA estimates from in situ data alone, especially when and where those in situ data are sparse. Below we update combined OHCA estimates of Willis et al. (2004) using in situ data and satellite altimetry maps collected and generated, respectively, through the end of October 2005. We also discuss how in situ sampling variability affects the temporal and spatial structure of error estimates for in situ OHCA maps.

Global in Situ Ocean Heat Content Anomaly Estimates

Yearly global upper (0 – 700 m) OHCA estimates for 1955 – 2003 and deeper (0 – 3000 m) pentadal (5-year) OHCA estimates for 1955 – 1959 through 1994 – 1998 (Fig. 1; Levitus et al. 2005a, b) are based on approximately seven million historical and modern temperature profiles that have become available as part of the *World Ocean Database 2001* (Conkright et al. 2002). In addition, approximately 310,000 additional temperature profiles that became available since the release of WOD01 have also been used in this analysis. Many of the recent data used represent real-time and delayed-mode data reported via the IOC Global Temperature Salinity Profile Project (IOC 1998). Many of the historical temperature data that have made these estimates possible have been recovered as part of "data archaeology and rescue" projects (Levitus et al. 2005c).

A large part of the total change in ocean heat content during the past 50 years occurred in the upper 700 m of the world ocean (Fig. 1). The difference between the 0 –700 m and 0 – 3000 m curves at the beginning of the record is likely owing to the lack of data for the yearly as compared to the pentadal compositing periods. Both time-series show similar variability. For the world ocean the linear trend of heat content (for the 0-3000 m layer for 1955-98) is 0.33×10^{22} J year^{-1}, corresponding to a rate of 0.2 W m^{-2} (per unit area of the earth's total surface), and the overall increase in heat content for the world ocean is 14.5×10^{22} J. The ocean warming is estimated to be about 84% of the total global warming since 1955 (Levitus et al. 2005b).

A large decrease in global ocean heat content is evident beginning around 1980 (Fig. 1). The 0 – 700 m layer

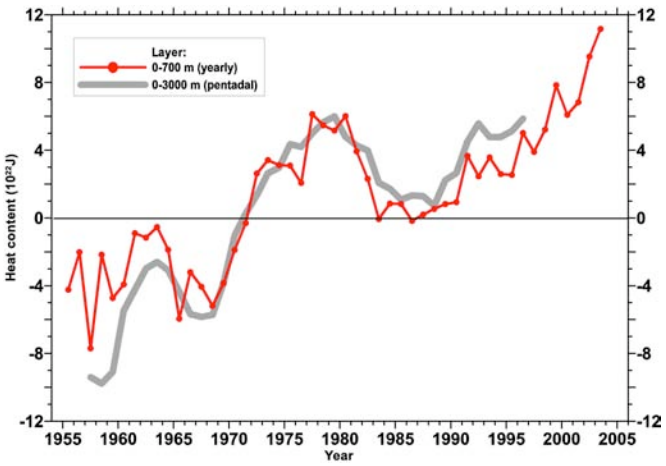

Figure 1. Time series of annual average global upper (0 – 700 m, red line with dots) Ocean Heat Content Anomaly (OHCA; J) estimated and deeper (0 – 3000 m, thick grey line) pentadal (5-year) global OHCA estimates for 1955 – 59 through 1994 – 98 from Levitus et al. (2005a). Annual and pentadal estimates are plotted at their temporal mid-points.

exhibits a decrease of approximately 5.8×10^{22} J between 1980 and 1983, corresponding to a cooling rate of 1.2 W m^{-2} (per unit area of the earth's total surface). Most of this decrease occurs in the Pacific Ocean and may be associated with a sign change of the Pacific Decadal Oscillation (Stephens et al. 2001; Levitus et al. 2005a, b). Estimates of ocean heat content changes for 1994 – 2003 (Willis et al. 2004) are in rough agreement with net radiation at the top-of-the-atmosphere, available only since 1985 (Wong et al. 2006). This agreement includes interannual variability of approximately 1.5 W m^{-2} (per unit area of the earth's total surface) associated with the 1997 – 98 El Niño**.** El Niño and the Pacific Decadal Oscillation appear linked (Zhang et al. 1997), leading to the suggestion that processes which may lead to changes in the net radiation at the top of the atmosphere associated with El Niño may have an analogue in the Pacific Decadal Oscillation, and the further suggestion that these processes are due to internal variability of the ocean-atmosphere system.

Global Combined in Situ and Altimeter Ocean Heat Content Estimates

We (JML, JKW, and GCJ) have also updated the in situ ocean temperature data and satellite altimetry maps that start in 1993 through 31 October 2005. We have used these in situ data and maps to produce annual average maps at quarterly intervals from 1993.5 through 2005.5 of upper (0 – 750 m) OHCA relative to a ten-year 1993 – 2002 baseline using the Willis et al. (2004) methodology. Maps of OHCA can be produced from the satellite data alone, the in situ data alone, and the two data sets combined. Here we will focus on the combined estimates only.

Since each OHCA map is normally based on a year's worth of data, the 2005.5 maps are suboptimal because at the time they were produced we were missing 2 months of data. In addition, the satellite only and combined OHCA maps for 2004.75 – 2005.25 are also suboptimal because only preliminary real-time satellite altimeter maps were available for dates after 7 January 2005 at the time of the analysis. Thus, maps during these periods use at least some real-time satellite data. Maps of OHCA for the last few years will be improved in the future by use of finalized satellite altimeter data and inclusion of more in situ data as profiles taken in the field but not yet publicly available are gradually reported to, gathered by, and made available from oceanographic data centers.

Because of differences in processing of the real-time and delayed mode altimeter data, these preliminary maps may not be optimal for looking at subtle (equivalent to order 1 W m^{-2}) global average OHCA variations (e.g. Willis et al. 2004; Levitus et al. 2005a,b). In addition, the Argo Project profiling CTD float array has significantly changed ocean sampling. First, floats sample at even 10-day intervals, whereas shipboard data sample more sporadically with potential seasonal biases. Second, the floats are distributed globally, whereas shipboard data are concentrated along shipping routes that miss wide swaths of the ocean. The effects of real-time altimetry on the maps and the change of in situ sampling patterns over the last few years preclude updating the combined estimate of globally averaged OHCA through the end of 2005 at this time. This curve will be updated as soon as delayed-mode altimeter data becomes available and any effects due to the new sampling regime can be more fully explored. However, local variations of the combined OHCA maps over interannual and even decadal time-scales are analyzed here because they are much larger than potential artifacts owing to sampling changes.

The 2005.5 combined OHCA map compared to a 1993 – 2002 baseline (Fig. 2, top) shows eddy and meander variability down to the 100-km mapping scales. Some large-scale patterns are also evident. OHCA is high in the subpolar N. Atlantic and low in the subtropical N.

Atlantic, consistent with a decreased strength of the North Atlantic Current. This pattern is probably related

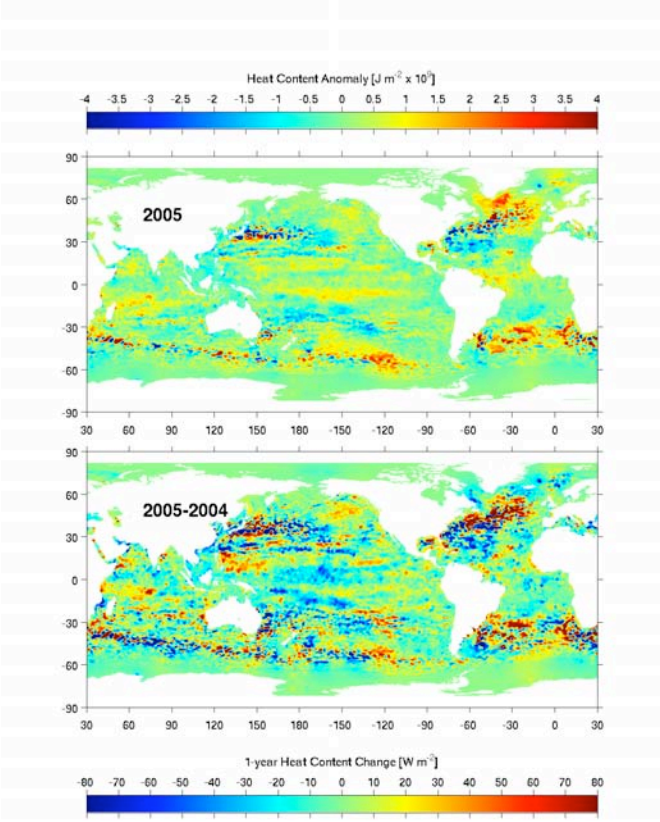

Figure 2. The 2005.5 satellite and in situ upper ocean (0 – 750 m) combined OHCA map following Willis et al. (2004) relative to a 1993 – 2002 baseline period (top; J m^{-2}) and the difference of the 2005.5 and 2004.5 combined OHCA maps (bottom) expressed as a surface heat flux equivalent (W m^{-2}).

to decadal changes in the North Atlantic Oscillation (e. g. Curry and McCartney 2001). This climate index was lower in 2005 than during the baseline period of 1993-2002, and has trended lower from 1993 through 2005. The tropics in 2005 have generally higher OHCA than for the baseline period, but not excessively so, reflecting the lack of an El Niño or La Niña in 2005. In 2005 OHCA is high throughout the South Pacific and South Atlantic Oceans in a belt located north of the Antarctic Circumpolar Current. There is a large amount of small-scale spatial variability associated with this current and the western boundary currents.

The difference in combined OHCA maps between 2005.5 and 2004.5 (Fig. 2, bottom) illustrates the large year-to-year variability in ocean heat storage, with changes reaching or exceeding the equivalent of an 80 W m^{-2} magnitude surface flux over a year in many places. Comparison with the global averaged absorption of solar radiation by the ocean and atmosphere of about 238 W m^{-2}, these variations are quite substantial. Ocean advection likely plays a large role in many of these changes. This difference between two years clearly shows the influence of eddies and meanders, as well as the larger scale patterns discussed above in the subtropical and subpolar regions. The decrease in OHCA in the central equatorial Pacific between 2005 and 2004 probably reflects the transition from a very weak El Niño to more normal conditions. Also of interest, given the strong 2005 hurricane season and the potential link between hurricane intensity and warm ocean waters (e.g. Shay et al. 2000; Emanuel 2005; Webster et al. 2004) are the large increases in OHCA around Florida and the Gulf of Mexico from 2004 to 2005.

Eddies and meanders are mostly absent from the 13-year linear trends in the combined OHCA maps (Fig. 3, top), since such features are smoothed out over decadal time-scales. The amplitudes of the decadal changes are smaller than the year-to-year changes by nearly an order of magnitude. Assuming every year is statistically independent and accurately estimated, the linear trends exceed the 95% confidence intervals in only a few locations (Fig. 3, bottom). Notable changes in OHCA include a strong increase in the subpolar N. Atlantic already discussed above. In addition, there is strong decrease in the subpolar N. Pacific that may be related to changes in the wind field (Qiu 2002; Cummins and Lagerloef 2004) likely associated with the Pacific Decadal Oscillation. Also interesting and apparently significant are the increases in OHCA in the southern Hemisphere, north of the Antarctic Circumpolar Current. This change has recently been studied in the South Pacific (Roemmich et al. 2006) and related to changes in the wind-stress field associated with an increase in the Antarctic Oscillation. Increases in OHCA in the southern hemisphere subtropical gyres in all three oceans may be related. Decadal changes in the tropics are mostly not significant, which is not surprising given the large amplitude of interannual variability and the relative shortness of the 13-year record.

Global Uncertainty Estimates and Sampling Metrics

We (JML, JKW, and GCJ) are expanding and improving the error analysis for the Willis et al. (2004) methodology. Previously, only the uncertainty of the trend in global average combined OHCA over the entire period studied was estimated. In reality, errors change with each in situ and combined map as in situ sampling

distributions vary (while remaining relatively constant for the satellite only map). We are presently working on systematically propagating all significant sources of uncertainty (including in situ sampling distributions, the seasonal cycle, instrument noise, and the model for combining in situ heat content and satellite altimetry) through the estimates.

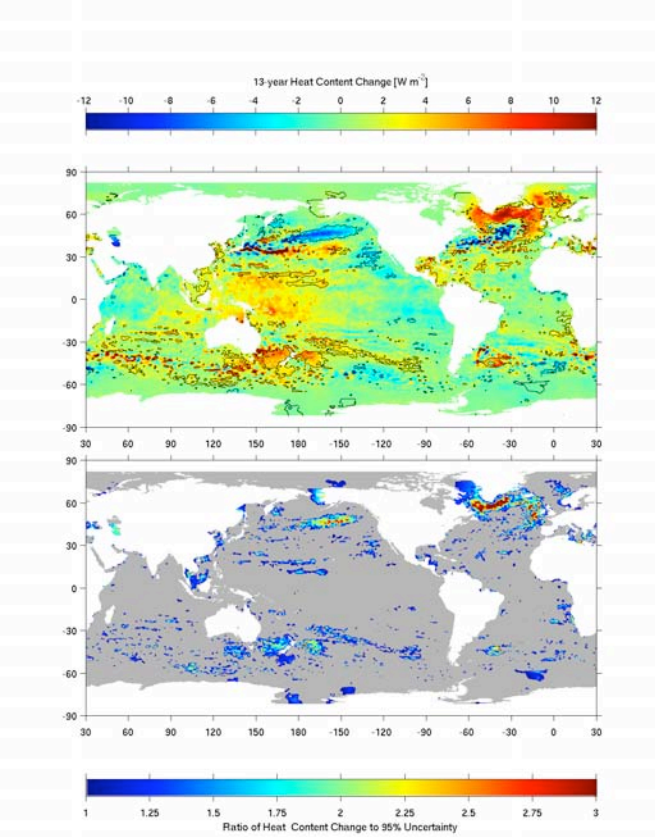

Figure 3. Linear trends in heat content change from combined OHCA maps 1993 – 2005 (top) expressed as a surface heat flux equivalent (W m^{-2}) with areas of significant slope outlined in black as estimated by the ratio of these trends to their 95% uncertainty estimates (bottom, where colored regions are increasingly significantly different from zero but grey are not).

As an illustration, we discuss the effect of year-to-year variations in the in-situ data sampling distribution on the uncertainties in the annual global averaged in situ OHCA estimates. Although this is just one of several terms that must be taken into account in the total uncertainty of the combined OHCA estimates, it may be the dominant one.

While satellite altimetry provides relatively complete nearly global coverage of SSHA, in situ data distributions can be sparser than optimal for estimating OHCA globally. Estimates of the annual 95% uncertainty in OHCA are made by sub-sampling every year of the 13-year record of SSHA in the same manner as the in situ sampling pattern for a given year. To derive the uncertainties, the global integral of SSHA, for the 13-year record, is constructed from maps of sub-sampled data set (Willis et al. 2004) and compared to the global integral of SSHA based on the complete SSHA maps. The uncertainty of the global mean in SSHA (Willis et al. 2004) must be added in quadrature to these uncertainties to account for unsampled geophysical variability. Then the SSHA uncertainty can be converted into an OHCA uncertainty using a global regression coefficient betwee the two quantities.

The contribution of this error source to the global averaged in situ estimate varies significantly from year

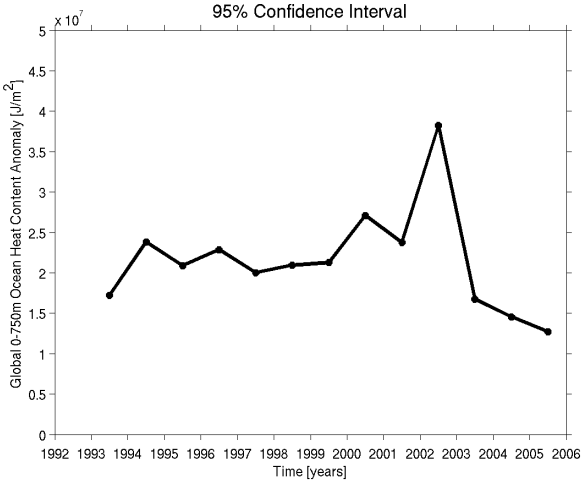

Figure 4. In situ annual global mean OHCA uncertainty from 1993 – 2005, estimated as discussed in the text. The sharp decrease in 2003 – 2005 is owed in large part to the growth of the Argo Project.

to year (Fig. 4). Most notably, while 2002 and 2005 globally averaged in situ only OHCA estimates make use of a similar number of temperature profiles (about 150,000 in each year), the 2005 estimate has a much smaller sampling uncertainty than the 2002 estimate. This change results because the Argo Project global array of profiling CTD floats grew dramatically from about 400 floats near the start of 2002 to about 2200 floats near the end of 2005, resulting in a more widespread sampling spatially and more uniform sampling temporally in 2005 than previous years. There may still be a lag of several years for non-Argo in situ data (such as ship-based XBT and CTD profiles) to make their way to the public archives we are using. In that case this component of uncertainty for subsequent analyses that include additional in situ data could be further reduced.

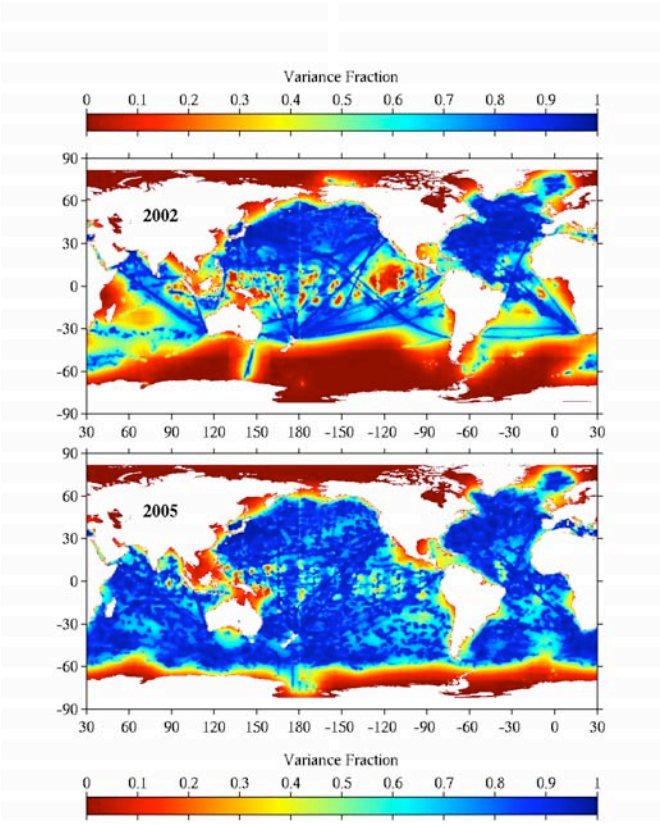

Figure 5. Energy of a global unit OHCA mapped with in situ sampling patterns for 2002 (top) and 2005 (bottom), a much better sampled year with the advent of the global Argo Project array of profiling CTD floats. Fields result from the sampling pattern and the geophysical mapping parameters from Willis et al. (2004), with 1 being very well sampled, and 0 being unsampled.

For each year's sampling pattern, we can map (e.g . Fig. 5) where the ocean sampling is good (approaching 1) and where it is poor (approaching 0). These maps for 2002 and 2005 (Fig. 5) reveal the reason that the in situ error for the global average OHCA in 2002 is larger than in 2005. In 2002 large swaths of the southern hemisphere, and other regions are badly undersampled. However, by 2005, the growing Argo Project array of profiling CTD floats is doing a much better job at sampling OHCA for the global ice-free ocean.

Monthly Atlantic Mixed Layer Properties from in situ Data for 1997 to 2005.

The ocean mixed layer is the portion of the ocean that interacts directly with the atmosphere. The temperature and thickness of this layer have wide-ranging importance in climate studies, from ocean-atmosphere carbon exchange to hurricane intensification. Here we (CS) analyze seasonal to interannual variability of mixed layer temperature and thickness in select Atlantic regions with sufficient data coverage using preliminary in situ data from 1997 through November 2005. Irregularly spaced in situ data are mapped to a uniform grid using a standard objective analysis technique that takes into account error energy as well as spatial and temporal scales of variability. Data coverage is best in the tropical Atlantic and the subtropical North Atlantic (Fig. 6). The data set for 2005 is not complete so annual means for 2003 and 2004 are compared. Large regions in the tropical Atlantic and the subtropical North Atlantic have sufficient data coverage (best centered near 30˚N) for comparisons in these years (Fig. 7). Monthly estimates for select regions over the full time period are also discussed.

The 2003 annual average temperature (not shown) looks quite similar to that for 2004 (Fig. 8, top left) mainly due to the large temperature range that masks differences an order of magnitude smaller. The difference between 2003 and 2004 (Fig. 8, top right) reveals about 1˚C higher temperatures around 5˚N, near 45˚W and 20˚W, in 2003. In the western equatorial region, temperature differences alternate in sign (positive near S. America, negative farther east). Northeast of the Bahamas the water is colder in 2004, whereas it is warmer farther east. Areas such as the eastern equatorial band have insufficent observations for comparison. Similarly, the colder water to the north, at about 15˚N, 35˚W is only based on few observations in both years. All differences south of about 25˚S may also be an artifact of much poorer local sampling in 2003 (Fig. 7).

Mixed layer thickness differences are about 10 m in regions with sufficient data coverage (Fig. 8, bottom right). Along 5˚N the mixed layer in the western basin is about 10 m thicker (positive difference) in 2004, whereas it is about 10 m thinner in the eastern basin. On the equator the mixed layer is thinner in 2004. Around 30˚N a region of negative differences is south of a region with positive differences. Here mixed layer heat storage differences (not shown; on the order of 10^9 Jm^{-2}) are very closely related to mixed layer thickness differences.

As noted above, sea surface temperature anomalies over the tropical North and South Atlantic have significant climate impacts over adjacent land masses. Here well-sampled subregions of the tropical North and South Atlantic are analyzed, so the tropical North Atlantic (TNA) is defined as 13 – 16˚N, 40 – 30˚W and the tropical South Atlantic (TSA) as 6˚S – 0, 30 –22˚W (Fig. 6, small rectangles). In the TNA monthly data

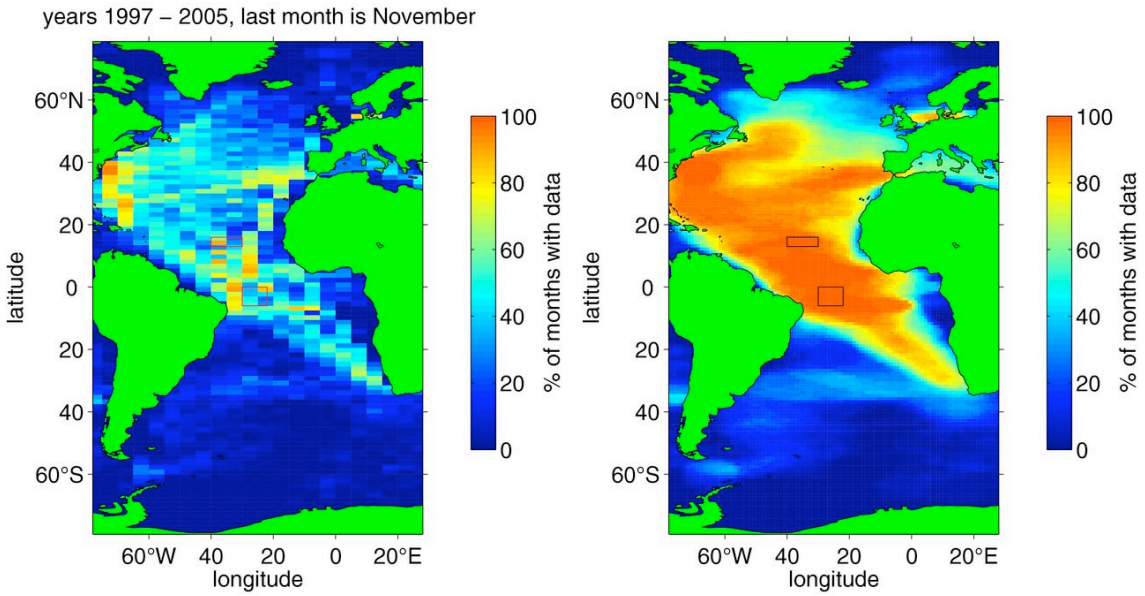

Figure 6. Data coverage for January 1997 - November 2005. Raw percentage of months with observations (left). Red rectangles indicate subregions of the tropical North and South Atlantic. Percentage of months with observations after objective analysis was used to interpolate the data for every month onto a regular grid before the data coverage was derived (right). Black rectangles indicate subregions of the tropical North and South Atlantic.

coverage varies between 25 and 100% and exceeds, on average 50%. In the TSA monthly data coverage is a little lower but the average is about 50%. In both regions the data coverage after objective analysis is 100% in most months and almost always exceeds 80%. This apparent increase in coverge occurs because the analysis smooths and interpolates data given the spatial and temporal scales of geophysical variability.

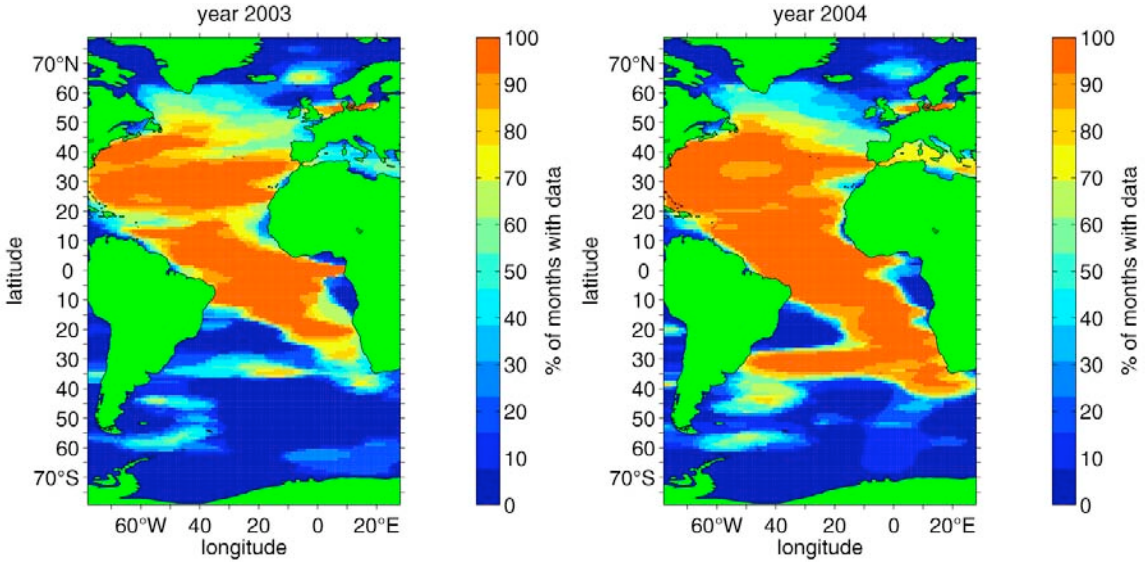

Figure 7. Data coverage, after objective mapping, for 2003 (left) and 2004 (right).

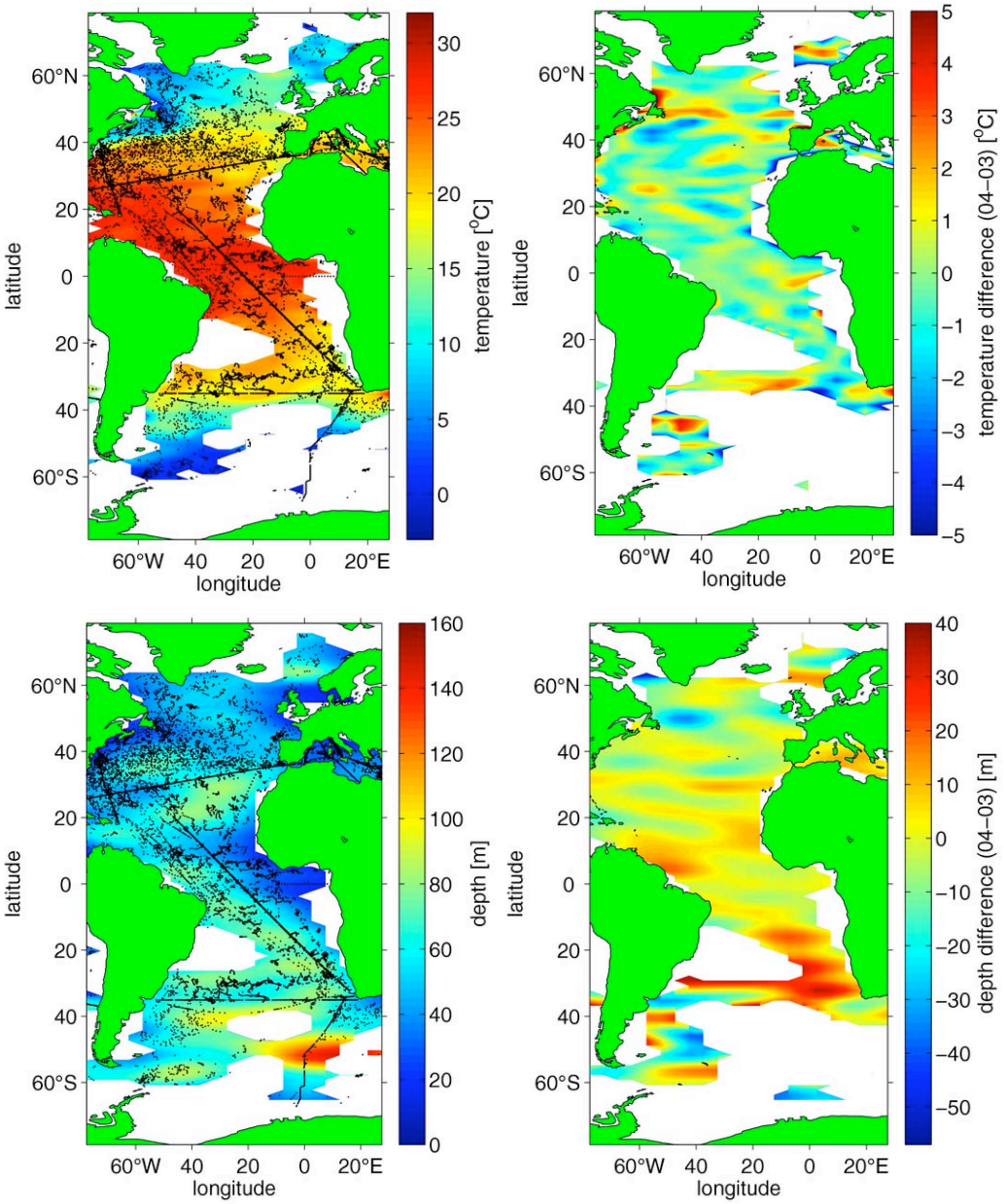

Figure 8. Annual mean mixed layer temperature (top left) and thickness (bottom left) for 2004. Black dots indicate profile positions. Differences of the 2003 and 2004 annual mean mixed layer temperature (top right) and thickness (bottom right).

TNA mixed layer temperatures vary from 23.5 – 28 ˚C (Fig. 9, top left) with lows in February-April and the highs in September-November. Interannual temperature minimum variations are about 1 ˚C and temperature maximum variations do not exceed 0.8 ˚C. Relatively low maximum temperatures are found in 1999-2000. This period, also containing the lowest minimum temperatures, is coincident with strong La Niña conditions. Over the last 5 years (2001-2005) the interannual variability is quite small, and there have been no strong El Niño or La Niña conditions.

TNA mixed layer thickness varies between about 30 m in boreal fall and up to 80 m in boreal spring (Fig. 9,

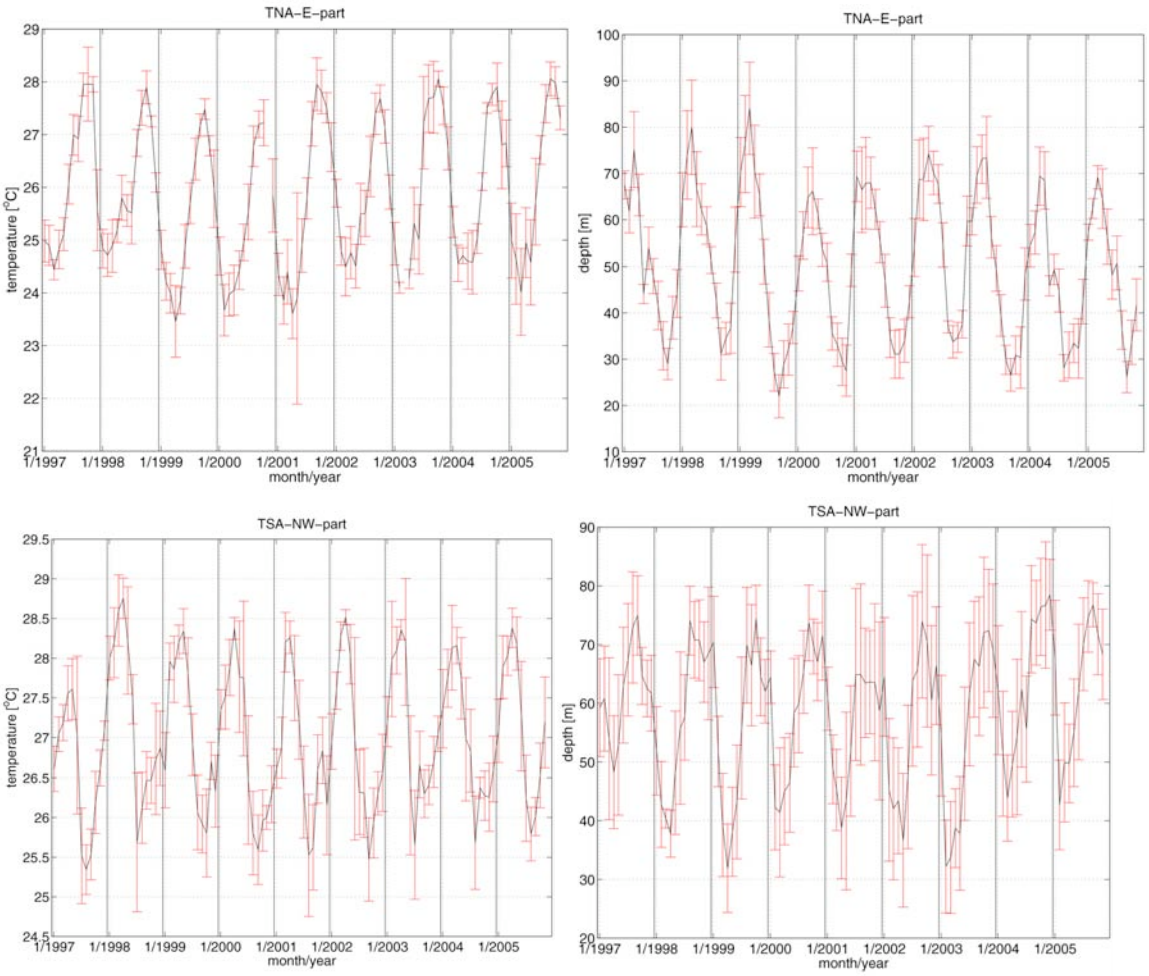

Figure 9. Time series of monthly mixed layer temperature (left, ˚C) and thickness (right, m) in the tropical North Atlantic (top; TNA; 13 – 16˚N, 40 – 30˚W) and the tropical South Atlantic (bottom; TSA; 6˚S – 0, 30 – 22˚W) with one standard deviation error bars.

top right). The highest maximum and lowest minimum occur in 1999, an exceptional year. The next year has the lowest maximum and an average minimum. Given the Strong 1997 – 98 El Niño and the 1999 – 2001 La Niña, a correlation between this climate variability and mixed layer thickness in this region seems unlikely**.** As for the temperature, interannual variability in the last 5 years is small. Mixed layer heat storage variations (not shown) correlated well with mixed layer thickness variations.

TSA mixed layer temperature (Fig. 9, bottom left) is roughly opposite in phase to TNA mixed layer temperature, with minima in austral fall and maximum in austral spring. However, the 25.5 – 28.5 ºC TSA temperature range is smaller than that in the TNA. From 1999 to 2005 interannual TSA variability is small. Satellite observations could be included to determine if the interannual variability at the beginning of the time series is owing to the sampling patterns.

As for the TNA, TSA mixed layer thickness (Fig. 9, bottom right) varies from 30 – 80 m, and is again a mirror image of the TNA in the sense that the TSA maxima occur in austral spring and the minima in austral fall. The thinnest mixed layers are in 1999 and 2003, and the thickest mixed layers are in 2004 and 2005, so a correlation with El Niño conditions is not evident. Again TSA heat storage (not shown) follows mixed layer thickness closely.

References

Banks, H., and R. Wood, 2002: Where to look for anthropogenic climate change in the ocean. *J. Climate*, **15**, 879-891.

Barnett, T. P., D. W. Pierce, and R. Schnur, 2001: Detection of anthropogenic climate change in the World's Oceans. *Science*, **292**, 270–274

Barnett, T. P. D. W. Pierce, K. M. AchutaRao, P. J. Gleckler, B. D. Santer, J. M. Gregory, and W. M. Washington, 2005: Penetration of Human-Induced Warming into the World's Oceans. *Science*, **309**, 284–287.

Boyer, T. P., S. Levitus, J. I Antonov, R. A. Locarnini, and H. E. Garcia, 2005: Linear trends in salinity for the World Ocean, 1955–1998. *Geophys. Res. Lett*., **32**, L01604, doi:10.1029/2004GL021791.

Bryden, H. L., E. L. McDonagh, and B. A. King, 2003: Changes in ocean water mass properties: Oscillations or trends? *Science*, **300**, 2086-2088.

Conkright, M. E., J. I. Antonov, O. K. Baranova, T. P. Boyer, H. E. Garcia, R. Gelfeld, D. Johnson, R. A. Locarnini, P. P. Murphy, T. O'Brien, I. Smolyar, and C. Stephens, 2002: *World Ocean Database 2001, Volume 1: Introduction. NOAA Atlas NESDIS 42, U.S.,* Ed. S. Levitus, Government Printing Office, Washington, D.C., 159 pp., CD-ROMs.

Cummins, P. F., and G. S. E. Lagerloef, 2004: Wind-driven interannual variability over the northeast Pacific Ocean. *Deep–Sea Res. I*, **51**, 2105–2112.

Curry, R. and C. Mauritzen, 2005: Dilution of the northern North Atlantic in recent decades. *Science*, **308**, 1772–1774.

Curry, R. G., and M. S. McCartney, 2001: Ocean gyre circulation changes associated with the North Atlantic oscillation. *J. Phys. Oceanog*., **31**, 3374 – 3400.

Emanuel, K. A., 2005: Increasing destructiveness of tropical cyclones over the past 30 years. *Nature*, **436**, 686–688.

Enfield, D. B., 1996: Relation of Inter-American rainfall to Tropical Atlantic and Pacific SST variability. *Geophys. Res. Lett*., **23**, 3305-3308.

Enfield, D. B., and E.J. Alfaro, 1999: The dependence of Caribbean rainfall on the interaction of the tropical Atlantic and Pacific Oceans, *J. Clim.*, **12**, 2093-2103.

Enfield, D.B., A.M. Mestas-Nunez, and P.J. Trimble, 2001: The Atlantic Multidecadal Oscillation and its relationship to rainfall and river flows in the continental U.S. *Geophys. Res. Lett.*, **28**, 2077-2080.

Gregory, J. M., H. T. Banks, P. A. Stott, J. A. Lowe, and M. D. Palmer, 2004: Simulated and observed decadal variability in ocean heat content. *Geophys. Res. Lett*., **31**, L15312, doi:10.1029/2004GL020258.

Hansen, J., L. Nazarenko, R. Ruedy, M. Sato, J. Willis, A. Del Genio, D. Koch, A. Lacis, K. Lo, S. Menon, T. Novakov, J. Perlwitz, G. Russell, G. A. Schmidt, and N. Tausnev, 2005: Earth's energy imbalance: Confirmation and implications. *Science*, **308**, 1431–1435.

Hurrell, J. W., 1995: Decadal trends in the North Atlantic Oscillation: regional temperatures and precipitation. *Science*, **269**, 676-679.

IOC, 1998: *Global Temperature-Salinity Profile Programme (GTSPP) Overview and Future*, *IOC Tech. Series, vol. 49*, Intergovernmental Oceanographic Commission, Paris, 12 pp.

Lamb, P.J., and R.A. Peppler, 1992: Further case studies of tropical Atlantic surface atmospheric and oceanic patterns associated with Subsaharan drought. *J. Clim.*, **5**, 476-488.

Levitus, S., J. Antonov, T. P. Boyer, and C. Stephens, 2000: Warming of the World Ocean. *Science*, **287**, 2225-2229.

Levitus, S., J. Antonov, J. Wang, T. L. Delworth, K. W. Dixon, and A. J. Broccoli, 2001: Anthropogenic warming of earth's climate system. *Science*, **292**, 267-270.

Levitus, S., J. I. Antonov, T. P. Boyer, H. E. Garcia, and R. A. Locarnini, 2005a: EOF analysis of upper ocean heat content. *Geophys. Res. Lett*., **32**, L18607, doi: 10.1029/2005GL023606.

Levitus, S., J. I. Antonov, and T. P. Boyer, 2005b: Warming of the World Ocean, 1955–2003. *Geophys. Res. Lett*., **32**, L02604, doi:10.1029/2004GL021592.

Levitus, S., S. Sato, C. Maillard, N. Mikhailov, P. Caldwell, and H. Dooley, 2005c: Building Ocean

Profile-Plankton Databases for Climate and Ecosystem Research, NOAA Technical Report NESDIS 117, U.S. Government Printing Office, Wash., D.C., 29 pp.

Mantua, N. J., S. R. Hare, Y. Zhang, J. M. Wallace, and R. C. Francis,1997: A Pacific interdecadal climate oscillation with impacts on salmon production. *Bull. Amer. Meteor. Soc.* **78**, 1069–1079.

National Research Council,1979: *Carbon Dioxide and Climate: A Scientific Assessment (Report of an Ad Hoc Study group on Carbon Dioxide and Climate)*, Nat. Acad. Sci., Wash., D.C., 22 pp.

Nobre, P., and J. Shukla, 1996: Variations of sea surface temperature, wind stress and rainfall over the tropical Atlantic and South America. *J. Clim.*, **9**, 2464-2479.

Qiu, B., 2002: Large-scale variability in the midlatitude subtropical and subpolar North Pacific Ocean: Observations and causes. *J. Phys. Oceanogr.*, **32**, 353–375.

Roemmich, D., J. Gilson, R. Davis, P. Sutton, S. Wijffels, and S. Riser, 2006: Decadal spin-up of the South Pacific subtropical gyre. *J. Phys. Oceanogr.*, **36**, in press.

Roemmich, D., S. Riser, R. Davis, and Y. Desaubies, Y 2004: Autonomous profiling floats: Workhorse for broadscale ocean observations. *J. Mar. Technol. Soc*., **38**, 31 – 39.

Rossby, C., 1959: Current problems in meteorology, in *The Atmosphere and Sea in Motion*, Rockefeller Institute Press, New York, pp. 9-50.

Shay L. K., G. J. Goni, and P. G. Black. 2000: Effect of a warm ocean ring on hurricane Opal. *Mon. Weath. Rev*., **128**, 1366-1383.

Stephens, C., S. Levitus, J. Antonov, and T. Boyer, 2001: The Pacific regime shift, *Geophys. Res. Lett*., **28**, 3721-3724.

Webster, P. J., G. J. Holland, J. A. Curry, and H.–R. Chang, 2005: Changes in tropical cyclone number, duration, and intensity in a warming environment, *Science*, **309**, 1844 – 1846.

White House, 1965: *President's Science Advisory Committee Report*- "Restoring the Quality of Our Environment- Report of the Environmental Pollution Panel", Appendix Y4 (by R. Revelle, W. Broecker, H. Craig, C. D. Keeling, J. Smagorinsky), Wash., D.C., 112-133.

Willis, J. K., D. Roemmich, and B. Cornuelle, 2003: Combining altimetric height with broadscale profile data to estimate steric height, heat storage, subsurface temperature, and sea-surface temperature variability. *J. Geophys. Res*., **108**, 3292, doi:10.1029/2002JC001755.

Willis, J. K., D. Roemmich, and B. Cornuelle, 2004: Interannual variability in upper ocean heat content, temperature, and thermosteric expansion on global scales. *J. Geophys. Res*., **109**, C12036, doi: 10.1029/2003JC002260.

Wong, T., B. A. Wielicki, and R. B. Lee III, 2006: Re-examination of the observed decadal variability of earth radiation budget using altitude-corrected ERBE/ERBS Nonscanner WFOV data. *J. Clim*., in press.

Zhang, Y., J. M. Wallace, and D. S. Battisti, 1997: ENSO-like interdecadal variability: 1900-93. *J. Clim*., **10**, 1004-1020.Banks, H., and R. Wood, 2002: Where to look for anthropogenic climate change in the ocean. *J. Climate*, **15**, 879-891.

Equatorial Pacific Ocean Variability (El Niño)

Michael J. McPhaden
NOAA/Pacific Marine Environmental Laboratory, Seattle, WA

A weak El Niño developed in the equatorial Pacific during the second half of 2004 and ended in March 2005. Anomalous warming was for the most part centered around the international date line, with near normal sea surface temperatures (SSTs) prevailing most of the time in the far eastern eastern Pacific and along the west coast of South America. SST anomalies in the NINO3.4 index region (5°N-5°S, 120°-170°W) were approximately 0.6°C on average from July 2004 to February 2005, with peak seasonal values of 0.8°C during August to December 2004. The Southern Oscillation Index (SOI), which is the normalized surface air pressure difference between Darwin, Australia, and Tahiti, French Polynesia, was on average –1.0 from July 2004 to February 2005. The trade winds were unusually weak west of the date line associated with the elevated central and western Pacific SSTs and negative SOI values throughout much of 2004 and early 2005. These oceanic and atmospheric anomalies were consistent with warm phase El Niño/Southern Oscillation (ENSO) conditions. The equatorial Pacific subsequently returned to near normal as surface wind, SST, and thermocline depth anomalies weakened after February 2005. Conditions remained near-normal until late in the year, when weak La Niña-like SST anomalies developed in the eastern Pacific and the trade winds became anomalously strong in the central and western Pacific (Fig. 1).

The 2004-05 El Niño was characterized by significant month-to-month variability in both the ocean and the atmosphere. The SOI for example was highly variable during the event, ranging from 0.3 in January 2005 to –4.1 in February 2005. The very low SOI value in Febuary 2005, the lowest since February 1983 during the 1982-83 El Niño, was associated with a category-5 tropical cyclone (Percy). Surface westerly wind anomalies near the equator during this storm were the strongest of any period in 2004-05 (Fig. 1). The

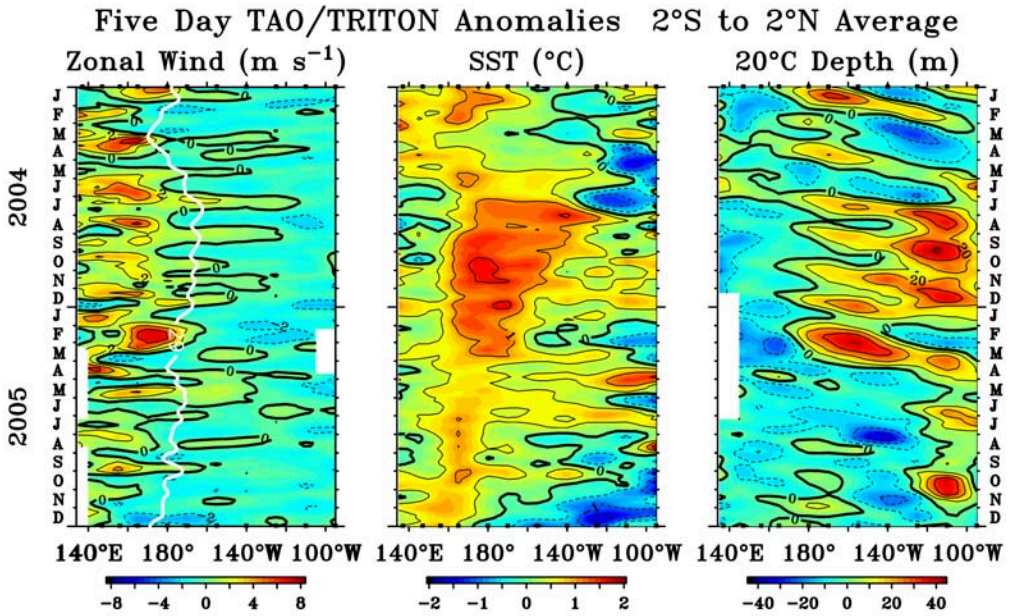

Fig. 1. Five-day average anomalies of zonal wind, SST, and 20°C depth (an index for the depth of the thermocline) relative to the mean seasonal cycle averaged 2°N–2°S based on TAO/TRITON moored time series data. White line on the zonal wind anomaly panel indicates the 29°C isotherms which marks the eastern edge of the western Pacific warm pool. Ticks on the horizontal axis indicate longitudes sampled at the start (top) and end (bottom) of record.

Madden-Julian Oscillation (MJO), initiated as convective flare-ups over the Indian Ocean and subsequently propagating eastward into the western Pacific, also contributed to the month to month variability in atmospheric and oceanic indices. The westerly phase of the MJO was linked to 2-3 week long westerly wind bursts in the western Pacific, which forced eastward propagating downwelling intraseasonal equatorial Kelvin waves. These waves deepened the thermocline in the eastern Pacific by 20-30 m and lead to warming of eastern Pacific SSTs, though this warming did not always persist beyond the passage of individual the Kelvin waves (Fig. 1).

An unusual feature of this event was that excess heat content along the equator, typically a precursor to subsequent ENSO SST anomaly development (Jin, 1997; Meinen and McPhaden, 2000), did not precede but rather developed in phase with NINO3.4 SST anomalies during 2004-05 (Fig. 2). The lack of a subsurface heat content precursor may account for the relative weakness of the 2004-05 El Niño and the difficulty in predicting its onset (Lyon and Barnston, 2005) since such precursors are indicative of large-scale deterministic processes controlling the evolution of ENSO. More prominent in relative terms was the influence of stochastic forcing associated with weather variability during the 2004-05 El Niño. The state of the climate report for 2004 (Levinson et al, 2005) provides additional information on the interplay between large-scale ocean-atmosphere dynamics and stochastic forcing during the onset and early evolution of the 2004-05 El Niño. By the end of 2005, the excess equatorial heat content prevalent during most 2004-05 had disappeared in association with the onset of cold La Niña conditions (Fig. 2).

During the 2004-05 El Niño, deep atmospheric convection was highly variable in the along the equator in the western and central Pacific, and persistent anomalous rainfall that characterizes mature warm phase ENSO conditions failed to develop near the date line except in February 2005. The relative absence of such persistent anomalous atmospheric convection indicated that the ocean and atmosphere were only weakly coupled during this event. As a result, the El Niño had only limited global climatic impacts. Those impacts included below normal rainfall in Indonesia, the Philippines, and portions of South Africa and Central America in the last quarter of 2004 and January 2005 (Lyon and Barnston, 2005). Likewise, the failure of persistent warm SST

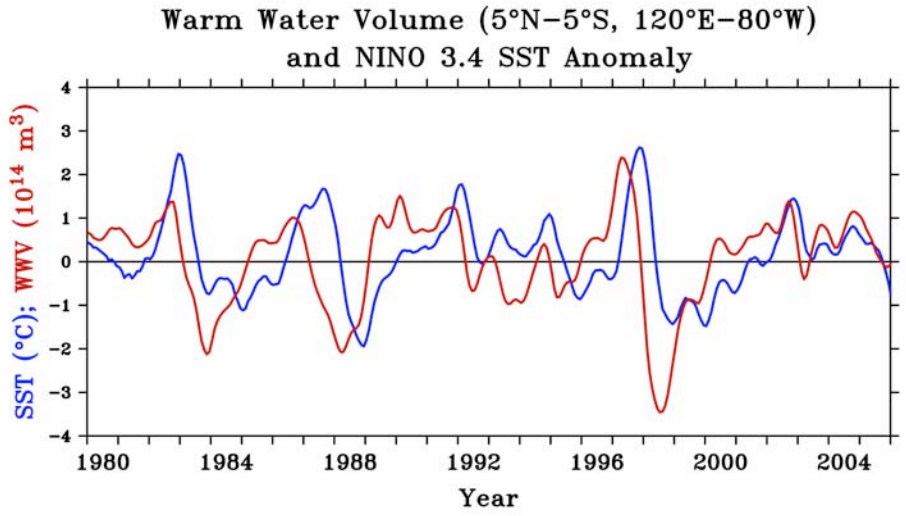

Fig. 2. Monthly anomalies of NINO3.4 SST and warm water volume (WWV) from January 1980 to December 2005. WWV, which is an index of heat content along the equator, is based on a blended thermal field analysis of TAO/TRITON moored time series data and ship-of-opportunity expendable bathythermograph (XBT) data integrated over the region 5°N–5°S, 80°W–120°E above the 20°C isotherm. NINO3.4 SST represents an average anomaly over the region 5°N–5°S, 120°W–170°W. Time series have been smoothed with a 5-month running mean filter for display.

anomalies to develop in the eastern equatorial Pacific and along the west coasts of the Americas limited the effects of this El Niño on marine ecosystems in those regions.

Weak warm SST anomalies in the equatorial Pacific, their concentration in the central basin, the weakness of equatorial ocean-atmosphere coupling, and the relatively muted impacts of Pacific SST anomalies on the global climate system lead to considerable controversy in the scientific community as to whether 2004-05 should be classified as an El Niño. Conditions in the Pacific met the definition for El Niño according to the criterion recently formulated by the National Centers for Environmental Prediction (NCEP), namely five consecutive overlapping 3-month seasons with NINO3.4 SST $\geq$ 0.5°C. However, this definition is not universally agreed upon, either because it is focused on a single region or defined only in terms of SST. Some putative impacts of this El Niño have likewise been actively debated, such as unusual dryness in the Pacific Northwest and extraordinarily rainy conditions in the Southwestern U.S. during boreal winter 2004-05.

The first two El Niños of the 21st century followed on the heels of a protracted, strong La Niña during 1998-2001, and were of moderate (2002-03) and weak (2004-05) intensity. This raises the question of whether the Pacific Decadal Oscillation (PDO) (Mantua et al, 1997) may be affecting the ENSO cycle. It has been argued (e.g. Peterson and Schwing, 2003) that the PDO shifted phase from positive to negative in the late 1990s, with the negative phase characterized by stronger than normal trade winds and colder than normal equatorial cold tongue SSTs. These conditions, which would favor weaker El Niño SST anomalies, have been observed in the tropical Pacific on average since the late 1990s (McPhaden and Zhang, 2004). Thus, a decadal change in background state may have contributed to the weakness of the 2004-05 El Niño, though the details of how ENSO and the PDO may interact with one another are not well understood at present.

References

Jin, F.F., 1997: An equatorial recharge paradigm for ENSO. Part I: Conceptual model. *J. Atmos. Sci.*, **54**, 811-829.

Levinson, D.H., et al, 2005: State of the Climate in 2004. *Bull. Am. Meteor. Soc., 86*(6), S1-S86.

Lyon, B., and A. G. Barnston, 2005: The evolution of the weak 2004-2005 El Niño. U.S. CLIVAR Variations, 3(2), US CLIVAR Office, Washington, DC, 1-4.

Mantua, N. J., S. J. Hare, Y. Zhang et al., 1997: A Pacific interdecadal oscillation with impacts on salmon production, Bull. Am. Meteorol. Soc., 76, 1069– 1079.

McPhaden, M.J. and D. Zhang, 2004: Pacific Ocean circulation rebounds. *Geophys. Res. Lett., 31*, L18301, doi:10.1029/2004GL020727.

Meinen, C.S. and M.J. McPhaden, 2000: Observations of warm water volume changes in the equatorial Pacific and their relationship to El Niño and La Niña. *J. Clim., 13*, 3551-3559.

Peterson, W. T., and F. B. Schwing, 2003: A new climate regime in the northeast Pacific Ocean, Geophys. Res. Lett., 30(17), 1896, doi:10.1029/2003GL017528.

Arctic Ocean and Sea Ice

Jackie Richter-Menge[1], Andrey Proshutinsky[2], Jean Claude Gascard[3], Michael Karcher[4], Jim Maslanik[5], Jamie Morison[6], Don Perovich[1], Ignatius Rigor[6] and Julienne Stroeve[7]
[1]ERDC-Cold Regions Research and Engineering Laboratory, Hanover, NH
[2]Woods Hole Oceanographic Institute, Woods Hole, MA
[3]Universite Pierre et Marie Curie, Paris, France
[4]Alfred Wegner Institute, Bremberhaven, Germany
[5]University of Colorado, Boulder, CO
[6]Polar Science Center, Applied Physics Laboratory, University of Washington, Seattle, WA
[7]National Snow and Ice Data Center, Boulder, CO

Introduction

The permanent presence of sea ice is a unique feature of the polar oceans. The Arctic is further distinguished because it sustains a human population in a harsh environment. These characteristics amplify the impact of global climate change on both the regional physical and societal systems. These impacts reach beyond the Arctic region. For instance, studies are underway to determine the extent to which the loss of sea ice cover over the last two decades has impacted multi-year persistence in the surface temperature fields, especially in the Pacific sector.

In this report we provide observations that indicate continuing trends in the current state of physical components of the Arctic system, including the ocean and sea ice cover. The temporal extent of the data provides a multi-decadal prospective and confirms the sensitivity of the Arctic to changes in the global climate system. The destabilization of several known relationships between climate indices (e.g. Arctic Oscillation (AO)) and Arctic physical system characteristics (e.g. continued reduced state of the sea ice cover) presents an intriguing and significant puzzle with respect to the contemporary global climate system.

Ocean Circulation

Data from satellites and drifting buoys indicate that the circulation of the ocean surface layer has been characterized by an anticyclonic regime for the entire 2000-2005 period (Figure 1, top panel). The anticyclonic regime is the result of a higher sea level atmospheric pressure over the Arctic Ocean, relative to the 1948-2005 mean, and the prevalence of anticyclonic winds. The dominance of the anticyclonic circulation regime of the ocean surface layer is consistent with the AO index which has exhibited relatively low and fluctuating values since 1996 (Figure 2).

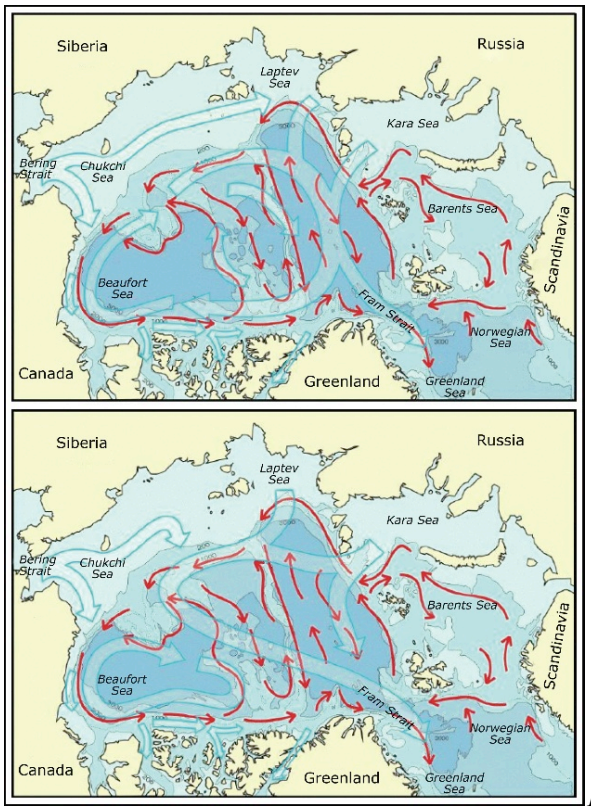

Figure 1. Idealized patterns of the dominant circulation regimes of the Arctic Ocean. Two circulation regimes of surface waters (anticyclonic – top, and cyclonic – bottom) are shown in wide blue arrows. In the cyclonic regime the clockwise circulation pattern in the Beaufort Sea region (Beaufort Gyre) weakens and the flow across the basin, from the Siberian and Russian coasts to the Fram Strait (Transpolar Drift), shifts poleward. The cyclonic pattern dominated during 1989-1996; the anticyclonic pattern has prevailed from 1997-present. The Atlantic water circulates cyclonically (red arrows) at approximately 200-800 m depth, independent of the circulation of the surface layer. (Adapted from Proshutinsky et al., 2005)

Climatological studies (e.g. Proshutinsky and Johnson, 1997) provide a foundation for understanding the significance of these ocean surface conditions. These studies indicate that the Arctic atmosphere and ocean surface layer motion alternates between cyclonic and anticyclonic circulation regimes, with each regime persisting from 4 to 8 years and resulting in a period of 8-16 years. Figure 1 illustrates idealized patterns of the two dominant wind-driven circulation regimes: anticyclonic and cyclonic. The cyclonic pattern dominated during the period 1989-1996 and the anticyclonic pattern has prevailed from 1997-present. Identification of the current or prediction of the future circulation regime is important because each regime is characterized by a set of environmental parameters that impact human activity in the Arctic. Atmospheric, ice and oceanic observational data, along with the results of numerical coupled ice-ocean models, provide evidence that during anticyclonic circulation regimes, compared to the cyclonic regimes, the arctic atmospheric pressure is higher, wind speed is lower, winter temperatures are colder, ocean waters are fresher, sea ice areal coverage is greater, and sea ice is thicker. When the cyclonic circulation regime dominates, the transport of sea ice from the Arctic Ocean increases, summer wind divergence produces more openings in the sea ice, allowing the upper ocean to accumulate heat. In addition, under a cyclonic circulation regime advection of heat with air masses to the Arctic also increases. This positive heat anomaly extends the ice melt season and leads to generally thinner ice. This description of oceanic and atmospheric conditions is consistent with environmental characteristics described by Thompson and Wallace (1998), who introduced the AO index. Figure 2 shows that during 2000-2005, the AO index fluctuated between positive and negative values and, on average, was relatively low. These recent characteristics correspond to the mean climatology, typified by a cold arctic and anticyclonic circulation regime as seen in Figure 2 prior to 1989.

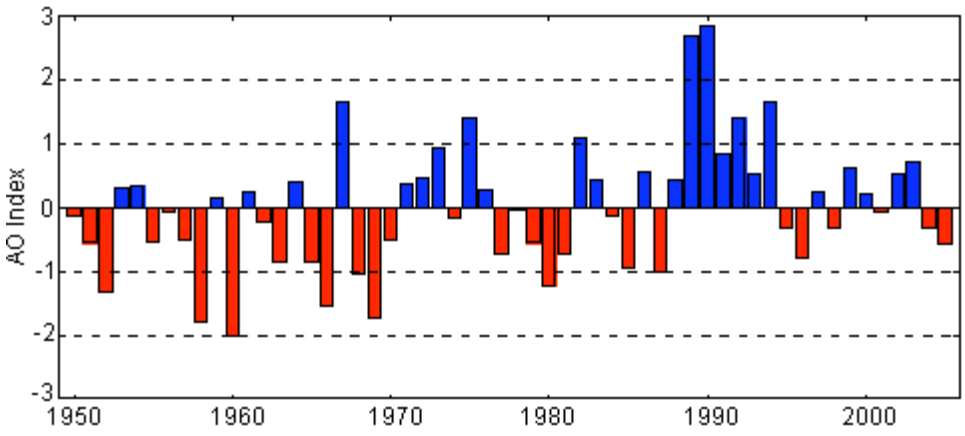

Figure 2. Time series of the annually-averaged Arctic Oscillation Index (AO) for the period 1950 – 2005, based on data from the website www.cpc.ncep.noaa.gov.

The circulation of Pacific water (located at the depths between 50 and 200 m) in the Arctic Ocean may be coherent with the surface currents but its pathways are not known from direct observations. Recently the vertical structure of this layer and its properties have been revised by Shimada et al. (2001) and Steele et al. (2004), where the presence of two types of summer Pacific halocline water and one type of winter Pacific halocline water in the Arctic Ocean were reported. According to the Environmental Working Group (EWG) analysis (EWG, 1997), the total thickness of the Pacific layer is approximately 150 m. This thickness is subject to temporal variability (McLaughlin et al., 2003) depending on wind stresses and circulation modes (Proshutinsky et al., 2002). Steele et al. (2004) found similar evidence in their examination of data from the 1980s and 1990s. The most recent studies by Shimada et al. (2006) and Maslowski (2006) speculate that the significant reduction of sea ice in the Canadian Basin observed in 2002-2005 (see Figure 10) is due to an increase of heat flux from the Pacific water layer to the bottom of sea ice which resulted in sea ice melt. Warming of the Pacific water is associated with the increase of heat flux via Bering Strait. In this region, preliminary observations from a mooring site, established and maintained since 1990, suggest that that annual mean water temperatures have been about a degree warmer since 2002, compared to 1990-2001(Woodgate, Aagaard and Weingartner, pers.comm., 2006). Since 2001, there has also been an increase in the annual mean water transport. Changes in the Pacific water circulation may also influence heat release from the Pacific water to the upper ocean layers.

The Atlantic water circulates in the Arctic Ocean at approximately 200-800 m depth. This water penetrates to the Arctic via Fram Strait and St. Anna Trough (Barents Sea). Under extensive surface cooling it sinks to intermediate depths and forms the warm Atlantic Layer with water temperature greater than 0°C. This layer is covered by low density surface waters and is thus prevented from undergoing heat exchange with the atmosphere. The most widely-accepted circulation scheme of

Atlantic water (Rudels et al., 1994) postulates that it circulates counterclockwise, forming several loops (Figure 1, red arrows) in the Arctic basins. Variability of the Atlantic water circulation pattern is not known from observations but model results show that its circulation has a pulsating character expressed in the propagation of warm and cold events, changing from seasonal to decadal time scales. An increase of the Atlantic water temperature in the Fram Strait and the Laptev Sea was observed in 2004 (Polyakov et al., 2005).

Heat and freshwater content

The heat and freshwater content of the Arctic Ocean are important integrated parameters and are indicative of the potential role of the Arctic Ocean in the global climate system. For example, the meridional overturning circulation in the Atlantic Ocean, an important component of the global ocean circulation, is significantly influenced by freshwater fluxes from the Arctic Ocean. It is suggested that the Arctic Ocean accumulates fresh water during anticyclonic circulation regimes and releases this water to the North Atlantic during cyclonic circulation regimes. The Beaufort Gyre (illustrated in Figure 1 by the closed clockwise circulation pattern in the Beaufort Sea region) is the major reservoir of fresh water in the Arctic Ocean and its dynamics (accumulation or release) is responsible for freshwater fluxes to the Atlantic Ocean. The heat content of the Arctic Ocean is potentially responsible for the sea ice melt and the Arctic atmosphere warm up. However, under the existing ocean state the majority of this heat is trapped in the Atlantic water layer and does not affect sea ice conditions. A change in the ocean vertical stratification or the ocean circulation could result in the release of this heat which could cause massive melting of the Arctic sea ice cover and, perhaps, even its disappearance.

From 2000 to 2005, the most complete observational data available to analyze changes in the freshwater and heat content of the Arctic Ocean are the intensive investigations conducted in the vicinity of the North Pole (North Pole Environmental Observatory, NPEO, Morison et al. (2002), http://psc.apl.washington.edu/northpole/) and the Western Arctic (Beaufort Gyre Observing System, BGOS, http://www.whoi.edu/beaufortgyre/index.html). Hydrographic data acquired in the North Pole region in the 1990s show a strong increase in upper ocean salinity relative to the Environmental Working Group Atlas of the Arctic Ocean (EWG, 1997) climatology (Figure 3, left panel), where water temperature and salinity from observations were averaged and gridded for the decades of 1950, 1960, 1970 and 1980. This increase was associated with a more cyclonic Arctic Ocean circulation in the 1990s. Under this condition, the fresh water from river runoff tended to circulate along ocean boundaries (see Figure 1, right panel, wide blue lines)

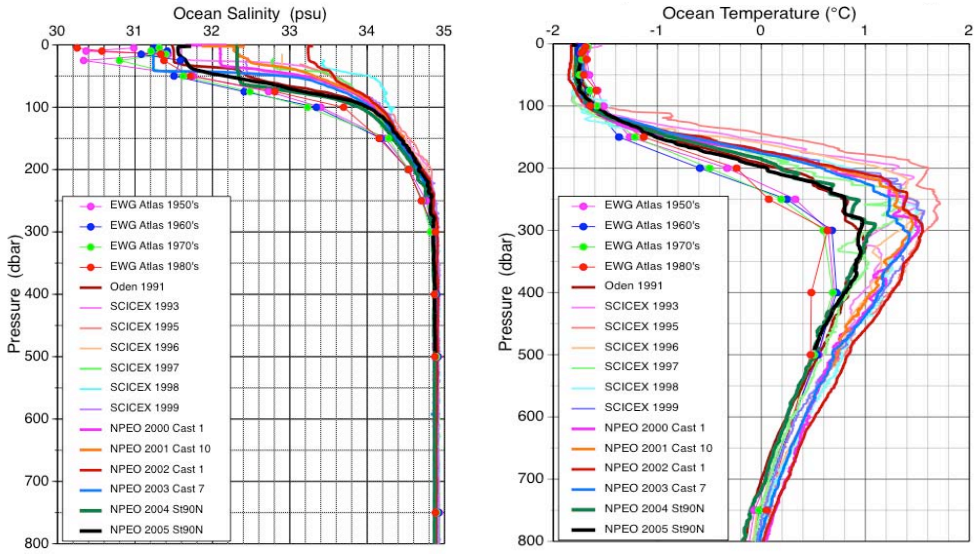

Figure 3. North Pole hydrography 1991-2005 (lines) compared with EWG climatology (lines with circles); left: salinity, right: temperature.

resulting in the decrease of salinity along coastlines and salinity increase in the central Arctic (North Pole). The NPEO-data also show a large increase in Atlantic Water temperature at depth relative to the EWG climatology (Figure 3m, right panel). This was also consistent with the cyclonic circulation regime conditions in the 1990s when more Atlantic water penetrated to the Arctic Ocean and, correspondingly, there was an increase in Atlantic water temperature. Hydrographic measurements made by the NPEO show that the conditions since 2000 have relaxed toward the pre-1990 climatology, but some changes still at least partially persist.

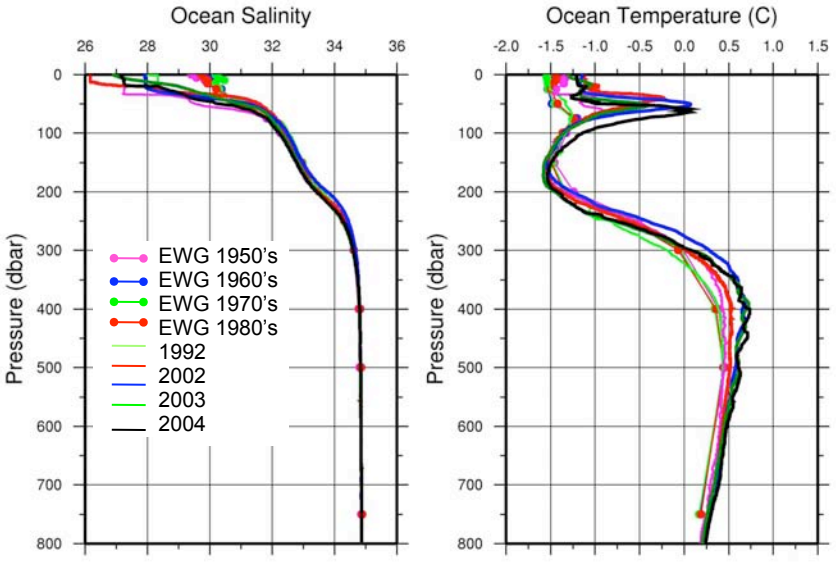

Figure 4. The Beaufort Gyre hydrography 1991-2005 (lines) compared with EWG climatology (lines with circles) for the vicinity of 75N and 150W; left: salinity, right: temperature.

The Beaufort Gyre (the major freshwater reservoir in the Arctic Ocean) hydrography has also changed dramatically relative to the 1990s (Figure 4). The results of several hydrographic surveys in this region in the 1990s compared to the EWG data indicate that, in opposition to the salinity increase at the North Pole, the salinity of the upper layer in the Beaufort Gyre was significantly reduced in the 1990s (Figure 4, left panel). This is a consequence of both sea ice melt during Arctic warming in the 1990s and the addition of fresh water from Siberian rivers. The shift in the pattern of fresh water transport is consistent with the presence of cyclonic winds, which redirect the ocean surface flow of fresh water from the Russian and Siberian coasts along the Siberian Seas to the Beaufort Sea. Under anticyclonic winds, this fresh water flows towards the Fram Strait (compare left and right circulation patterns in Figure 1, wide blue arrows). In the 2000s relative to 1990s, the salinity in the Beaufort Gyre was increased but was still approximately 1 unit less than the EWG climatology. There was also a very small salinity decrease in the 50-300 meter layer of the ocean but this change was within the range of interannual variability. Interestingly, the total freshwater content in the Beaufort Gyre in the 2000s has not changed dramatically relative to climatology but there has been a significant change in the freshwater distribution (Figure 5, panels 3 and 4). The center of the freshwater maximum has shifted toward Canada and significantly intensified relative to climatology.

In the 1990s, the water temperature in the Beaufort Gyre increased significantly relative to EWG data (Figure 4, right panel). As discussed in section 2.1, the most pronounced warming (up to 1°C) was observed in the Pacific water layer (50-100m), but the maximum heat accumulation was observed in the Atlantic waters between 200 and 800 meter layer. These waters, propagating cyclonically from the Fram Strait (Figure 1, red arrows), reached the Beaufort Sea in the late 1990s – much later than when they reached the North Pole. The combination of warming water temperatures and a change in the circulation pattern resulted in a significant increase of the heat content in the Beaufort Gyre in the 2000s relative to the EWG climatology and observations made in the beginning of the 1990s (Figure 5, panels 1 and 2).

Sea Level

Figure 6 shows sea level time series from several coastal stations in the Siberian Seas. There is a positive sea level trend along the arctic coastlines. From 1954-1989 the rate of sea level rise was estimated as 0.185 cm/year (Proshutinsky et al., 2004). Adding 1990-2004 data increases the estimated rate to 0.191 cm/year. Sea level time series correlates relatively well

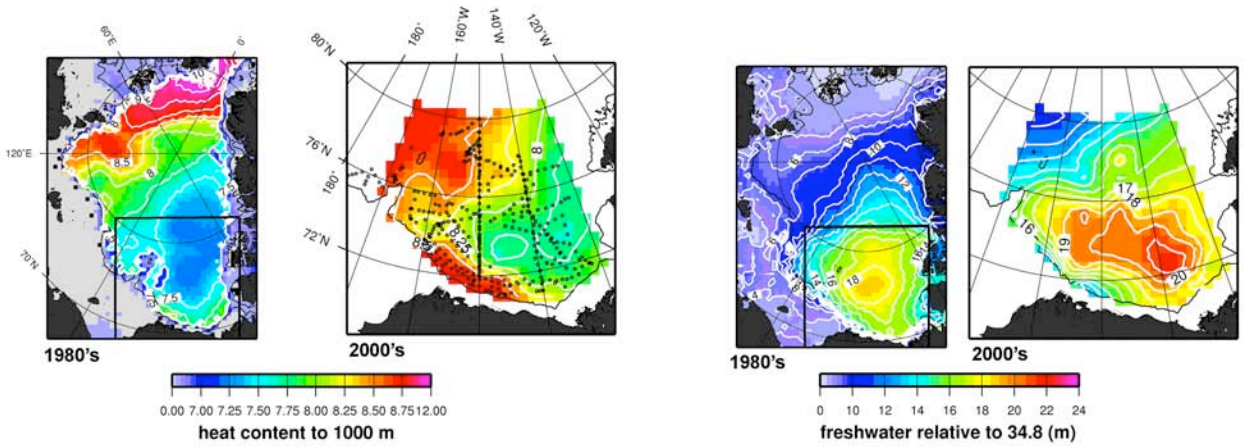

Figure 5. Summer heat (10^9 J/m^2, left) and freshwater (m, right) content. Panels 1 and 3 show heat and freshwater content in the Arctic Ocean based on 1980s climatology (EWG, 1998). Panels 2 and 4 show heat and freshwater content in the Beaufort Gyre in 2000-2005 based on hydrographic surveys (black dots depict locations of hydrographic stations). For reference, this region is outlined in black in panels 1 and 3. The heat content is calculated relative to the water temperature freezing point in the upper 1000m ocean layer. The freshwater content is calculated relative to reference salinity of 34.8.

with the AO index (correlation coefficient is 0.83). Consistent with the influences of AO-driven processes, sea level dropped significantly after 1990 and increased after the circulation regime changed from cyclonic to anticyclonic in 1997. In contrast, from 2000 to 2004 the sea level rise rate has increased in spite of a steady decrease of the AO index. At this point, because of the large interannual variability, it is difficult to evaluate the significance of this change.

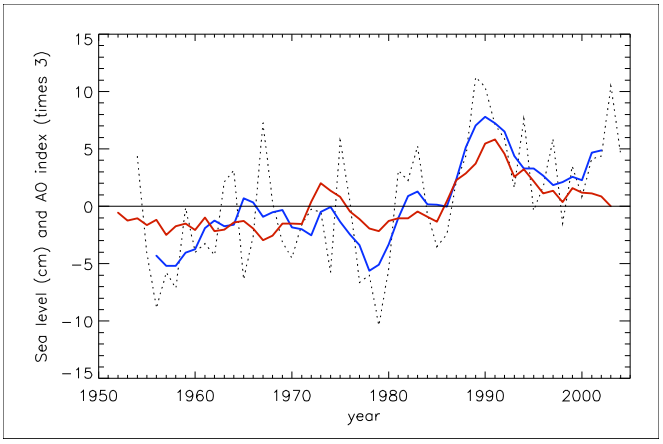

Figure 6. Annual mean relative sea level from 9 tide gauge stations in the Siberian Seas (dotted line). The blue line is the 5-year running mean sea level. The red line is the 5-year running mean AO index.

Sea Ice Cover - Extent and Thickness

During 2005 every month, except May, showed record minima sea ice extent in the Northern Hemisphere for the period 1979-2005. The extent of the sea ice cover is typically at or near its maximum in March and its minimum in September. The ice extent in March 2005 was 14.8 million km^2. In September 2005 the ice extent was 5.6 million km^2. In comparison, the mean ice extent for March and September, for the period 1979-2005, was 15.7 million km^2 and 6.9 million km^2, respectively (Figure 7). It is notable that in March 2005 the ice extent fell within the mean contour at almost every location. In September 2005, the retreat of the ice cover was particularly pronounced along the Eurasian and North American coastlines.

To put the 2005 minimum and maximum ice extent into context, the time series of the variability of ice extent in March and September for the period 1979-2005 are presented in Figure 8. In both cases, a negative trend is apparent, with a rate of 2% per decade for March and 7% per decade for September. The summers of 2002-2005 have marked an unprecedented series of extreme ice extent minima (Stroeve et al., 2005).

The state of the sea ice cover is intrinsically linked to the state of the ocean and atmosphere. This is confirmed by the observation that during this same period (1978-2005), the annual surface temperatures over land areas north of 60° N have generally been rising and

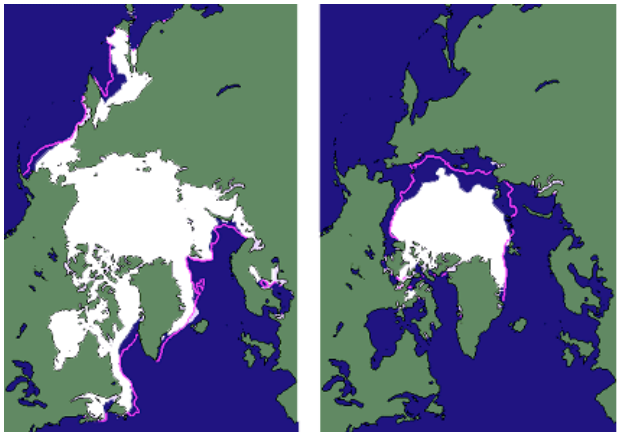

Figure 7. Sea ice extent in March and September 2005, when the ice cover was at or near its maximum and minimum extent, respectively. The magenta line indicates the median maximum and minimum extent of the ice cover, for the period 1979-2000. In both cases, the ice extent reached a record minimum in 2005, for the period 1979-2005. (Courtesy of National Snow and Ice Data Center, NSIDC)

have been above the mean value for the 20th century since the early 1990s (Figure 9).

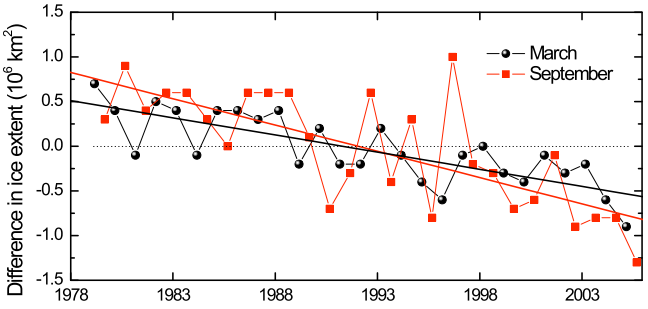

Figure 8. Time series of the difference in ice extent in March (maximum) and September (minimum) from the mean values for the time period 1979-2005. Based on a least squares linear regression, the rate of decrease in March and September was 2% per decade and 7% per decade, respectively.

Ice thickness is intrinsically more difficult to monitor, compared to ice extent. With satellite-based techniques (Laxon et al., 2003; Kwok et al., 2004) only recently introduced, observations have been spatially and temporally limited. Data from submarine-based observations, indicate that at the end of the melt season the permanent ice cover (ice located towards the center of the Arctic basin that survives is present all year round; see Figure 7, right panel) thinned by an average of 1.3 m between

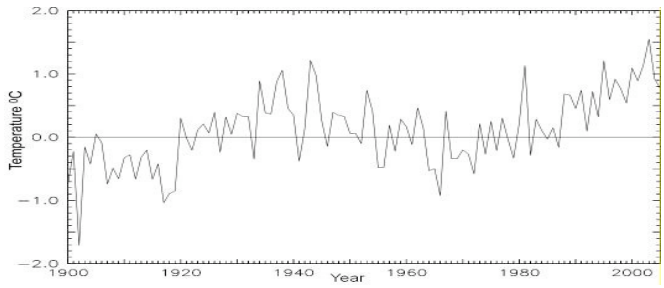

Figure 9. Arctic-wide and annual averaged surface air temperature anomalies (60° – 90° N) over land for the 20th century based on the CRU TEM2V monthly data set (courtesy of J. Overland).

the period 1956-1978 and the 1990s, from 3.1 m to 1.8 m (Rothrock et al., 1999). On the other hand, measurements of the seasonal ice cover (ice around the periphery of the Arctic basin that melts during the summer) do not indicate any statistically significant change in thickness in recent decades (Melling et al., 2005; Haas, 2004; Polyakov et al., 2003).

The trends in the extent and thickness of the cover are consistent with observations of a significant loss of older, thicker ice out of the Arctic via the Fram Strait (e.g. Rigor and Wallace, 2004; Pfirman et al., 2004; Yu et al., 2004) in the late 1980s and early 1990s (Figure 10). This event coincides with the strong, positive AO period which extended from 1989-1995 (see Figure 2). When the AO is positive, atmospheric and oceanic conditions favor a thinner ice cover. A relatively younger, thinner ice cover, like the one left behind from this event, is intrinsically more susceptible to atmospheric or oceanic warming. It is of great interest to observe whether the sea ice cover will continue its decline or rebound under the recent more neutral AO conditions.

Sea Ice Surface Conditions

Data from 1982-2004, derived from Advanced Very High Resolution Radiometer (AVHRR) Polar Pathfinder extended (APP-x) products (updated from Wang and Key, 2005a,b), indicate an overall negative trend for summer (June-August) mean albedo of –0.4%/year (Figure 11a). The trend increases slightly to –0.5%/year for the period from April through September (Figure 11b), suggesting a possible increase in the duration of the melt season. In both cases, the surface albedo is relatively low from 2001 to 2004 and is consistent with observations of an earlier, more spatially extensive onset of melt and decreases in ice concentration (Belchansky et al., 2004; Stroeve et al., 2005).

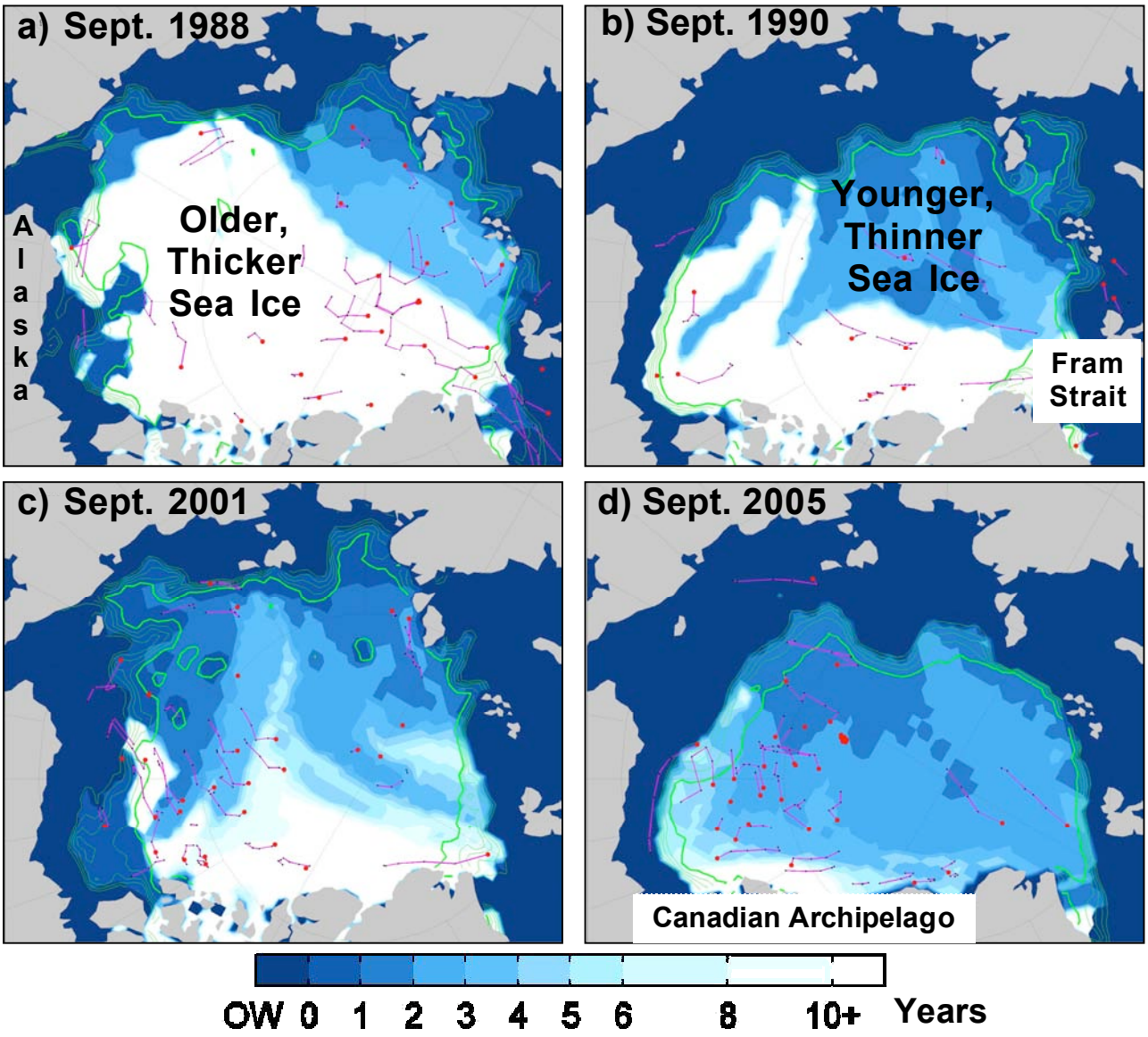

Figure 10. Change in the age of ice on the Arctic Ocean, compared for September and based on results from a simulation using drifting buoy data and satellite-derived ice concentration data (Rigor and Wallace, 2004). Open water (OW) is shown in dark blue and the oldest ice is shown in white. The darker green line marks 90% ice concentration and the lighter green lines mark ice concentrations of 80, 70, 60 and 50%. This sequence shows (a) most of the Arctic Ocean was covered by older, thicker sea ice in Sept. 1988; (b) coincident with a transition to high AO conditions in 1989 (see Fig. 2) most of the older, thicker sea ice was rapidly flushed out of Arctic Ocean through Fram Strait, so that by 1990 only 30% of the Arctic Ocean was covered by older, thicker sea ice; (c) persistence of the relative distribution between older thicker and younger, thinner sea ice during the 1990's, in spite of a shift back towards a more neutral AO condition in the mid-1990's; and d) extension of this work through 2005, suggesting a continued decrease in the average ice age over the Arctic Ocean, with older, thicker ice now limited to the area north of the Canadian Archipelago.

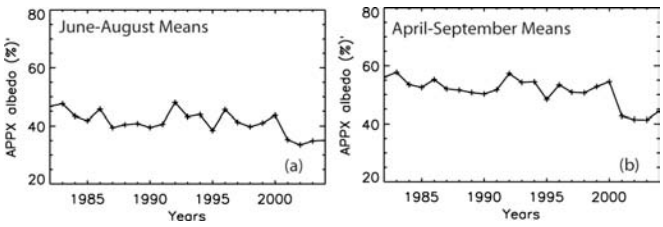

Figure 11. Time series of APP-x surface albedo for areas between 60° – 90° N and with ice concentrations of 15-100%. (a) Means averaged over June-August. (b) Means averaged over April-September.

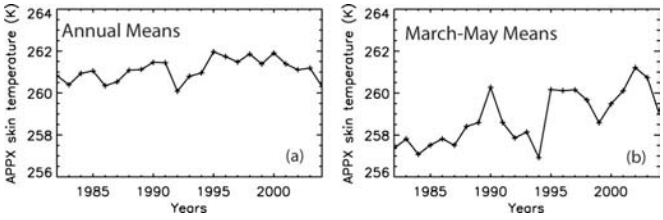

Figure 12. Time series of APP-x skin temperatures for areas between 60° – 90° N and with ice concentrations of 15-100%. (a) Means averaged over 12 months. (b) Means averaged over March-May.

The time series of APP-x annual mean skin temperatures (Figure 12a) over the same period shows less consistent change over time, with a general increase in annual mean temperatures through the early 1990's and a decrease from 1995 onward. When the time series is limited to spring (March-May) temperatures the 23-year linear trend is positive (0.14K/year), with greater interannual variability (Figure 12b), indicative of the seasonal dependence of warming trends.

Large regional variability, typical of arctic conditions, is observed in albedo, skin temperature and ice concentration (Cavalieri et al., 1997). From 1996-2004, the largest decreases in surface albedo correspond to a reduction in ice extent in the Beaufort and Chukchi seas, while lower albedos over the central ice pack appear consistent with the lower total ice concentrations over this same period. It remains to be determined how much of the albedo change is due to the presence of more open water vs. more extensive ice-surface melt and ponding. In either case, the changes represent significant modifications of the ice pack.

.

References

Belchansky, G.I., D.C. Douglas and N.G. Platonov (2004) Duration of the Arctic sea ice melt season: Regional and interannual variability, J. Climate, 17(1): 67-80.

Cavalieri, D., C. Parkinson, P. Gloerson, and H.J. Zwally (1997, updated 2005) Sea ice concentrations from Nimbus-7 SMMR and DMSP SSM/I passive microwave data, June to September 2001. Boulder, CO, USA: National Snow and Ice Data Center. Digital media.

Environmental Working Group (EWG), Arctic Climatology Project (1997) /Environmental Working Group joint U.S.-Russian atlas of the //Arctic Ocean// - winter period/. Edited by L. Timokhov and F. Tanis. Ann Arbor, MI: Environmental Research Institute of Michigan in association with the National Snow and Ice Data Center. CD-ROM.

Haas, C. (2004) Late-summer sea ice thickness variability in the Arctic Transpolar Drift 1991--2001 derived from ground-based electromagnetic sounding, *Geophys. Res. Let.*, 31(L09402), doi: 10.1029/2003GL019394.
Kwok, R., H.J. Zwally and D. Yi (2004) ICESat observations of Arctic sea ice: A first look, *Geophys. Res. Let.*, 31(L16401), doi: 10.1029/2004GL020309.

Laxon, S., N. Peacock and D. Smith (2003) High interannual variability of sea ice thickness in the Arctic Region, *Nature*, 425, 947-950.

Maslowski, W., J. L. Clement, W. Walzowski, J.S. Dixon, J. Jakacki, T. P. McNamara (2006) Oceanic forcing of Arctic sea ice at Gateways and Margins of Pacific and Atlantic water inflow, *Eos Trans. AGU*, 87(36), Ocean Sci. Meet. Suppl., Abstract OS32P-05.

McLaughlin, F., E. Carmack, R. W. MacDonald, A. J. Weaver, and J. Smith (2003) The Canada Basin 1989-1995: Upstream events and far-field effects of the Barents Sea, J. of Geophys. Res., 107(C7): 3233, doi:10.1029/2002JC001537.

Melling, H., D. A. Riedel, and Z. Gedalof (2005), Trends in the draft and extent of seasonal pack ice, Canadian Beaufort Sea, *Geophys. Res. Lett.*, 32(L24501), doi:10.1029/2005GL024483.

Morison, J. H., K. Aagaard, K. K. Falkner, K. Hatakeyama, R. Moritz, J. E. Overland, D. Perovich, K. Shimada, M. Steele, T. Takizawa, R. Woodgate (2002)

North Pole environmental observatory delivers early results, *Eos Trans. AGU*, 83(33), 357, 10.1029/2002EO000259.

Pfirman, S., W.F. Haxby, R. Colony and I. Rigor (2004) Variability in Arctic sea ice drift, *Geophys. Res. Lett.*, 31, L16402, doi: 10.1029/2004GL020063.

Polyakov, I. V., et al. (2005), One more step toward a warmer Arctic, *Geophys. Res. Lett.*, 32, L17605, doi:10.1029/2005GL023740.

Polyakov, I., G. V. Alekseev, R. V. Bekryaev, U. Bhatt, R. Colony, M. A. Johnson, V. P. Karklin, D. Walsh, and A. V. Yulin (2003), Long-term ice variability in arctic marginal seas, *J. Climate*, 16(12), 2078-2085.

Proshutinsky, A., J. Yang, R. Krishfield, R. Gerdes, M. Karcher, F. Kauker, C. Koeberle, S. Hakkinen, W. Hibler, D. Holland, M. Maqueda, G. Holloway, E. Hunke, W. Maslowski, M. Steele, J. Zhang (2005) Arctic Ocean Study: Synthesis of Model Results and Observations, *Eos Trans. AGU*, 86(40), 368, 10.1029/2005EO400003.

Proshutinsky A., I. M. Ashik, E. N. Dvorkin, S. Häkkinen, R. A. Krishfield, W. R. Peltier (2004) Secular sea level change in the Russian sector of the Arctic Ocean, *J. Geophys. Res.*, 109, C03042, doi:10.1029/2003JC002007.

Proshutinsky, A., R. H. Bourke and F. A. McLaughlin (2002) The role of the Beaufort Gyre in Arctic climate variability: Seasonal to decadal time scales, *Geophys. Res. Lets*, 29(23), doi: 10.1029/2002GL015847.

Rigor, I. and J.M. Wallace (2004) Variations in the age of Arctic sea-ice and summer sea-ice extent, *Geophys. Res. Lett*., 31, L09401, doi: 10,1029/2004GL019492.

Proshutinsky, A. Y. and M. A. Johnson (1997) Two circulation regimes of the wind-driven Arctic Ocean, *J. Geophys. Res.*, 102(C6): 12,493–12,514.

Rothrock, D.A., Y. Yu and G.A. Maykut, Thinning of the Arctic sea-ice cover, *GRL*, 26, 3469-3472, 1999.

Rudels, B., E. P. Jones, L. G. Anderson, and G. Kattner (1994) On the intermediate depth waters of the Arctic Ocean. In: The Polar Oceans and Their Role in Shaping the Global Environment: The Nansen Centennial Volume, ed., O. M. Johannessen, R. D. Muench, and J. E. Overland, *American Geophysical Union*, Washington DC 20009, 33-46.

Shimada, K., E. C. Carmack, K. Hatakeyama, and T. Takizawa (2001) Varieties of shallow temperature maximum waters in the western Canadian Basin of the Arctic Ocean, *Geophys. Res. Let*., 28(18), 3441-3444.

Shimada, K., F. McLaughlin, E. Carmack, A. Proshutinsky, S. Nishino, and M. Itoh (2004), Penetration of the 1990s warm temperature anomaly of Atlantic Water in the Canada Basin, *Geophys. Res. Let.*., 31, L20301, doi:10.1029/2004GL020860.

Shimada K., T. Kamoshida, M. Itoh, S. Nishino, E. Carmack, F. McLaughlin, S. Zimmermann, A. Proshutinsky, M. (2006) Influence of Pacific Summer water on the recent anomalous reduction of ice cover in the Arctic Ocean, *Eos Trans. AGU*, 87/(36), Ocean Sci. Meet. Suppl., Abstract OS33N-01.

Steele M., J. Morison, W. Ermold, I. Rigor, M. Ortmeyer, K. Shimada (2004) Circulation of summer Pacific halocline water in the Arctic Ocean, *J. Geophys. Res*., 109, C02027, doi:10.1029/2003JC002009.

Stroeve, J. C., M.C. Serreze, F. Fetterer, T. Arbetter, W. Meier, J. Maslanik, K. Knowles (2005) Tracking the Arctic's shrinking ice cover: Another extreme September minimum in 2004 Geophys. Res. Lett., Vol. 32, No. 4, L04501, doi:10.1029/2004GL021810.

Thompson, D.W.J. and M. Wallace, 1998. The Arctic Oscillation signature in the wintertime geopotential height and temperature fields, *Geophys. Res. Let*., 25(9), 1297-1300.

Yu, Y., G.A. Maykut and D.A. Rothrock (2004) Changes in the thickness distribution of Arctic sea ice between 1958-1970 and 1993-1997, *J. Geophys. Res*., 109(C08004), doi: 10.1029/2003JC001982.

Wang, X and J.R. Key (2005a) Arctic surface, cloud, and radiation properties based on the AVHRR Polar Pathfinder dataset. Part I: Spatial and temporal characteristics. J. Climate, vol. 18, 2558-2574.

Wang, X and J.R. Key (2005b) Arctic surface, cloud, and radiation properties based on the AVHRR Polar Pathfinder dataset. Part II: Recent trends. J. Climate, vol. 18, 2575-2593.

The Global Ocean Carbon Cycle: Inventories, Sources and Sinks

Christopher L. Sabine[1], Richard A. Feely[1] and Rik Wanninkhof [2]
[1]NOAA/Pacific Marine Environmental Laboratory
[2]NOAA/Atlantic Oceanographic and Meteorological Laboratory

Background

The global utilization of fossil fuels is rapidly changing the trace gas composition of the Earth's atmosphere. These "greenhouse gases" play a critical role in controlling the Earth's climate because they increase the infrared opacity of the atmosphere, causing the planetary surface to warm. Carbon dioxide (CO_2) is the major anthropogenic greenhouse gas, contributing about 60% to the total change in radiative forcing due to human perturbations. As of the early 2000s, the release of CO_2 to the atmosphere from burning fossil fuels and cement manufacturing had grown to more than 7 Pg C per year (1Pg = 10^{15}g = 1 billion metric tons) (Marland et al., 2005). Of this amount, approximately 3 Pg C of this so-called "anthropogenic CO_2" accumulates in the atmosphere with distributions that are well documented through a global measurement network. The remaining 4 Pg C is sequestered by the terrestrial biosphere and global ocean. Where and how these two major sink regions (ocean and terrestrial biosphere) vary in their uptake of CO_2 from year to year is the subject of much scientific research (Prentice, 2001). Understanding this partitioning is critical because the ocean is believed to be a long-term sink for anthropogenic CO_2 while the terrestrial sink is more labile.

Several approaches have been used to estimate the ocean uptake of anthropogenic CO_2 for the decade of the 1990s (Table 1). There is a general consensus that the average oceanic sink for the 1980s and 1990s was about 1.9 ± 0.7 Pg C yr^{-1} (Figure 1; Sabine et al., 2004a). Most of these estimates, however, can not be used, a priori, to predict what the future ocean uptake will be or how feedbacks between the ocean carbon system and climate may alter the controls on sea-air CO_2 fluxes. Future policy decisions regarding possible

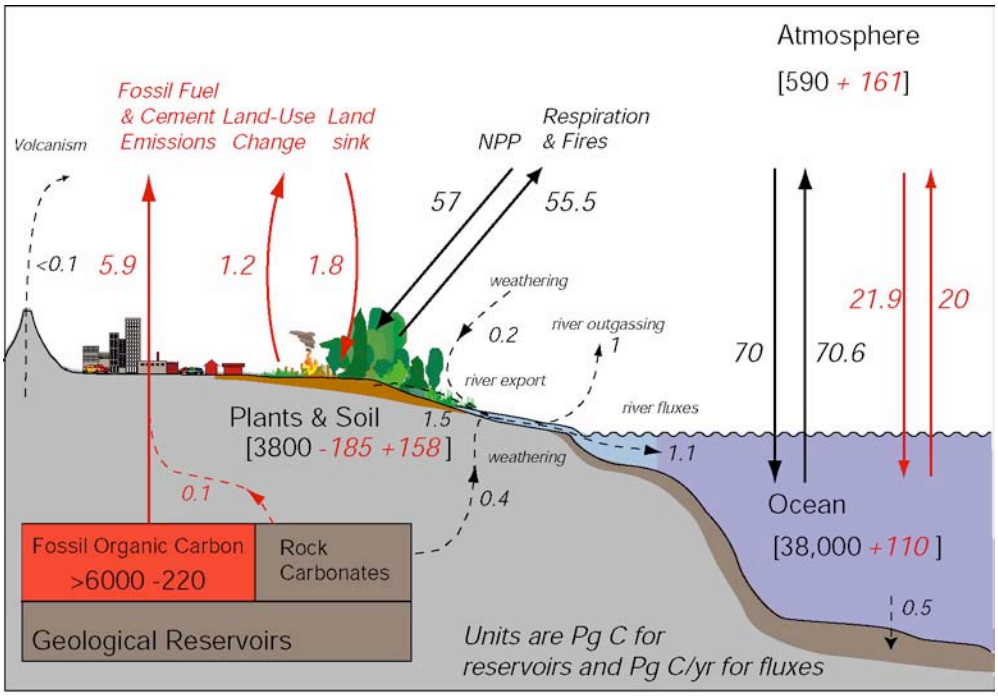

Figure 1. Schematic of global carbon cycle during the 1980s and 1990s. Black arrows represent natural fluxes and red arrows are anthropogenic fluxes (adapted from Sabine et al., 2004a).

Table 1. *Estimates of Oceanic Anthropogenic CO_2 Uptake in Pg C/yr.*

Method	Carbon Uptake (Pg C/yr)	Reference
Measurements of sea-air pCO_2 Difference	2.1 ± 0.5	Takahashi et al. (2002)
Inversion of atmospheric CO_2 observations	1.8 ± 1.0	Gurney et al. (2002)
Inversions based on ocean transport models and observed DIC	2.0 ± 0.4	Gloor et al. (2003)
Model simulations evaluated with CFC's and pre-bomb radiocarbon	2.2 ± 0.4	Matsumoto et al. (2004)
OCMIP-2 Model simulations	2.4 ± 0.3	Orr (2004)
Based on measured atmospheric O_2 and CO_2 inventories corrected for ocean warming and stratification	2.2 ± 0.5	Keeling et al. (2005)
GCM Model of Ocean Carbon	1.93	Wetzel *et al*. (2005)
CFC ages	2.0 ± 0.4	McNeil *et al*. (2003)

Fluxes are normalized to 1990-1999 (except Keeling & Manning which is for 1993-2004) and corrected for pre-industrial degassing flux of ~0.6 Pg C/yr.

greenhouse gas emission controls need to be based on predictive models of CO_2 sources and sinks and these models need to be adequately validated against sustained ocean carbon observing system measurements. Moreover, tracking the increases in ocean carbon content, and the associated ocean acidification, will contribute to an improved understanding of the effects of elevated CO_2 on ocean biota (Feely et al., 2004a; Orr et al., 2005).

Two basic approaches are being used to document changes in the ocean carbon system: 1) repeated trans-basin hydrographic sections (surveys of ocean properties in the water column along a cruise track) provide information on decadal scale changes in ocean inventories and transport within the ocean interior; and 2) high frequency (in space and time) observations of surface ocean and atmospheric CO_2 concentrations that can be used to estimate sea-air exchanges on seasonal to interannual time-scales. These two approaches provide information on ocean carbon changes over a complimentary range of time and space scales. The latest findings from the ocean carbon program are presented here. These findings are placed in context with a growing body of evidence documenting the carbon cycle changes in the ocean.

Ocean Inventories

In the 1990s, researchers from several countries worked together through two international programs, the World Ocean Circulation Experiment (WOCE) and the Joint Global Ocean Flux Study (JGOFS), to conduct an extensive survey of the chemical and physical properties of the global ocean (Feely et al., 2001; Wallace, 2001). An analysis of more than 70,000 carbon measurements from this survey, found that the ocean accumulated approximately 118 Pg C between 1800 and 1994 (Sabine et al., 2004b). This accumulation accounts for 48% of the CO_2 released from burning fossil fuels over this same time period. Because the ocean mixes much more slowly than the atmosphere, more than half of this carbon can still be found in the upper 400 meters (Figure 2). The average penetration depth for CO_2 generated

from human activity is about 1000 meters, roughly one quarter of the average global ocean depth. Most of the ocean volume, therefore, has not been exposed to the higher atmospheric CO_2 concentrations of the industrial era so we would anticipate that the ocean would continue to take up CO_2 for at least the next thousand years.

Because there were no ocean carbon measurements prior to the industrial revolution, the anthropogenic CO_2 component of the total dissolved inorganic carbon (DIC) concentration had to be estimated using a back calculation technique based on our understanding of the physical and biological contributions to the measured DIC. As a consequence, assumptions about steady state circulation and biology over these time scales had to be made. By repeating a subset of the cruises run in the 1990s, many of the assumptions required for the back calculation technique can be avoided and the changes in ocean carbon along a cruise track run at two different times can be directly evaluated.

The U.S. CLIVAR/CO_2 Repeat Hydrography Program started in 2003 with three cruises in the North Atlantic (Figure 3). Analysis of these repeated lines has indicated that several biogeochemical parameters are changing with time (Feely et al., 2005a). For example, changes of -10 to +30 μmol kg^{-1} of DIC have been observed in the upper 1000 m of the water column between the 1993 and 2003 occupations of A16N along 25°W in the North Atlantic (Figure 4a). Although the magnitude of the changes is expected, the patchiness of the changes was not anticipated. More surprisingly is the fact that there have been comparable changes in the Apparent Oxygen Utilization (AOU, a measure of the decomposition of organic matter in the ocean) of the waters indicating significant changes in the organic matter cycling over the last decade (Figure 4b). The complicated patterns of these changes clearly show that carbon is being influenced by more than simple secular changes in anthropogenic tracers. In some cases changes in circulation and organic matter decomposition may be masking the anthropogenic changes and in other cases these changes may enhance the apparent ocean carbon uptake.

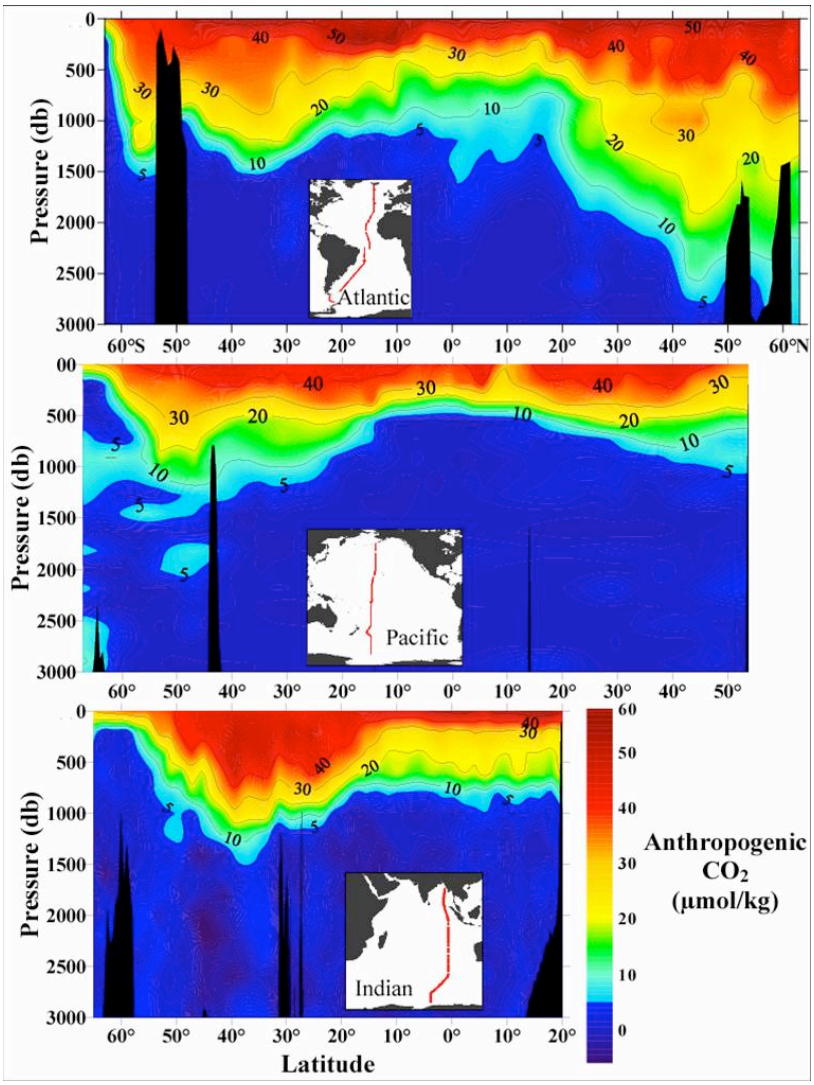

Figure 2. Example sections of anthropogenic CO_2 that has accumulated in the Atlantic, Pacific, and Indian oceans between 1800 and 1994 (modified from Sabine et al., 2004b).

Another intriguing preliminary finding from a comparison of recent cruises in the North Pacific and North Atlantic is an indication that anthropogenic carbon inventories may be increasing in the Pacific at about twice the rate of the Atlantic over the last 10 years (Feely et al., 2005a). This is in contrast to the long-term anthropogenic CO_2 inventory that shows larger column inventories in the North Atlantic, thus highlighting the variability in oceanic

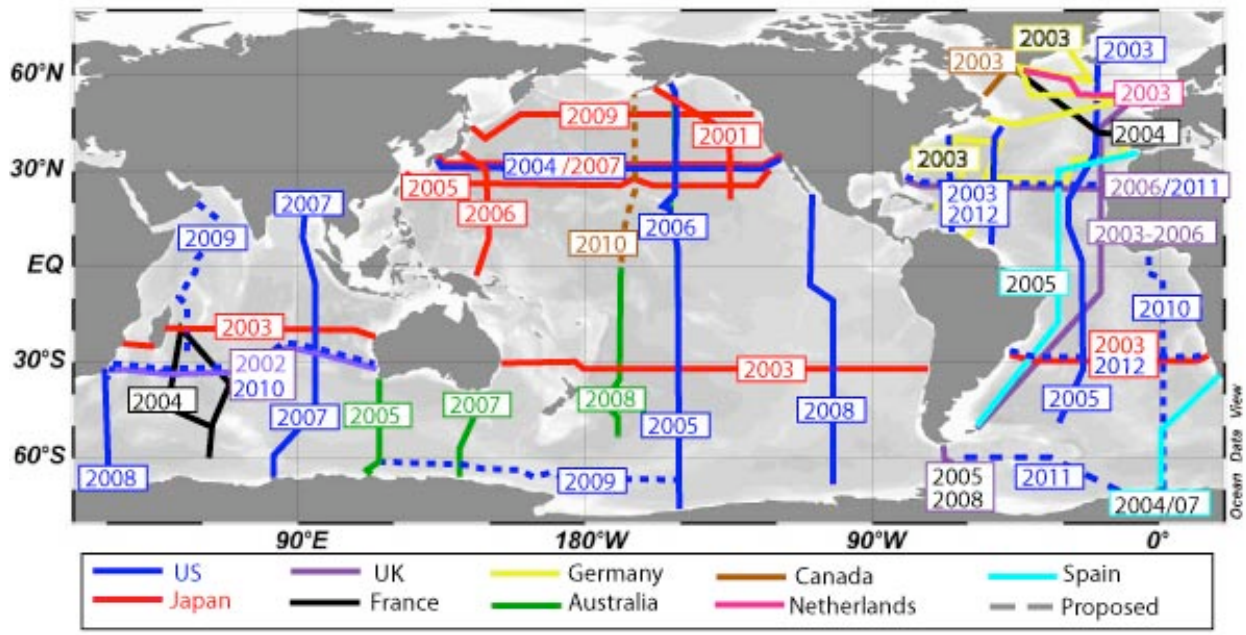

Figure 3. Map indicating recently completed and planned international repeat hydrography cruises. The U.S. CLIVAR/CO_2 Repeat Hydrography Program (indicated in blue) started in 2003 with three cruises in the North Atlantic.

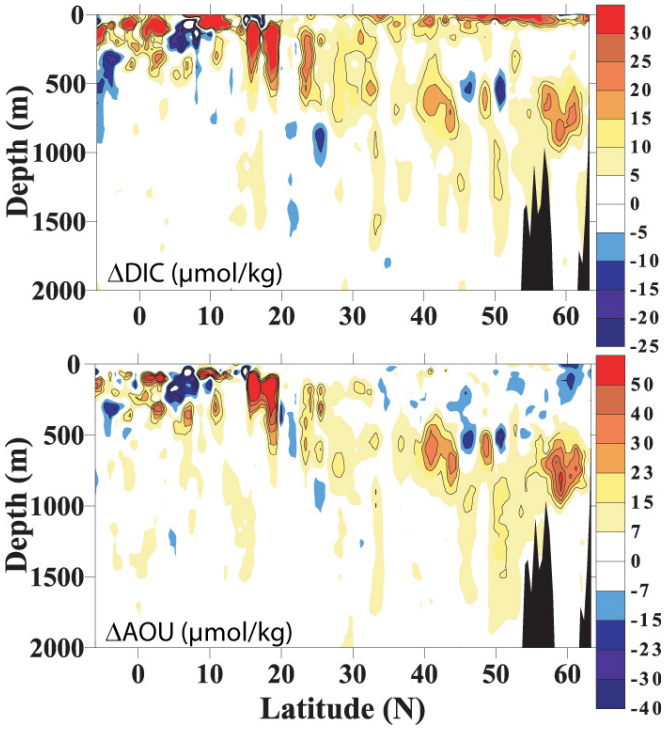

Figure 4. Changes in DIC (a) and AOU (b) between the 2003 and the 1993 occupations of A16N. Positive values represent an increase in concentrations between 1993 and 2003 (modified from Feely et al., 2005a).

sinks with time, and underscoring the challenge of predicting future oceanic uptake of atmospheric CO_2. The explanation for these recent findings may lie in understanding the effects of climate modes like the North Atlantic Oscillation (NAO) or the Pacific Decadal Oscillation (PDO) on the decadal scale circulation. These results also point to the need for improved techniques for isolating the anthropogenic and natural components of the observed variability.

Ocean-Atmosphere CO_2 Fluxes

The temporal and spatial variability of the partial pressure of CO_2 (i.e. the contribution of CO_2 pressure to total gas pressure, pCO_2) in the surface ocean is large compared to the atmospheric pCO_2 variability. Atmospheric pCO_2 is well resolved by weekly flask sampling at ~50 stations around the world (Tans and Conway, 2005). Because of the greater variability, surface ocean pCO_2 distributions are only known in a climatological sense. Inferring a global CO_2 uptake rate is challenging because, the average pCO_2 of the atmosphere need only be ~7μatm higher than the global ocean pCO_2 to account for an ocean uptake of ~2 Pg of carbon each year. Taro Takahashi of Lamont-Doherty Earth Observatory and his collaborators have amassed adatabase of more

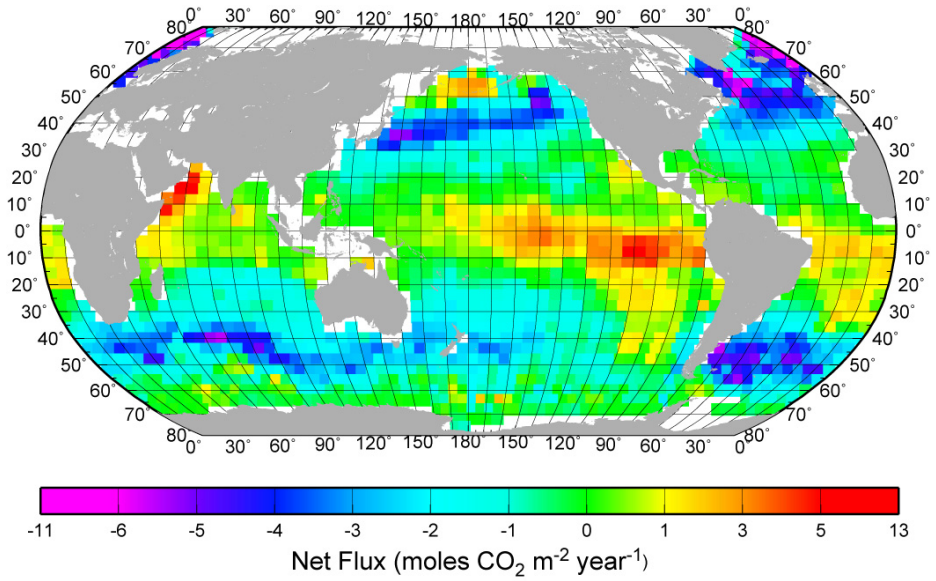

Figure 5. Annual sea-air fluxes for a nominal year of 1995. Positive values indicate a flux of CO_2 out of the ocean (Takahashi, 2002).

than 1.7 million surface ocean pCO_2 measurements, spanning more than 30 years, and derived a pCO_2 climatology for the global ocean (Takahashi et al., 2002). These data have been used to determine global and regional sea-air CO_2 fluxes with an average annual global open-ocean uptake of 1.5 ± 0.4 Pg C/yr for a nominal year of 1995 (Takahashi et al., 2002; revised by T. Takahashi, New York, 2005, personal communication). This flux estimate represents the total net flux in 1995. This is significant because prior to human intervention the oceans were a net source of CO_2 to the atmosphere of approximately 0.6 Pg C yr^{-1} (Sabine et al., 2004a). The total anthropogenic flux is the difference between the 1995 net sea-air flux and the estimated pre-industrial net sea-air flux (i.e. -1.5 – 0.6 = -2.1 Pg C/yr; see Table 1).

Figure 5 shows the global distribution of total net sea-air CO_2 fluxes. The yellow-orange-red colors indicate oceanic areas where there is a net source of CO_2 to the atmosphere, and the blue-purple colors indicate regions where there is a net sink of CO_2. The Equatorial Pacific is a strong source of CO_2 to the atmosphere throughout the year as a result of upwelling, which brings deep, high CO_2 waters to the surface in the central and eastern regions. This upwelling, and thus the CO_2 flux to the atmosphere, is heavily modulated by the El-Niño Southern Oscillation (ENSO) cycle (Feely et al., 2002, 2004b; Takahashi et al., 2003). During strong El-Niño years the equatorial Pacific CO_2 source can drop to zero as the upwelling is suppressed. During La Niña the upwelling, and thus the CO_2 source to the atmosphere, is enhanced**.** CO_2 outgassing fluxes are also observed in the tropical Atlantic and Indian oceans.

The CO_2 flux in the high-latitude ocean is governed primarily by deep convection in winter and biological uptake during the spring and summer months (i.e. outgassing in the winter and uptake in the spring/summer), whereas in the temperate and subtropical regions, the flux is governed primarily by water temperature (i.e., spring/summer warming causes outgassing and fall/winter cooling causes uptake). Outside of the equatorial belt and coastal upwelling regions, the ΔpCO_2 (seawater pCO_2 - atmospheric pCO_2, which drives the air sea exchange) is highest during winter in subpolar and polar waters, whereas it is highest during summer in the temperate regions. Thus, the seasonal variation of ΔpCO_2 and, consequently, the shift between net uptake and release of CO_2 in subpolar and polar regions is about 6 months out of phase with that in the temperate regions (Takahashi et al., 2002).

Although the Takahashi pCO_2 climatology has greatly improved our understanding of the sea-air flux patterns, it does not address the temporal variability in these patterns or the variability in the global net uptake. Substantial inter-annual variability in the Equatorial Pacific CO_2 flux (± 0.4 Pg C/yr peak-to-peak amplitude) has been well documented through sustained shipboard and moored time series measurements (e.g. Feely et al., 1995; Chavez et al., 1999; Feely et al., 2005b), but a

paucity of measurements have limited similar assessments in other regions of the global ocean.

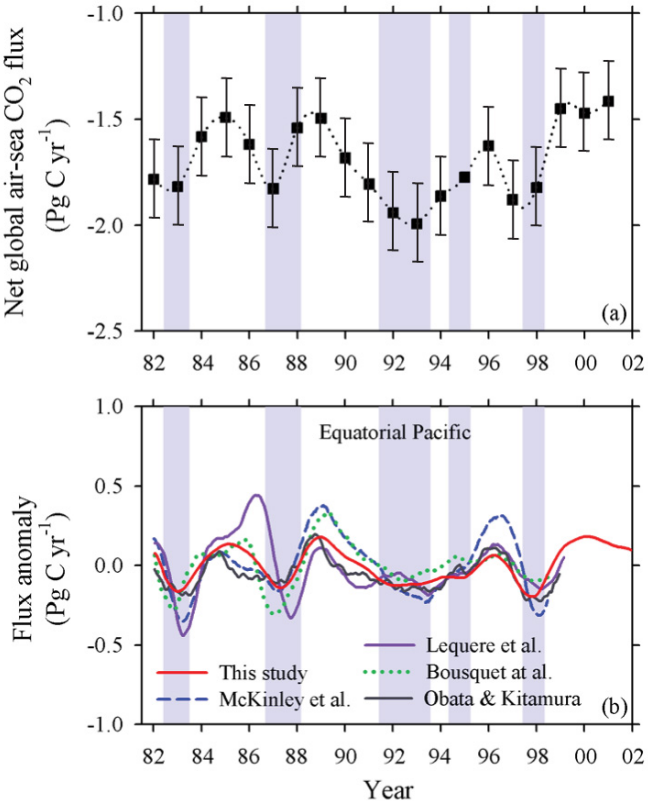

Figure 6. (a) Net global sea-air CO_2 fluxes in Pg C yr^{-1} from 1982 through 2001. The dotted line is a spline fit and error bars indicate estimated uncertainty in seasonal pCO_{2sw}/SST relationships only. Negative values correspond to net oceanic CO_2 uptake. Shaded bars indicate El Niño events (when SST anomoly is greater than 0.4°C in the Niño 3.4 region). (b) Comparisons of modeled CO_2 flux anomalies for the Equatorial Pacific (10°N–10°S, 80°W–135°E). For the period over which four independent estimates are available (1982–1997), modeled interannual variabilities obtained from Le Quéré et al. (2003), McKinley et al. (2004), Bousquet et al. (2000), Obata and Kitamura (2003), and the present study (Park et al., 2005) are ±0.18, ±0.18, ±0.14, ±0.13, and ±0.12 Pg C yr^{-1}, respectively (modified from Park et al., 2005).

.Recently, Park et al. (2005) used regional algorithms relating pCO_2 to satellite derived sea surface temperature anomalies to estimate CO_2 variability globally. They found the average inter-annual deviation of the global ocean CO_2 flux from the Takahashi climatology to be ±0.18 Pg C yr^{-1} for the period from 1982 to 2001. However, there are large uncertainties in this approach. The estimated uncertainty from the seawater pCO_2/SST relationships alone is as large as the estimated global inter-annual variability (Figure 6a).

In an effort to improve these regional algorithms, the international CO_2 community is developing a surface CO_2 observational network using volunteer observing ships, moorings, and drifting floats. These measurements together with modeling efforts can be used to better understand the controls on sea-air CO_2 fluxes. For example, approximately 70% of the global CO_2 flux variability is currently attributed to flux anomalies in the Equatorial Pacific (Figure 6b). The regional algorithm approach estimates a smaller inter-annual variability than most ocean model studies in this region. Our growing observational data base will allow us to make improved algorithms for the Equatorial Pacific (e.g. Feely et al., 2004b). Similar efforts are going on in subtropical regions where temperature exerts a dominant control on sea surface pCO_2 levels (e.g. Olsen et al., 2004, Wanninkhof et al, 2005).

In the high-latitude oceans the algorithms will require additional input parameters to account for the effects of deep convection and biological uptake on surface pCO_2. For example, the inclusion of mixed layer depth, obtained from the ARGO profiling floats, in the algorithms for these regions looks promising (Lueger et al., 2005). An expansion of the global observational network is needed in all parts of the global ocean to evaluate the uncertainties in the regional algorithm assessment of global inter-annual variability and to develop improved algorithms relating pCO_2 to satellite observations. With the proper observational program, the documentation of inter-annual CO_2 flux variability in the global ocean can be achieved.

References

Bousquet, P., P. Peylin, P. Ciais, C. Le Quéré, P. Friedlingstein, and P. P. Tans (2000) Regional changes in carbon dioxide fluxes of land and oceans since 1980, *Science*, *290*, 342–1346.

Chavez, F. P., P. G. Strutton, G. E. Friederich, R. A. Feely, G. Feldman, D. Foley, and M. J. McPhaden (1999), Biological and chemical response of the equatorial Pacific Ocean to the 1997–1998 El Niño, *Science, 286*(5447), 2126–2131.

Feely, R. A., R. Wanninkhof, C. E. Cosca, P. P. Murphy, M. F. Lamb, and M. D. Steckley (1995), CO_2 distributions in the equatorial Pacific during the 1991–1992 ENSO event, *Deep Sea Res., Part II*, 42(2–3), 365–386.

Feely, R.A., C.L. Sabine, T. Takahashi, and R. Wan-

ninkhof (2001) Uptake and storage of carbon dioxide in the oceans: The global CO_2 survey. *Oceanography*, 14(4), 18–32.

Feely, R.A., J. Boutin, C.E. Cosca, Y. Dandonneau, J. Etcheto, H.Y. Inoue, M. Ishii, C. Le Quere, D. Mackey, M. McPhaden, N. Metzl, A. Poisson, and R. Wanninkhof (2002) Seasonal and interannual variability of CO_2 in the Equatorial Pacific. *Deep-Sea Res. Pt. II,* 49(13–14), 2443–2469.

Feely, R.A., C.L. Sabine, K. Lee, W. Berelson, J. Kleypas, V.J. Fabry, and F.J. Millero (2004a) Impact of anthropogenic CO_2 on the $CaCO_3$ system in the oceans. *Science*, 305(5682), 362–366.

Feely, R.A., R. Wanninkhof, W. McGillis, M.-E. Carr, and C.E. Cosca (2004b) Effects of wind-speed and gas exchange parameterizations on the air-sea CO_2 fluxes in the equatorial Pacific Ocean. *J. Geophys. Res.,* 109(C8), C08S03, doi: 10.1029/2003JC001896.

Feely, R.A., L.D. Talley, G.C. Johnson, C.L. Sabine, and R. Wanninkhof (2005a) Repeat hydrography cruises reveal chemical changes in the North Atlantic. *Eos, Trans. AGU,* 86(42), 399, 404–405.

Feely, R.A., T. Takahashi, R. Wanninkhof, M.J. McPhaden, C.E. Cosca, S.C. Sutherland, and M.-E. Carr (2005b) Decadal Variability of the Air-Sea CO_2 Fluxes in the Equatorial Pacific Ocean, *J. Geophys. Res. Ocean*, submitted.

Gloor, M., Gruber, N., Sarmiento, J.L., Sabine, C.L., Feely, R.A. and Rödenbeck, C. (2003) A first estimate of present and preindustrial air-sea CO_2 flux patterns based on ocean interior carbon measurements and models. *Geophysical Research Letters,* 30, 1, 1010, doi: 10.1029/2002GL015594.

Gurney, K.R., Law, R.M., Denning, A.S., Rayner, P.J., Baker, D., Bousquet, P., Bruhwiler, L., Chen, Y.H., Ciais, P., Fan, S., Fung, I.Y., Gloor, M., Heimann, M., Higuchi, K., John, J., Maki, T., Maksyutov, S., Masarie, K., Peylin, P., Prather, M., Pak, B.C., Randerson, J., Sarmiento, J., Taguchi, S., Takahashi, T. and Yuen, C.W. (2002) Towards robust regional estimates of CO_2 sources and sinks using atmospheric transport models. *Nature* 415 (6872), 626-630.

Keeling, R.F., Keeling, C.D. and Manning, A.C. (2005) Interannual variations in carbon sinks deduced from measurements of atmospheric O_2/N_2 and CO_2, *Global Biogeochemical Cycles*., submitted.

Le Quéré, C., O. Aumont, L. Bopp, P. Bousquet, P. Ciais, R. Francey, M. Heimann, C.D. Keeling, R.F. Keeling, H. Kheshgi, P. Peylin, S.C. Piper, I.C. Prentice and P.J. Rayner (2003) Two decades of ocean CO_2 sink and variability, *Tellus*, *55B*, 649−656.

Lueger, H., Wanninkhof, R., Olsen, A., Trinanes, J., Johannessen, T., Wallace, D., Koertzinger, A.,(2005) The CO_2 air-sea flux in the North Atlantic estimated from satellite data. *Tellus* , submitted.

Marland, G., T.A. Boden, and R. J. Andres (2005) Global, Regional, and National Fossil Fuel CO_2 Emissions. In *Trends: A Compendium of Data on Global Change*. Carbon Dioxide Information Analysis Center, Oak Ridge National Laboratory, U.S. Department of Energy, Oak Ridge, Tenn., U.S.A.

Matsumoto, K., Sarmiento, J.L., Key, R.M., Aumont, O., Bullister, J.L., Caldeira, K., Campin, J.M., Doney, S.C., Drange, H., Dutay, J.C., Follows, M., Gao, Y., Gnanadesikan, A., Gruber, N., Ishida, A., Joos, F., Lindsay, K., Maier-Reimer, E., Marshall, J.C., Matear, R.J., Monfray, P., Mouchet, A., Najjar, R., Plattner, G.K., Schlitzer, R., Slater, R., Swathi, P.S., Totterdell, I.J,, Weirig, M.F., Yamanaka, Y., Yool, A. and Orr, J.C. (2004) Evaluation of ocean carbon cycle models with data-based metrics, *Geophysical Research Letters* 31 (7): Art. No. L07303.

McKinley, G. A., M. J. Follows, and J. Marshall (2004) Mechanisms of air-sea CO_2 flux variability in the equatorial Pacific and the North Atlantic, *Global Biogeochem. Cycles*, *18*, GB2011, doi:10.1029/2003GB002179.

McNeil, B.I., Matear, R.J., Key, R.M., Bullister, J.L. and Sarmiento, J.L. (2003) Anthropogenic CO_2 uptake by the ocean based on the global chlorofluorocarbon data set. *Science, 299*(5604), 235–239.

Obata, A., and Y. Kitamura (2003) Interannual variability of the air-sea exchange of CO_2 from 1961 to 1998 simulated with a global ocean circulation-biogeochemistry model, *J. Geophys. Res.*, *108*, 3337, doi:10.1029/2001JC001088

Olsen, A., Triñanes, J., Wanninkhof, R. (2004) Sea-air flux of CO_2 in the Caribbean Sea estimated using in situ and remote sensing data. *Remote Sensing of Environment* , *89*, 309–325.

Orr, J.C. (2004) *Modelling of ocean storage of CO_2--- The GOSAC study*, Report PH4/37, IEA Greenhouse Gas R&D Programme, 96 pp.

Orr, J.C., V.J. Fabry, O. Aumont, L. Bopp, S.C. Doney, R.A. Feely, A. Gnanadesikan, N. Gruber, A. Ishida, F. Joos, R.M. Key, K. Lindsay, E. Maier-Reimer, R. Matear, P. Monfray, A. Mouchet, R.G. Najjar, G.-K. Plattner, K.B. Rodgers, C.L. Sabine, J.L. Sarmiento, R. Schlitzer, R.D. Slater, I. Totterdell, M.-F. Weirig, Y. Yamanaka, and A. Yool (2005) Anthropogenic ocean acidification over the twenty-first century and its impact on calcifying organisms. *Nature*, 437(7059), 681–686.

Park, G.-H., K. Lee, R. Wanninkhof and R.A. Feely (2005) Empirical ocean data-based estimates of variability of oceanic uptake of CO_2 over the last two decades, *J. Geophys. Res.*, submitted.

Prentice, I.C., G.D. Farquhar, M.J.R. Fasham, M.L. Goulden, M. Heimann, V.J. Jaramillo, H.S. Kheshgi, C. LeQuéré, R.J. Scholes, and D.W.R. Wallace (2001) The carbon cycle and atmospheric CO_2, In: *Climate Change: The Scientific Basis*, Contribution of working group I to the Third Assessment Report of the Intergovernmental Panel on Climate Change, J. Houghton, and D. Yihui (eds.), Cambridge University Press, Cambridge, UK.

Sabine, C.L., Heimann, M., Artaxo, P., Bakker, D., Chen, C.-T.A., Field, C.B., Gruber, N., LeQuéré, C., Prinn, R.G., Richey, J.E., Lankao, P.R., Sathaye, J. and Valentini, R. (2004a) Chapter 2: Current status and past trends of the global carbon cycle. In: Field, C.B. and Raupach, M.R. (eds.), *The Global Carbon Cycle: Integrating Humans, Climate, and the Natural World*, Scope 62, Island Press, Washington D.C., 17-44.

Sabine, C.L., R.A. Feely, N. Gruber, R.M. Key, K. Lee, J.L. Bullister, R. Wanninkhof, C.S. Wong, D.W.R. Wallace, B. Tilbrook, F.J. Millero, T.-H. Peng, A. Kozyr, T. Ono, and A.F. Rios (2004b) The oceanic sink for anthropogenic CO_2. *Science*, 305(5682), 367–371.

Takahashi, T., Sutherland, S.C., Sweeney, C., Poisson, A., Metzl, N., Tilbrook, B., Bates, N., Wanninkhof, R., Feely, R.A., Sabine, C. and Olafsson, J. (2002), Biological and temperature effects on seasonal changes of pCO_2 in global ocean surface waters, *Deep Sea Research* 49 (9–10), 1601–1622.

Takahashi, T., S.C. Sutherland, R.A. Feely, and C.E. Cosca (2003) Decadal variation of the surface water PCO_2 in the western and central equatorial Pacific. *Science*, 302, 852–856.

Tans, P.P. and T.J. Conway (2005) Monthly Atmospheric CO_2 Mixing Ratios from the NOAA CMDL Carbon Cycle Cooperative Global Air Sampling Network, 1968-2002. In *Trends: A Compendium of Data on Global Change*. Carbon Dioxide Information Analysis Center, Oak Ridge National Laboratory, U.S. Department of Energy, Oak Ridge, Tenn., U.S.A.

Wallace, D.W.R. (2001) Storage and transport of excess CO_2 in the oceans: The JGOFS/WOCE Global CO_2 Survey, In: Siedler, G., Church, J. and Gould, J. (eds.) *Ocean Circulation and Climate: Observing and Modelling the Global Ocean*, Academic Press, San Diego, CA, 489-521.

Wanninkhof, R., Olsen, A., Triñanes, J. (2005) Air-Sea CO_2 Fluxes in the Caribbean Sea from 2002-2004. *Journal of Marine Systems,Proceedings of the 37th International Colloquium on Ocean Dynamics:Gas Transfer at Water Surfaces*, accepted.

Wetzel, P., Winguth, A. and Maier-Reimer, E. (2005) Sea-to-air CO_2 flux from 1948 to 2003: A model study, *Global Biogeochemical Cycles* 19 (2): Art. No. GB2005.